


The GAPS Programme at TNG

XXXVII. A precise density measurement of the young ultra-short period planet TOI-1807 b^{★,★★}

D. Nardiello^{1,2} , L. Malavolta^{3,1}, S. Desidera¹, M. Baratella⁴, V. D'Orazi¹, S. Messina⁵, K. Biazzo⁶, S. Benatti⁷, M. Damasso⁸, V. M. Rajpaul⁹, A. S. Bonomo⁸, R. Capuzzo Dolcetta¹⁰, M. Mallonn⁴, B. Cale¹¹, P. Plavchan¹¹, M. El Mufti¹¹, A. Bignamini¹², F. Borsa¹³, I. Carleo¹⁴, R. Claudi¹, E. Covino¹⁵, A. F. Lanza⁵, J. Maldonado⁷, L. Mancini^{16,17,8}, G. Micela⁷, E. Molinari¹⁸, M. Pinamonti⁸, G. Piotto^{3,1}, E. Poretti^{19,13}, G. Scandariato⁵, A. Sozzetti⁸, G. Andreuzzi^{19,6}, W. Boschin^{19,20,21}, R. Cosentino¹⁹, A. F. M. Fiorenzano¹⁹, A. Harutyunyan¹⁹, C. Knapic¹², M. Pedani¹⁹, L. Affer⁷, A. Maggio⁷, and M. Rainer¹³

(Affiliations can be found after the references)

Received 8 April 2022 / Accepted 1 June 2022

ABSTRACT

Context. Great strides have been made in recent years in the understanding of the mechanisms involved in the formation and evolution of planetary systems. Despite this, many observational findings have not yet been corroborated by astrophysical explanations. A fine contribution to the study of planetary formation processes comes from the study of young, low-mass planets, with short orbital periods ($\lesssim 100$ days). In the last three years, the NASA/TESS satellite has identified many planets of this kind and their characterization is clearly necessary in order to understand how they formed and evolved.

Aims. Within the framework of the Global Architecture of Planetary System (GAPS) project, we performed a validation and characterization (radius and mass) of the ultra-short period planet TOI-1807 b, which orbits its young host star BD+39 2643 (~ 300 Myr) in only 13 h. This is the youngest ultra-short period planet discovered so far.

Methods. Thanks to a joint modeling of the stellar activity and planetary signals in the TESS light curve and in new HARPS-N radial-velocity measurements, combined with accurate estimation of stellar parameters, we validated the planetary nature of TOI-1807 b and measured its orbital and physical parameters.

Results. By using astrometric, photometric, and spectroscopic observations, we found that BD+39 2643 is a young, active K dwarf star and a member of a 300 ± 80 Myr old moving group. Furthermore, it rotates in $P_{\text{rot}} = 8.8 \pm 0.1$ days. This star hosts an ultra-short period planet, exhibiting an orbital period of only $P_b = 0.54937 \pm 0.00001$ days. Thanks to the exquisite photometric and spectroscopic series, along with the accurate information on its stellar activity, we measured both the radius and the mass of TOI-1807 b with high precision, obtaining $R_{p,b} = 1.37 \pm 0.09 R_{\oplus}$ and $M_{p,b} = 2.57 \pm 0.50 M_{\oplus}$. These planet parameters correspond to a rocky planet with an Earth-like density ($\rho_b = 1.0 \pm 0.3 \rho_{\oplus}$) and no extended H/He envelope. From the analysis of the age- R_p distribution for planets with well measured ages, we inferred that TOI-1807 b may have already lost a large part of its atmosphere over the course of its 300 Myr lifetime.

Key words. planets and satellites: fundamental parameters – stars: fundamental parameters – stars: individual: BD+39 2643 – techniques: photometric – techniques: spectroscopic – techniques: radial velocities

1. Introduction

Over the last decade, the space missions *Kepler* (Borucki et al. 2010), K2 (Howell et al. 2014), and TESS (Transiting Exoplanet Survey Satellite, Ricker et al. 2015) have allowed us to identify a large number of transiting planets and planetary systems with ages younger than 1 Gyr. The study of these young planets is important for bettering our understanding of the mechanisms that come into play in the early stages of planetary formation

and evolution, such as migration, planetary impacts, atmospheric evaporation, and so on. (see, e.g., Terquem & Papaloizou 2007; Ida & Lin 2010; Hansen & Murray 2012; Lopez & Fortney 2013; Owen & Wu 2013; Schlichting et al. 2015; Owen & Lai 2018; Schlichting 2018; Bonomo et al. 2019). Identifying and characterizing planets around young stars is not always an easy task because of the magnetic activity of the host star. Indeed, the strong starspot activity on the stellar surface (typical of young stars with ages $\lesssim 1$ Gyr) generates (periodical) important variations in the star's flux, both in terms of the photometric and spectroscopic time series, which can mask the planets' signals if not appropriately modeled. Despite this, in recent years, the population of young planets has been growing significantly and planets have been found around young stellar cluster members like M44 and the Hyades (Quinn et al. 2012, 2014; Malavolta et al. 2016; Mann et al. 2016a; Rizzuto et al. 2018; Vanderburg et al. 2018), young stellar associations and moving

* Spectroscopic series, lightcurve are only and Table B.1 is also available at the CDS via anonymous ftp to cdsarc.u-strasbg.fr (130.79.128.5) or via <http://cdsarc.u-strasbg.fr/viz-bin/cat/J/A+A/664/A163>

** Based on observations made with the Italian Telescopio Nazionale Galileo (TNG) operated by the Fundación Galileo Galilei (FGG) of the Istituto Nazionale di Astrofisica (INAF) at the Observatorio del Roque de los Muchachos (La Palma, Canary Islands, Spain).

groups (Benatti et al. 2019; Mann et al. 2020, 2022; Rizzuto et al. 2020; Tofflemire et al. 2021; Newton et al. 2021), and single young stars (David et al. 2019; Plavchan et al. 2020; Carleo et al. 2021; Bouma et al. 2022a). However, only a few sample of young exoplanets with ages $<0.5\text{--}1$ Gyr have well-constrained ages, (upper-limit) masses, and radii, demonstrating a broad variety of planets with densities included between $<0.5\text{--}1 \rho_{\oplus}$ (see, e.g., Benatti et al. 2021) and $2\text{--}3 \rho_{\oplus}$ (see, e.g. Barragán et al. 2019, 2022b).

Ultra-short period (USP) planets are planetary objects with orbital periods $P \lesssim 1$ day (Sahu et al. 2006). These “exotic” objects can provide many information on the processes of formation and evolution of planetary systems, especially if they are observed orbiting young stars. Even if this kind of planet may seem fairly easy to detect because of the short orbital period, only about a hundred of them have been discovered so far, with an occurrence rate of $0.4\text{--}0.5\%$ (Sanchis-Ojeda et al. 2014; Winn et al. 2018; Zhu & Dong 2021). The majority of USP planets have radii of $R_p < 2 R_{\oplus}$, and they could be shown to be the remnant rocky cores of gaseous giant planets following processes of atmospheric evaporation or they could be rocky planets that migrated inward with regard to their planetary systems (Chiang & Laughlin 2013; Valsecchi et al. 2014; Lee & Chiang 2017; Petrovich et al. 2019).

To date, we have not yet identified USP planets around very young stars (<100 Myr) and we thus still lack information on the very early stages of formation and evolution for these kinds of planets. In the context of the Global Architecture of Planetary Systems (GAPS) Young Objects project (see Carleo et al. 2020), we are monitoring young stars ($2\text{--}600$ Myr), using HARPS-N (Cosentino et al. 2012) at Telescopio Nazionale Galileo (TNG), with the aim of identifying and characterizing young planets around them, including USP planets. In this paper, we present the results obtained for the youngest USP planet discovered so far: with an age of ~ 300 Myr, TOI-1807 b orbits the K dwarf BD+39 2643 (TOI-1807) in about 0.55 days. This paper is structured as follows: Sect. 2 describes the photometric and spectroscopic data used in this work to characterize the host star and the planet. Section 3 reports the stellar properties. The procedures adopted to identify and confirm TOI-1807 b in the TESS light curve are explained in Sect. 4. The modeling of photometric and RV series and the planet’s properties are reported in Sect. 5. In Sect. 6, we discuss and summarize the results obtained in this work.

2. Observations and data reduction

2.1. TESS Photometry

The star TOI-1807 was observed by TESS both in short- (2 min) and long-cadence (30 minutes) mode in Sectors 22 and 23 (Table 1). In this work, we use light curves extracted from both datasets.

For the long-cadence data, we extracted the light curves from TESS Full Frame Images (FFIs, see Fig. 1), adopting the software IMG2LC developed by Nardiello et al. (2015) and used for the extraction of light curves of stars in stellar clusters from images obtained with ground-based instruments (Nardiello et al. 2016b), *Kepler* (Libralato et al. 2016a,b; Nardiello et al. 2016a), and TESS (Nardiello et al. 2019, 2021; Nardiello 2020). The routine allows us to minimize the neighbor contamination and extract high-precision photometry even for very faint stars (see, e.g., Apai et al. 2021). We corrected the light curves for systematic effects by fitting to them the Cotrending Basis Vectors (CBVs) extracted by Nardiello et al. (2020).

Table 1. Summary of the observations.

TOI	1807
TESS observations	
Sectors	22,23
HARPS-N RV monitoring	
Nr. spectra	161
Time-span (days)	474
$\langle RV_{\text{err}} \rangle$ (m s^{-1})	1.74
σ_{RV} (m s^{-1})	23.0
$\langle S/N \rangle$	67.9

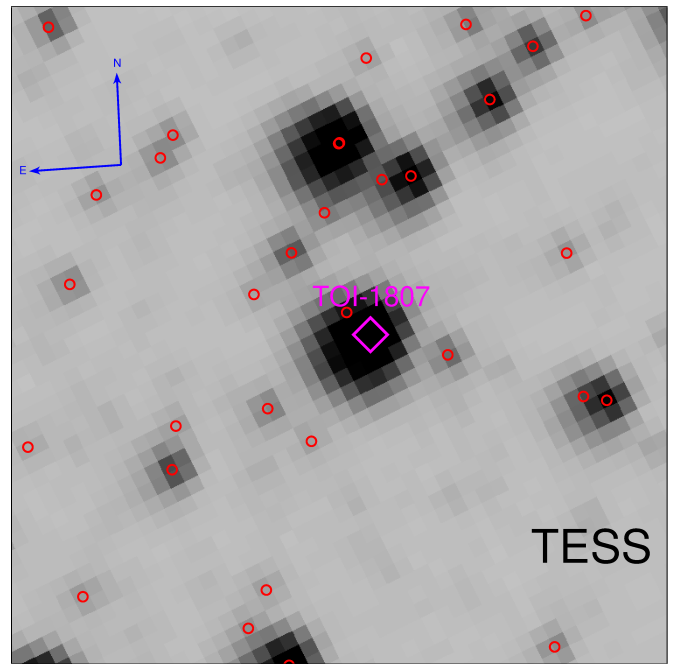


Fig. 1. Finding chart of TOI-1807 (magenta diamond) from the TESS FFI `tess2020090105920-s0023-2-2-0177-s_ffic`; red circles are the neighbor stars in the *Gaia* EDR3 catalog with $G \leq 17$. The field of view is 15×15 arcmin², and it is oriented with north up and east left.

For the short-cadence data, we corrected the Simple Aperture Photometry (SAP) light curves by using CBVs obtained with the routines developed by Nardiello et al. (2020) and all the SAP light curves in the same Camera and CCD in which TOI-1807 was located. This correction was mandatory because the Pre-search Data Conditioning Simple Aperture Photometry (PDCSAP) light curves (Smith et al. 2012; Stumpe et al. 2012, 2014) of the target suffered of many systematic effects due to over-corrections and/or injection of spurious signals. In Appendix A, we report the differences between PDCSAP light curves and those corrected by us. For the analysis carried out in this paper, for both long and short cadence light curves, we used the points flagged with $DQUALITY=0$.

We also excluded from the long cadence light curve the points associated with values of local background $>4\sigma_{\text{sky}}$ above the mean value of the local background. After the selections, the short and long cadence light curves contain 27866 and 1784 points, respectively, spanning 55.5 days. We calculated the simple RMS and the P2P RMS as done in Nardiello (2020); the first parameter is sensitive to the stellar variability, while the P2P RMS is not sensitive to the variations in the light curve.

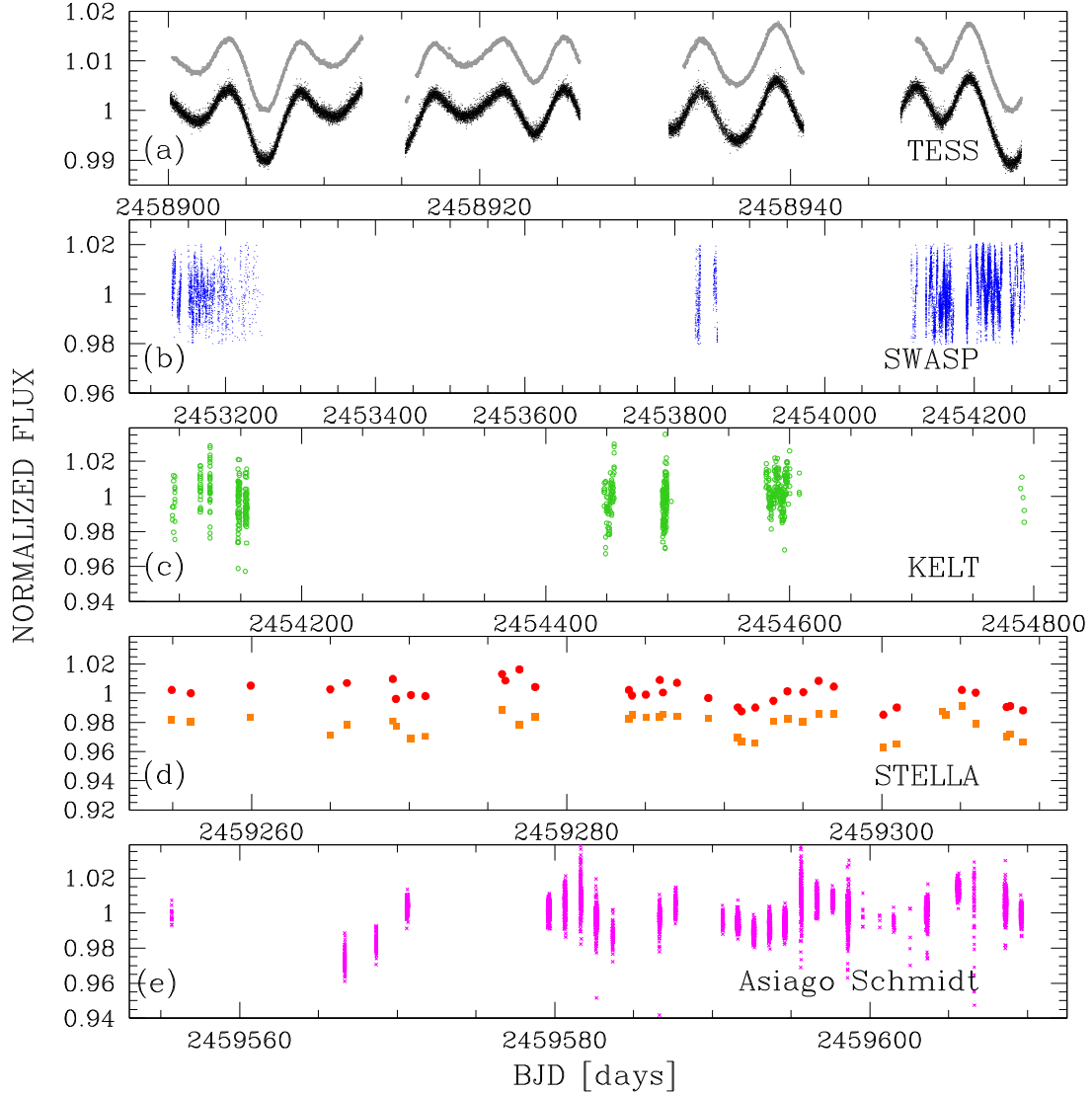


Fig. 2. Light curves of TOI-1807 used in this work. *Panel a* shows the long- (gray points) and the short-cadence (black points) TESS light curve; *panels b and c* illustrate the SuperWASP and KELT light curves, respectively. *Panel d* shows the STELLA light curves obtained in *V* (orange points) and *I* (red points) bands. *Panel e* shows the light curve obtained with the Asiago Schmidt 67/92 cm telescope.

We obtained an RMS of 4 parts-per-thousand (ppt) both for the short- and the long-cadence light curve; we measured a P2P RMS of 0.9 ppt for the short cadence light curve and 0.2 ppt for the long-cadence light curve. The short- and long-cadence light curves are shown in panel a of Fig. 2.

2.2. SuperWASP

We downloaded the publicly available light curves obtained with SuperWASP observations (Pollacco et al. 2006; Butters et al. 2010) and from them we removed all the points with the quality flag FLAG=0 (not-corrected photometric points) and all the outliers. The light curve of TOI-1807 we used contains 13038 points collected between May 2004 and June 2007 (1138.2 days, see panel b of Fig. 2). The simple and P2P RMS are 9 ppt and 6 ppt, respectively.

2.3. KELT

We used the light curves obtained from data collected during the Kilodegree Extremely Little Telescope (KELT) survey

(Pepper et al. 2007), and available online¹. We did not do any selection on these light curves (556 points, panel c of Fig. 2). Observations of TOI-1807 were carried out between December 2006 and November 2008 (698 days). The KELT light curve has an RMS of 10 ppt and a P2P RMS of 7 ppt.

2.4. STELLA

We collected data on TOI-1807 with the WiFSIP imager mounted at the robotic STELLA telescope (Strassmeier et al. 2004) between February and April 2021 (52 days). Observations were carried out in the *V*-Johnson ($t_{\text{exp}} = 8$ s) and *I*-Cousin bands ($t_{\text{exp}} = 5$ s). Differential light curves were extracted as described by Mallonn et al. (2015, 2018). The *V* and *I* light curves contain 35 and 36 points, respectively, and are shown in panel d of Fig 2; each point is the average of five individual exposures. The RMS of the light curves is about 10 ppt, while the P2P RMS is 8 ppt.

¹ <https://exoplanetarchive.ipac.caltech.edu/docs/KELT.html>

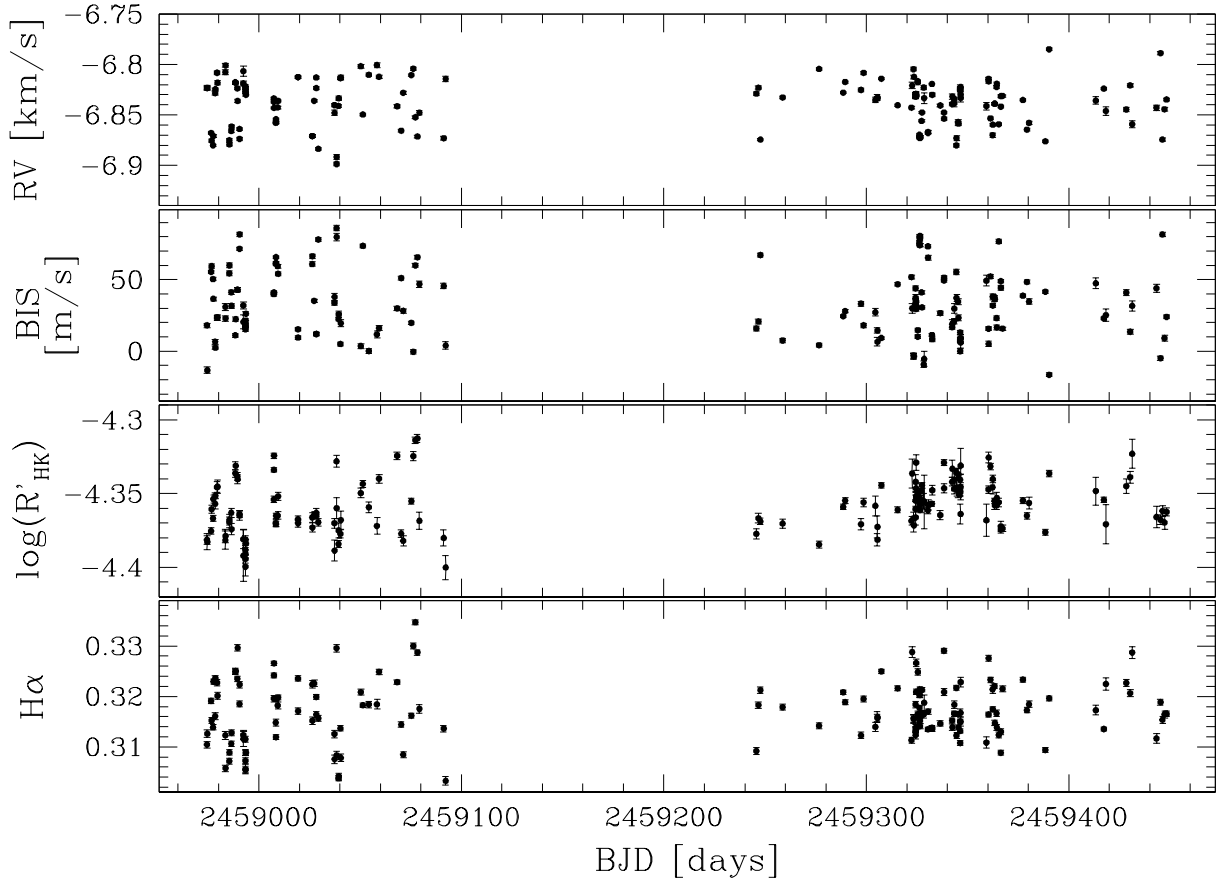


Fig. 3. Spectroscopic time series obtained with HARPS-N and used in this work. *From the top to the bottom panels:* the RV, BIS, $\log R'_{\text{HK}}$, and $H\alpha$ time series. See text for details.

2.5. Asiago Schmidt 67/92 cm

We collected images of TOI-1807 with the Asiago Schmidt 67/92 cm telescope. Observations were carried out between December 2021 and January 2022 (54 days) in the *i*-sloan filter with an exposure time of 7s. We extracted the light curve of TOI-1807 by adopting the pipeline developed by Nardiello et al. (2015). The light curve contains 4771 points (panel e of Fig. 2) and is characterized by an RMS of 9 ppt and a P2P RMS of 6 ppt.

2.6. HARPS-N data

We monitored TOI-1807 with HARPS-N at TNG within the GAPS Young Objects program (Carleo et al. 2020). We obtained 161 spectra between May 2020 and August 2021, with exposure times of 1200 s. We followed an observational strategy specifically suited for ultra-short period planets, which consists of gathering at least two observations every night (Lacedelli et al. 2021). We collected 161 spectra in 474 nights. The spectra have, on average, a signal-to-noise ratio (S/N) ~ 68 . Details about the number of spectra collected, the total time-span of the observations and the typical S/N are also reported in Table 1. In this work, we excluded measurements collected during the night between May 5th and 6th, 2020 because they had been obtained during bad weather conditions and thus stand as outliers in the time series.

The spectra were reduced by using the HARPS-N Data Reduction Software (DRS), providing the RV extraction through the Cross-Correlation Function (CCF) method (see Pepe et al. 2002 and references therein). With this technique, the scientific spectra are cross-correlated with a binary mask depicting the

typical features of a star with a selected spectral type. We used a K5 mask for TOI-1807. The resulting CCFs provide a proxy for the mean line profile changes of each spectrum. To improve the fitting of the continuum of the CCF, we reprocessed our data by enlarging the width of the CCF evaluation window by using the offline version of the HARPS-N DRS which is implemented at the INAF Trieste Observatory² through the YABI workflow interface (Hunter et al. 2012). The resulting RVs have a typical dispersion of a few tens of m s^{-1} ($\sim 23 \text{ m s}^{-1}$). RV internal errors are of the order of a few m s^{-1} ($\sim 1.7 \text{ m s}^{-1}$). A summary of these values is also reported in Table 1. We compared the RVs obtained by the HARPS-N DRS with those provided by the TERRA pipeline (Anglada-Escudé & Butler 2012), for an independent extraction with a template matching method, generally employed in case of active stars. Since we found no differences between the two data sets (same RV dispersion and RV error bars), we decided to adopt the DRS RVs data sets for our analysis.

We also extracted the time series of a set of activity indices, which are useful for evaluating the jitter in the RV series due to stellar activity. The HARPS-N DRS provides the value of the CCF bisector span (BIS), while the $\log R'_{\text{HK}}$ index from the Ca II H&K lines was obtained by using a procedure available on YABI (described in Lovis et al. 2011 and references therein). Finally, we used the ACTIN Code³ (Gomes da Silva et al. 2018) to extract the $H\alpha$ index. The spectroscopic time series are illustrated in Fig. 3.

² <https://www.ia2.inaf.it/>

³ <https://github.com/gomesdasilva/ACTIN>

3. Stellar parameters

Here, we present the methods we used for the determination of the stellar parameters, combining photometric, spectroscopic, astrometric data and additional information, with special focus on the stellar age.

3.1. Kinematics and membership to moving groups

The U , V , and W space velocities were derived for our target using the kinematic data from Table 2 and the formalism by Johnson & Soderblom (1987). We also searched for membership to known groups, exploiting the BANYAN Σ on-line tool (Gagné et al. 2018)⁴ and the literature regarding TOI-1807. Finally, we performed our own search for comoving objects, as described in Appendix B.

TOI-1807 was not previously identified as a member of known groups. As previously done by Hedges et al. (2021), we noticed that the young planet host TOI-2076 has very similar kinematic parameters (their space velocities differ by just 0.5 km s^{-1} and their separation on the sky is of 12.46 deg , 9.2 pc at their common distance). We then searched for additional comoving objects, as detailed in Appendix B; 76 comoving objects were identified. Among them, we found 26 objects which are found to be similar in terms of age. All but three of these objects are also rather close on the sky and at a similar distance (median distance 42 pc , rms 7 pc), strengthening the case for a common origin. These objects were considered to refine the age of TOI-1807, assuming that they are coeval and formed together. The case of TOI-2076 system will be discussed in more detail in a forthcoming paper.

3.2. Photometric T_{eff} and reddening

Reddening toward our target was estimated from interpolation of the 3D reddening maps of Lallement et al. (2018). Reddening is negligible for TOI-1807 as expected from its close distance from the Sun ($E(B - V) \approx 0.002 \text{ mag}$, $d \sim 42.6 \text{ pc}$). Photometric T_{eff} using the tables by Pecaut & Mamajek (2013)⁵ results in $4830 \pm 100 \text{ K}$, corresponding to K3V spectral type.

3.3. Atmospheric parameters

The star TOI-1807 has a relatively young age ($\tau \sim 300 \text{ Myr}$), as further discussed below. We derived atmospheric parameters applying the standard spectroscopic method (i.e., using only Fe lines) and the new spectroscopic approach described in Baratella et al. (2020a,b). The spectroscopic analysis of intermediate-age and young dwarf stars may be hampered by the presence of intense magnetic fields that alter the structure of the upper layers of the photosphere. These affect the formation of strong spectral lines, for which the abundances show a trend with optical depths (Baratella et al. 2020b). As a consequence, when deriving the micro-turbulence velocity (ξ) by imposing the condition that weak and strong Fe lines have the same abundance, its value must be increased until it reaches $\sim 2\text{--}2.5 \text{ km s}^{-1}$. An overestimation of ξ results in an underestimation of the iron abundance ([Fe/H]) and all the abundance ratios that rescale accordingly. Following the same strategy as in Baratella et al. (2020a), we applied a new method that consists of using a combination of

Table 2. Stellar parameters.

Parameter	TOI-1807	Reference
Other target identifiers		
TIC	180695581	(1)
2MASS	J13250800+3855210	(2)
<i>Gaia</i> DR2	1476485996883837184	(3)
Astrometric information		
α (J2016.0) (deg)	201.28260370719	(4)
δ (J2016.0) (deg)	+38.92236336733	(4)
μ_{α^*} (mas yr ⁻¹)	-124.608 ± 0.008	(4)
μ_{δ} (mas yr ⁻¹)	-27.300 ± 0.009	(4)
Parallax (mas)	23.4804 ± 0.0142	(4)
Distance (pc)	42.58 ± 0.06	(5)
Photometric information		
T (mag)	9.036 ± 0.006	(1)
G (mag)	9.6752 ± 0.0003	(3)
B (mag)	11.082 ± 0.057	(1)
V (mag)	10.000 ± 0.030	(1)
J (mag)	7.646 ± 0.037	(2)
H (mag)	7.605 ± 0.018	(2)
K (mag)	< 7.568	(2)
W_1 (mag)	7.395 ± 0.032	(6)
W_2 (mag)	7.508 ± 0.020	(6)
W_3 (mag)	7.445 ± 0.017	(6)
W_4 (mag)	7.368 ± 0.115	(6)
Fundamental parameters		
RV (km s ⁻¹)	-7.33 ± 0.59	(3)
RV (km s ⁻¹)	-6.8380 ± 0.0031	(7)
U (km s ⁻¹)	-16.40 ± 0.02	(7)
V (km s ⁻¹)	-20.90 ± 0.05	(7)
W (km s ⁻¹)	-2.07 ± 0.19	(7)
T_{eff} (spectroscopic) (K)	4730 ± 75	(7)
T_{eff} (photometric) (K)	4830 ± 100	(7)
$\log g_{\star}$ (cgs)	4.55 ± 0.05	(7)
[Fe/H] (dex)	-0.04 ± 0.02	(7)
[Ti/H] (dex)	0.01 ± 0.08	(7)
L_{\star} (L_{\odot})	0.215 ± 0.016	(7)
M_{\star} (M_{\odot})	0.76 ± 0.03	(7)
R_{\star} (R_{\odot})	0.690 ± 0.036	(7)
Age (Myr)	300 ± 80	(7)
$E(B - V)$ (mag)	$0.002^{+0.014}_{-0.002}$	(7)
$v \sin i_{\star}$ (km s ⁻¹)	4.2 ± 0.5	(7)
P_{rot} (days)	8.8 ± 0.1	(7)
S-index (MW)	0.918 ± 0.005	(7)
$\log R'_{\text{HK}}$	-4.363 ± 0.002	(7)
$\log L_X$ (erg s ⁻¹)	$28.36^{+0.16}_{-0.26}$	(7)
$\log L_X/L_{\text{bol}}$	-4.55 ± 0.25	(7)
EW_{Li} (Å)	100.0 ± 2.5	(7)
A(Li) _{NLTE}	1.67 ± 0.09	(7)

Notes. ⁽¹⁾TESS Input Catalogue v8 (Stassun et al. 2018). ⁽²⁾Two Micron All Sky Survey (2MASS, Skrutskie et al. 2006). ⁽³⁾*Gaia* DR2 (Gaia Collaboration 2018). ⁽⁴⁾*Gaia* EDR3 (Gaia Collaboration 2021a). ⁽⁵⁾Bailer-Jones et al. (2018). ⁽⁶⁾Wide-field Infrared Survey Explorer (WISE, Wright et al. 2010). ⁽⁷⁾This work.

Ti and Fe lines to derive T_{eff} (by imposing the excitation equilibrium) as well as using only Ti lines to derive $\log g_{\star}$ and ξ (by imposing the ionization equilibrium and by zeroing the trend between individual abundances and strength, or equivalent

⁴ <http://www.exoplanetes.umontreal.ca/banyan/banyansigma.php>

⁵ Updated version, available at https://www.pas.rochester.edu/~emamajek/EEM_dwarf_UBVIJHK_colors_Teff.txt

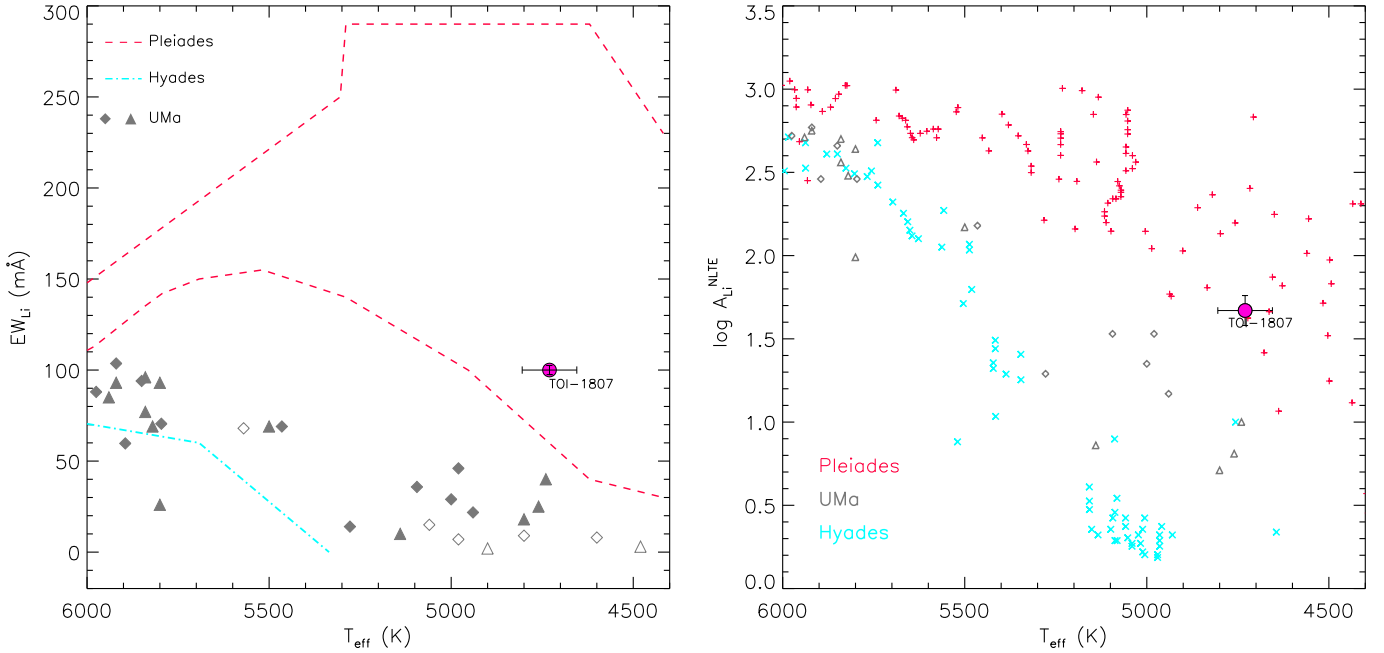


Fig. 4. *Left panel:* equivalent width of the Li I $\lambda 6707.8$ Å line plotted as a function of the spectroscopic effective temperature. The lines show the upper boundary for Hyades (dash-dotted; Sestito & Randich 2005) and the lower and upper envelopes of the Pleiades cluster (dashed; Soderblom et al. 1993a). The position of targets in the UMa group is represented by diamonds and triangles (open symbols are upper limits), as found by Ammler-von Eiff & Guenther (2009) and Soderblom et al. (1993b), respectively. *Right panel:* lithium abundance as a function of T_{eff} . Plus, diamond, triangle, and cross symbols represent the position of targets in Pleiades, UMa, and Hyades clusters, respectively, by the same authors.

width EW, of the lines, respectively). We used the driver called abfind of the code MOOG (Snedden 1973; Sobeck et al. 2011). The EWs were measured with the software ARESv2.0 (Sousa et al. 2015): we discarded lines with errors larger than 10% and with $EW > 120$ mÅ. We used 1D Local Thermodynamic Equilibrium (LTE) model atmospheres linearly interpolated from the ATLAS9 grid of Castelli & Kurucz (2003), with new opacities (ODFNEW).

As input parameters for the analysis, we used the photometric T_{eff} derived in Sect. 3.2 and we estimated the gravity from the classical equation using the *Gaia* parallaxes ($\log g_{trig}$). Initial values of ξ were derived following Dutra-Ferreira et al. (2016).

The final spectroscopic values of T_{eff} , $\log g_{\star}$, [Fe/H] and [Ti/H] derived with the new approach are reported in Table 2. We obtained a $T_{eff} = 4730 \pm 75$ K, which is 100 K cooler than the photometric temperature. Nonetheless, our spectroscopic T_{eff} was confirmed also using the standard analysis. Regarding the $\log g_{\star}$ values, the spectroscopic estimates (obtained with both methods) are slightly smaller than the input estimates obtained from the *Gaia* parallaxes. The difference between the spectroscopic $\log g_{\star}$ and the input $\log g_{trig}$ is $\Delta(\log g_{\star} - \log g_{trig}) = -0.07$ dex. Such discrepancies are expected for such cool stars (see e.g. Maldonado et al. 2015). The final ξ values obtained with the new spectroscopic approach confirm the input estimates ($\xi = 0.67$ km s $^{-1}$). Overall, the star has solar [Fe/H] and [Ti/H].

3.4. Lithium content

The lithium equivalent width (EW_{Li}) at $\sim \lambda = 6707.8$ Å of TOI-1807 was estimated using three measurements performed with the IRAF⁶ task splot and its error was computed from the standard deviation of the resulting values. The lithium

⁶ <https://iraf-community.github.io/>

abundance ($\log A(Li)^{NLTE}$) was derived from the measured EW_{Li} , the spectroscopic parameters (T_{eff} , $\log g$, [Fe/H]), and using the non-LTE (NLTE) prescriptions given by Lind et al. (2009). Errors in $\log n(Li)$ were estimated considering the errors in the EW_{Li} measurement and quadratically adding the uncertainties on spectroscopic parameters. The values of EW_{Li} and $\log A(Li)^{NLTE}$ are reported in Table 2 and plotted in Fig. 4 as a function of effective temperature: TOI-1807 seems to be close to the lower envelope of the Pleiades cluster.

3.5. Coronal and chromospheric activity

The chromospheric activity was measured on the HARPS-N spectra following the dedicated tool implemented in the YABI environment. The procedure mirrors that developed for HARPS spectra (Lovis et al. 2011). The S-index tabulated in Table 2 is then calibrated in the M. Wilson scale (Baliunas et al. 1995). The value $\log R'_{HK} = -4.36$ is intermediate between Hyades and Pleiades.

We also searched for X-ray emission on ROSAT and other public X-ray catalogs. TOI-1807 has X-ray detection (source 1RXS J132508.6+385517) within ~ 8.1 arcsec from the optical position on ROSAT Faint Source Catalog (Voges et al. 2000). The corresponding $RX = \log L_X/L_{bol} = -4.55$ is in agreement with that of the Hyades members of similar color (Desidera et al. 2015).

3.6. Projected rotational velocity

We derived the projected rotational velocity $v \sin i_{\star}$ through spectral synthesis of two wavelength regions around 6200 and 6700 Å and fixing the macro-turbulence velocity (v_{macro}), as previously done by our team (see, e.g., Barbato et al. 2020, and references therein). Using the same grid of model atmospheres and codes as those considered to derive the stellar atmospheric

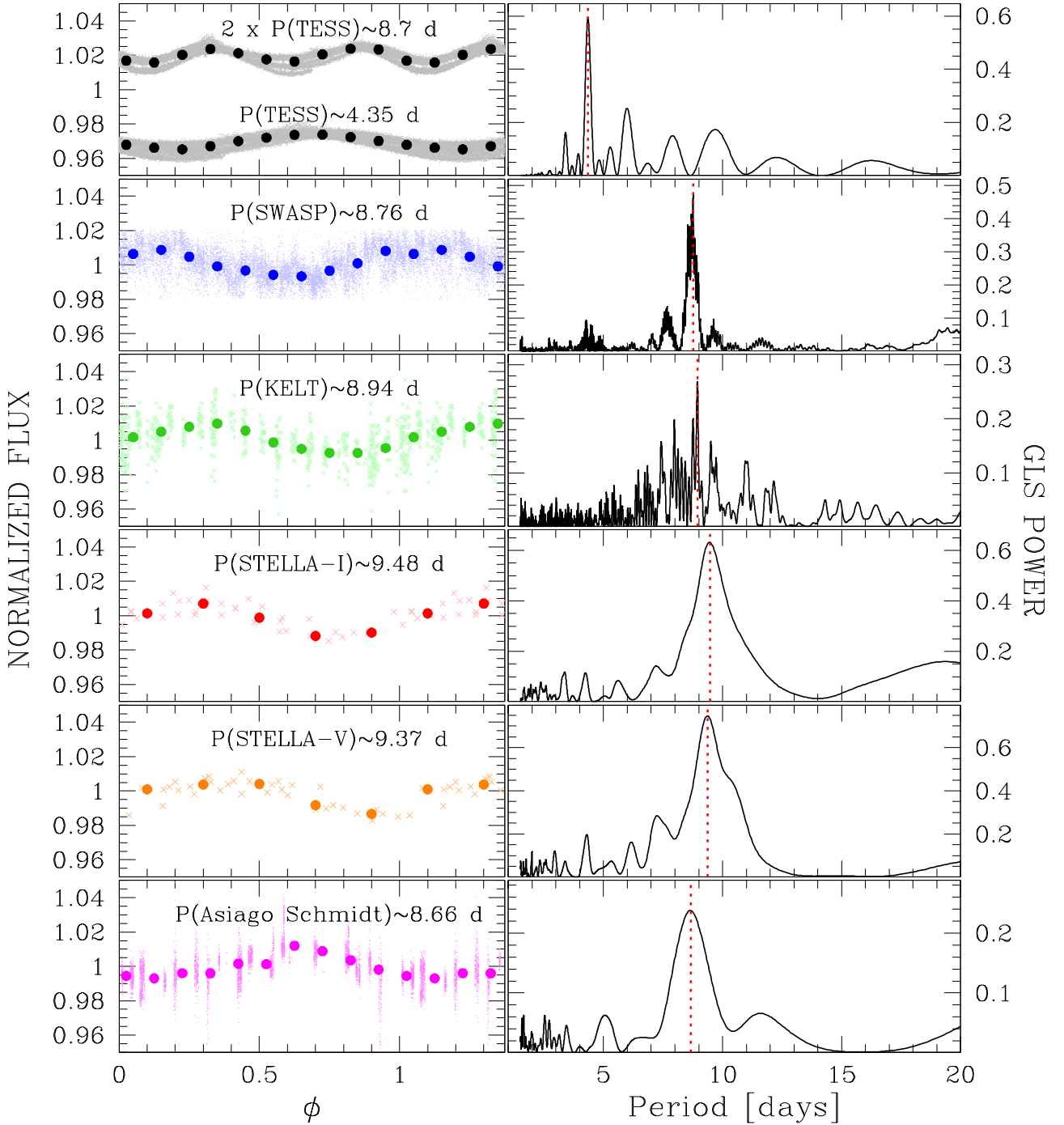


Fig. 5. Analysis of the light curves of TOI-1807 obtained with ground-based telescopes and TESS. *Left panels:* phased light curves obtained with SuperWASP (blue), KELT (green), TESS (gray), Asiago Schmidt 67/92 cm Telescope (magenta), and STELLA (red and orange for *I*- and *V*-band, respectively) by using the periods found by GLS. *Right panels:* GLS periodograms obtained from the corresponding light curves in the left panels; the red dashed line indicates the period of the peak.

parameters in Sect. 3.3 and fixing v_{macro} at the value of 1.6 km s^{-1} from the relations by Brewer et al. (2016), we found a rotational velocity of $v \sin i_{\star} = 4.2 \pm 0.5 \text{ km s}^{-1}$ (see Table 2).

3.7. Rotation and activity

3.7.1. Rotation from light curves

We used a ground-based photometric series and TESS light curves to obtain a first guess estimate of the rotation period

of TOI-1807. In order to identify the best rotation period, we extracted the Generalized Lomb-Scargle (GLS) periodograms (Zechmeister & Kürster 2009) of the light curves and we identified the period associated with the most powerful peak in the periodogram and the associated power (P_w).

We used the light curves of TOI-1807 obtained with SuperWASP, KELT, STELLA, Asiago Schmidt 67/92 cm and TESS surveys. In the case of SuperWASP we measured a single strong peak in the periodogram ($P_w \sim 0.47$) at $P = 8.7633 \pm 0.0004$ days. From the KELT light curve we obtained a period

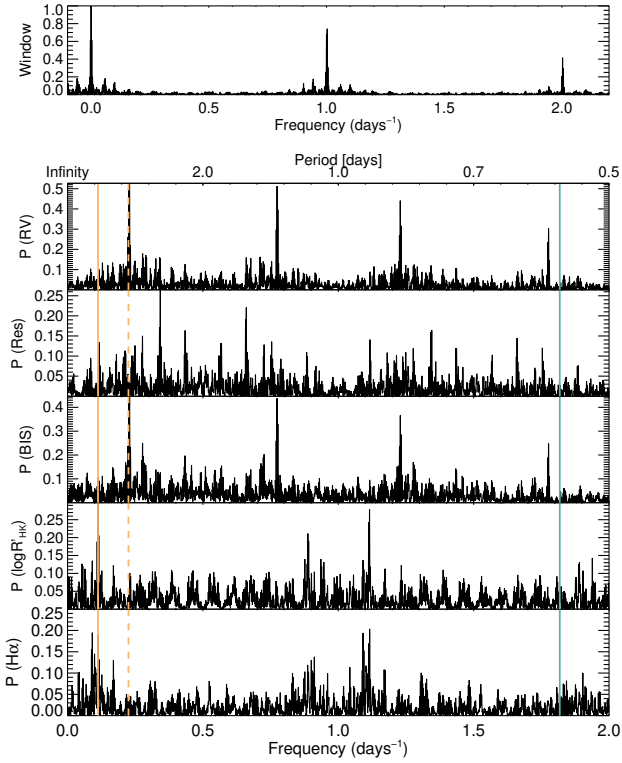


Fig. 6. GLS periodograms of the spectroscopic time series from HARPS-N data. The window function is depicted on the top panel while the periodograms of the RVs, the corresponding residuals, the bisector, the $\log R'_{\text{HK}}$ and the $\text{H}\alpha$ time series are reported in the following panels. The orange vertical lines represent the location of the rotation period (solid) and its first harmonic (dashed), while the cyan solid line indicates the position of the planet orbital period.

$P = 8.945 \pm 0.006$ day ($Pw \sim 0.27$). We measured the rotation period of TOI-1807 from the V - and I -band observations obtained with STELLA, finding a single strong peak ($Pw \sim 0.75$) at $P = 9.37 \pm 0.11$ days and $P = 9.48 \pm 0.16$; however, we highlight that the small number of points (35–36) spread out on 54 days can bias the detection of the real rotation period. Using the light curve obtained with the Asiago Schmidt 67/92 cm telescope, we found a peak in the periodogram at $P = 8.66 \pm 0.04$ days ($Pw \sim 0.24$). Finally, we measured the rotation period from the TESS light curve, obtaining a period $P = 4.350 \pm 0.001$ days ($Pw \sim 0.60$); in any case, looking the light curve and to its features, it appears more likely that the period is twice the detected one, namely, $P \sim 8.7$ days, in correspondence with the first harmonic in the periodogram ($Pw \sim 0.35$) and in agreement with the other measurements. Indeed the light curve is a double dip, that is, a variability that is due to the presence of spots that rotate on opposite sides of the star. Figure 5 shows the phased light curves of TOI-1807 obtained with the different instruments and the periodograms associated with them.

3.7.2. Frequency analysis of the HARPS-N data and stellar activity

We evaluated the GLS periodogram for the HARPS-N time series described in Sect. 2.6, aiming to obtain the activity-related periodicities. Figure 6 shows the window function of our sampling and the periodograms of the RVs, the corresponding residuals after removing the most prominent signal, and the spectroscopic activity indices. The GLS of both the RVs and BIS shows a very well defined and isolated peak at the first

harmonic of the rotation period (4.36 days, dashed orange line), while the GLS of both the $\log R'_{\text{HK}}$ and $\text{H}\alpha$ shows a periodicity of 8.8 days, in agreement with the photometric time series and the adopted rotation period (solid orange line). The periodicities at the first and the second harmonic are expected when the RV variations are dominated by the flux perturbations due to dark spots (Winn et al. 2018; Boisse et al. 2011). We removed a sinusoidal model from the RVs and obtained the GLS of the RV residuals (second panel of the second block of periodograms). Besides a marginal signal at 8.8 days, we found a large periodicity at 2.9 days, corresponding to the second harmonic of the rotation period. The high level of the stellar activity of our target is then well represented in the GLS periodograms. The rotational frequency $f_{\text{rot}} = 1/8.7$ day = 0.12 day $^{-1}$ generates an alias at $2 - f_{\text{rot}} = 1.88$ day $^{-1}$, close to the expected orbital frequency $f_{\text{orb}} = 1/0.55$ day = 1.82 day $^{-1}$. The two peaks should be clearly separated thanks to the very long time baseline of our monitoring, but the stellar activity strongly increases the noise level (up to 4 m s $^{-1}$) around f_{orb} . Therefore, no peak can be seen at the orbital frequency of the planet (cyan solid line).

3.7.3. Rotation period from $\log R'_{\text{HK}}$

In Sects. 3.7.1 and 3.7.2, we obtained, in the periodograms of the large part of the analyzed time series, a peak corresponding to a rotation period between 8.7 and 8.9 days. However, the analysis of the GLS periodograms of the TESS light curve, the RVs and BIS show a strong peak at ~ 4.35 days. In order to confirm that the real rotation period of TOI-1807 is $P_{\text{rot}} = 8.8 \pm 0.1$ days, we calculated the expected rotation period by using the equation and the coefficients for K stars reported by Suárez Mascareño et al. (2016) and the value of $\log R'_{\text{HK}}$ calculated in Sect. 3.5. We obtained a result of $P_{\text{rot}} = 8.7 \pm 1.2$ days, in agreement with the period of ~ 8.8 days found in this work for TOI-1807.

3.8. Stellar age, radius, and mass

3.8.1. Stellar age

In order to determine the stellar age of TOI-1807, we followed the approach of Desidera et al. (2015), combining the results of several indirect methods (rotation, chromospheric emission, coronal emission, and lithium content) and identification of comoving and coeval members (Appendix B). Isochrone fitting does not provide significant age constraints in this case.

The indicators agree quite consistently on an age intermediate between Pleiades and Hyades (125 Myr and 625 Myr, respectively), although the Li EW of TOI-1807 is close to the lower envelope of Pleiades members. The rotation period vs color for TOI-1807, TOI-2076 and the other comoving objects (see Fig. 7) matches well the sequence of Group X recently obtained by Messina et al. (2022). Group X is a sparse association overlapping on the sky with the Coma Ber open cluster, but with distinct kinematics and age. Messina et al. (2022) derived an age of 300 ± 60 Myr for this group, considering both the rotation sequence and isochrone fitting of turn-off members, making it an ideal reference for objects with age intermediate between Hyades and Pleiades. From the overall similitude to Group X age, we adopted 300 ± 80 Myr for TOI-1807.

3.8.2. Stellar mass, radius, and luminosity

Stellar luminosity and radius were derived as in Carleo et al. (2020), exploiting Stefan-Boltzmann law and Pecaut & Mamajek (2013) tables (updated version 2021.03.02) and adopting the

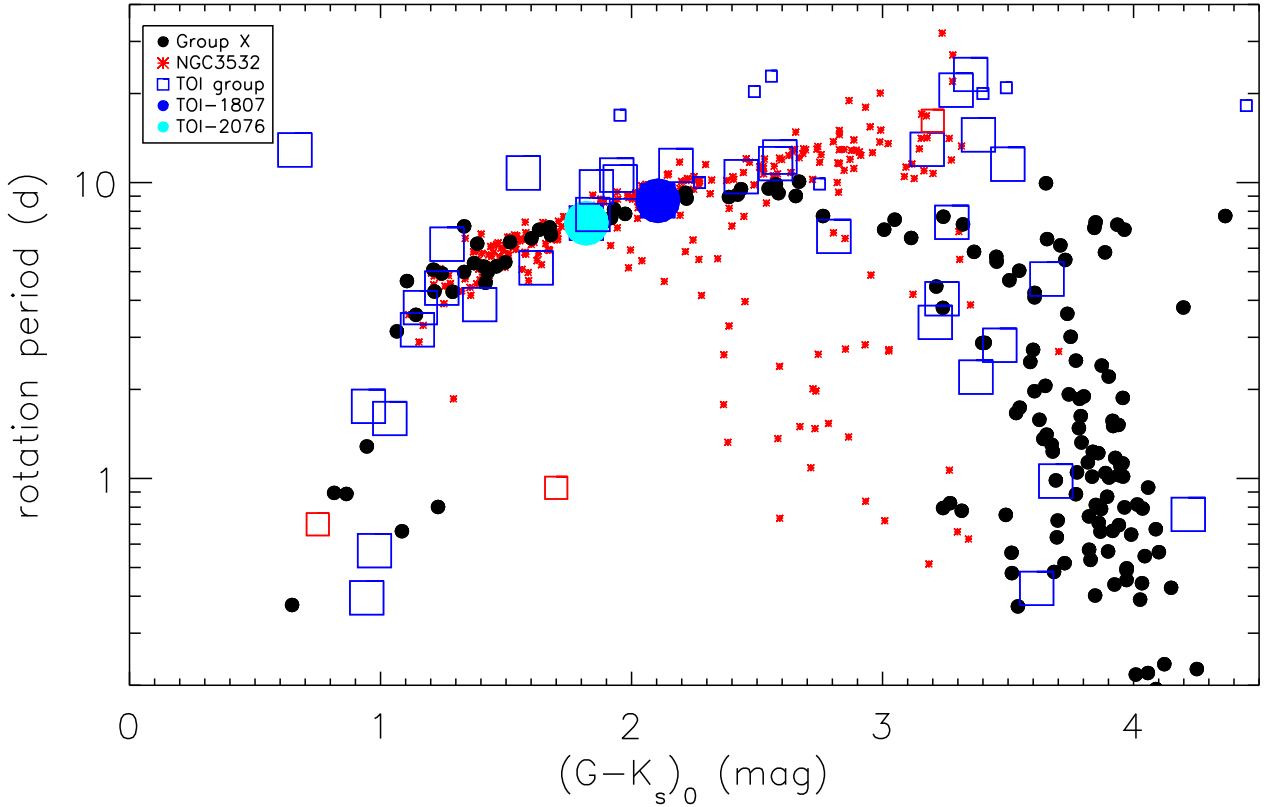


Fig. 7. Rotation period distribution of members of Group X (black points) and NGC 3532 (red starred points) with a quoted age of 300 Myr and of the wide companions and comoving stars identified in this study (blue squares). Big bullets indicate TOI-1807 and TOI-2076. Small squares are used to indicate grade B rotation periods, whereas the three red squares are periods from the literature (see Appendix B).

spectroscopic T_{eff} . The stellar radius results of $0.690 \pm 0.036 R_{\odot}$ and the luminosity $0.215 \pm 0.016 L_{\odot}$. For the stellar mass we exploited the PARAM (da Silva et al. 2006) Bayesian interface⁷, selecting the range of ages allowed by indirect methods. A stellar mass of $0.76 \pm 0.03 M_{\odot}$ is derived. These values are used as priors in the transit fitting, where stellar density is derived again.

3.9. System inclination

Coupling the rotation period from Sect. 3.7, and the stellar radius from Sect. 3.8.2, an equatorial velocity of $4.0 \pm 0.2 \text{ km s}^{-1}$ is derived. This is fully compatible with the observed $v \sin i_{\star}$ from Sect. 3.6 ($4.2 \pm 0.5 \text{ km s}^{-1}$), and suggesting that the star is seen very close to equator-on and that likely the stellar rotation and planetary orbit are aligned.

4. Planet detection and vetting

The candidate exoplanet orbiting the star TOI-1807 has been identified by the TESS official pipelines. In particular, the Science Processing Operations Center (SPOC) pipeline (Jenkins et al. 2016) detected one candidate ultra-short period exoplanet around TOI-1807 ($P \sim 0.55$ day). The planetary nature of the object has also been confirmed by Hedges et al. (2021).

We used the short-cadence light curve corrected by us to further confirm the candidate exoplanet. In order to detect the transit signals, we followed the procedure adopted by Nardiello et al. (2020). In brief, we modeled and removed the variability of the star interpolating to the light curve a fifth-order spline defined

⁷ http://stev.oapd.inaf.it/cgi-bin/param_1.3

over a grid of N_{knots} knots at intervals of 13-h. We removed bad quality measurements clipping away all the points of the light curve above 4σ and below 20σ the mean value of the flattened light curve. We extracted the Transit Least Squares (TLS) periodograms (Hippke & Heller 2019) of the flattened light curve, searching for transit signals with periods between 0.5 day and $T_{\text{LC}}/2$, where T_{LC} is the maximum temporal interval covered by the light curve. We confirmed the presence of one periodic signal of period $P_b \sim 0.549$ day (with a signal detection efficiency, SDE ~ 30). The position of the transits and the folded light curve of this candidate are shown in panels a and c of Fig. 8, respectively. We also looked for other transiting exoplanets in the TESS light curve as follows: we removed the transits of TOI-1807 b from the light curve and extracted again the TLS periodogram of the light curve searching for transit signals with periods between 1.0 day and $T_{\text{LC}}/2$. We obtained a (weak) peak in the periodogram at ~ 24.986 days, corresponding to a very low SDE ~ 5 . From a visual inspection of the phased light curve, we did not see any transit feature. Also after inspecting the entire light curve looking for single transits, we did not detect any presence of a second transiting exoplanet around TOI-1807 in the TESS light curve of Sectors 22 and 23.

TOI-1807 is an isolated star with few very faint neighbor stars. However, we performed a series of vetting tests to check if the transit signals belong to the star subject of our study or are due to contamination or systematic effects. By using the long-cadence light curves, for which we have photometries extracted with five different photometric methods, we checked if the transit depths vary changing the aperture. As demonstrated in panel a of Fig. 9, there is no dependence of the transit depth on the

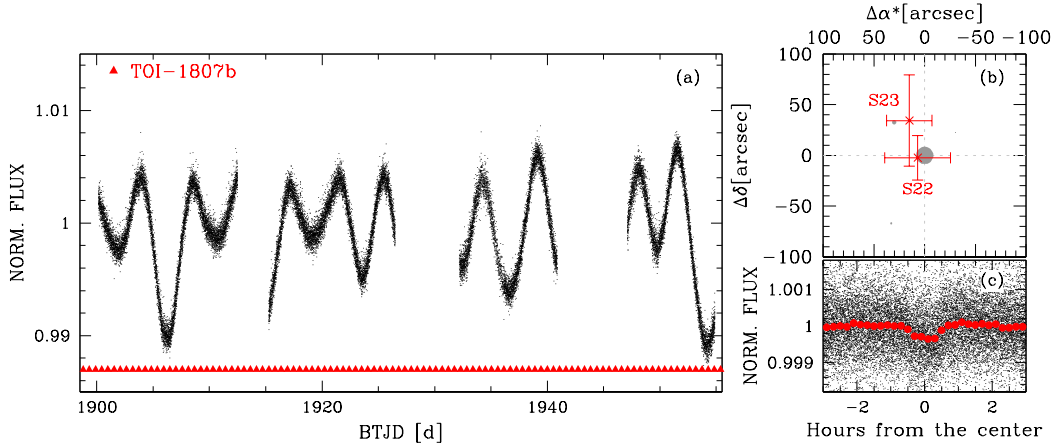


Fig. 8. Overview of some validation tests of TOI-1807 b. *Panel a* shows the flux normalized short-cadence light curve of TOI-1807; red triangles indicate the central time of the TOI-1807 b’s transits. *Panel b* illustrates the in- or out-of-transit centroid test, for sectors 22 and 23; within the errors, the transits are associated with the central star. *Panel c* is the flattened light curve, folded with the period of TOI-1807 b (~ 0.549 day).

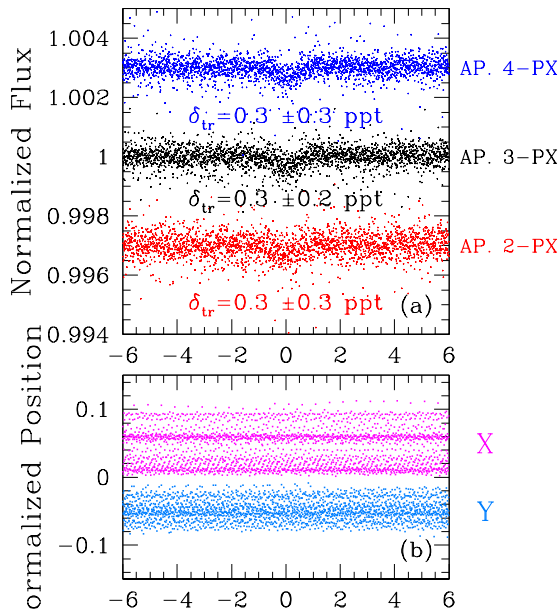


Fig. 9. Two validation tests for confirming the planetary nature of the transits. *Panel a* shows the phased long-cadence, flattened light curves of TOI-1807 obtained with different photometric apertures (2-pixel in red, 3-pixel in black, and 4-pixel in blue). The mean transit depth (δ_{tr} , in parts-per-thousand, ppt) is the same in all the cases within the errors. *Panel b* shows the normalized position X/Y folded with the period found for TOI-1807 b. No particular features correspond to the transit events.

photometric aperture⁸. We also confirm that there is no correlation between the (X,Y)-positions of the star (measured with PSF-fitting on FFIs) during the photometric series and the transit signals (see panel b of Fig. 9). We checked the mean depths of odd and even transits, finding that, within the errors, all the transits have the same depth. Finally, we performed an analysis of the in- or out-of-transit centroid to be sure that the transits are not due to contaminant neighbors. For a detailed description of this analysis we refer the reader to Nardiello et al. (2020) and

⁸ For this test we excluded PSF-fitting and 1-pixel aperture photometries (that work better for stars with $T > 12$) because the light curves extracted with these techniques show scatters larger than the transit depths.

Nardiello (2020). The results are reported in panel b of Fig. 8: within the errors, the in- or out-of-transit mean centroids, calculated for each sector, are in agreement with the position of our target star.

5. Properties of the planetary system TOI-1807

We used PyORBIT⁹ (Malavolta 2016; Malavolta et al. 2016, 2018) to model both the stellar activity and the planetary signal in both the TESS light curve and the RV series. PyORBIT is a package for modeling planetary transits and radial velocities, taking also into account the effects of stellar activity. It is mainly based on the combined use of the optimization algorithm PyDE¹⁰ (Storn & Price 1997) and the affine invariant Markov chain Monte Carlo (MCMC) sampler emcee (Foreman-Mackey et al. 2013). For this analysis, we first attempted to retrieve the semi-amplitude of the planet by applying the floating chunk offset method (Hatzes 2014); however, the prominent stellar activity prevented a precise detection of the planetary signal, despite our dedicated observational strategy. An attempt to substitute the nightly offset with a nightly linear trend (considering only the nights with at least three observations) did not end in success either. We therefore tested several approaches to model stellar activity though the use of Gaussian processes (GP, Rasmussen & Williams 2006; Haywood et al. 2014), characterized by different forms for the model covariance function (or kernel) and different combination of data sets to constraint the GP hyper-parameters, and considering different planetary system architectures (one or more planets). In this manuscript, we report the three most significant cases: (i) Case 1: Single planet system and activity modeling trained on photometry; (ii) Case 2: Single planet system and activity modeling trained on spectroscopy; (iii) Case 3: Two-planet system.

These three cases are described in the following sections.

5.1. Case 1: Single planet system and activity modeling trained on photometry

First, we tested the model of a planetary system formed by only the transiting USP TOI-1807 b. For this case, we considered both the photometric and the spectroscopic observations to constrain all the planet parameters.

⁹ <https://github.com/LucaMalavolta/PyORBIT>

¹⁰ <https://github.com/hpparvi/PyDE>

Simultaneously to the activity, PyORBIT modeled the signals of TOI-1807 b both in the light curve and in the RV series. The parameters of the host star, such as the stellar radius (R_\star) and mass (M_\star), effective temperature (T_{eff}), and gravity ($\log g$), come from the analysis performed in Sect. 3. For the transit modeling, we included the central time of the first transit ($T_{0,b}$), the orbital period (P_b), the impact parameter (b_b), the planetary-to-stellar-radius ratio ($R_{p,b}/R_\star$), and the stellar density (ρ_\star). On the basis of the $\log g$ and T_{eff} , we calculated the limb darkening (LD) coefficients by using the grid of values reported by Claret (2018), adopting the LD parametrization by Kipping (2013), and we used them as priors of the fitting¹¹. Transit modeling was carried out by using the package batman (Kreidberg 2015) and taking into account the 2-min cadence of TESS data (Kipping 2010). For the RV modeling, we included the RV semi-amplitude $K_{\star,b}$ and we considered a circular orbit ($e = 0$, a legitimate choice for an USP planet). Uniform priors on P_b and $T_{0,b}$ and a Gaussian prior on ρ_\star were used in the model procedure.

Since the periodogram of the RV variations analyzed in Sect. 3.7.2 suggests that the activity-induced variations are dominated by the flux effect (Lanza et al. 2010), we began our analysis by considering the photometric variations as a proxy for those RV intrinsic variations. We modeled the stellar activity in the light curve, in the RV, and in the $\log R'_{\text{HK}}$ series simultaneously, through Gaussian process (GP) regression. We employed two different kernels having in common the value of the stellar rotation period P_{rot} . For the RV and $\log R'_{\text{HK}}$ series we used a quasi-periodic kernel as defined by Grunblatt et al. (2015), setting the characteristics decay time scale P_{dec} , the coherence scale w , and the amplitudes of the covariance matrix h_{RV} and h_{act} as the hyper-parameters. GP regression was performed with the package george (Ambikasaran et al. 2015) for the RV and $\log R'_{\text{HK}}$ data-sets, and the package celerite2 (Foreman-Mackey et al. 2017; Foreman-Mackey 2018) for the light curve. Activity in the light curve was treated with a stochastically driven, damped harmonic oscillator term (SHOTerm) to model the stellar granulation, together with a combination of two SHOTerms at the rotation period and its first harmonic (RotationTerm) to model stellar rotation modulation, as proposed by Barros et al. (2020). For the granulation SHOTerm (grn) we fixed the quality factor $Q = 1/\sqrt{2}$, while leaving the undamped period of the oscillator P_{grn} and the standard deviation of the process σ_{grn} as free hyper-parameters (Foreman-Mackey et al. 2017); for the RotationTerm we left as free hyper-parameters the quality factor for the secondary oscillation $Q_{0,\text{rot}}$, the difference between the quality factors of the first and the second modes ΔQ_{rot} , the fractional amplitude of the secondary mode compared to the primary $f_{\text{rot}}^{\text{mix}}$, and the standard deviation of the process σ_{rot} , while the rotation period P_{rot} is in common with the quasi-periodic kernel (David et al. 2019; Gillen et al. 2020). A uniform prior on the rotation period P_{rot} was assigned on the basis of the analysis performed in Sect. 3.7¹². All the priors adopted for planet and activity modeling are reported in Table 3. We employed $8n_{\text{dim}}$ walkers for the chains, with n_{dim} being the dimensionality of the model. We ran the sampler with the standard ensemble method from Goodman & Weare (2010) for 200 000 steps (excluding the first 20 000 as burn-in) and using a thinning factor of 100 to reduce the effect of the chain auto-correlation. According to the Gelman-Rubin statistics (Gelman & Rubin 1992) and

¹¹ We also tested the case with no priors on LD parameters, finding no differences on the final planet parameters obtained.

¹² We also tested the modeling of the spectroscopic series only, while using larger uniform priors $\mathcal{U}(1.0, 100.0)$ days, obtaining the same results described in the paper.

auto-correlation analysis of the chains (see Lacedelli et al. 2021 for more details), convergence was always reached well before the (conservative) number of steps chosen as burn-in. The same sampler configuration and methodology has been applied to all the following instances of emcee, unless explicitly stated otherwise.

Figure 10 shows the results obtained for the modeling of the activity both in the photometric (panel a) and in spectroscopic series (panels b and c). We obtained a rotation period of $P_{\text{rot}} = 8.83 \pm 0.08$ days. The results of the modeling are reported in Table 3, while Fig. 11 shows an overview of the planet modeling after the subtraction of the activity signals from the light and RV curves. The resulting semi-amplitude K_b is about 2.4 m s^{-1} only, and this explains why it cannot be seen in the noisy RV periodogram of the original data (Fig. 6, see also discussion in Sect. 3.7.2).

5.2. Case 2: Single planet system and activity modeling trained on spectroscopy

In the second case, we modeled stellar activity through the multi-dimensional GP framework developed by Rajpaul et al. (2015), re-implemented in PyORBIT following the prescription in the paper (see also Barragán et al. 2022a). Given the high computational cost of this approach, we modeled only the spectroscopic data-sets, namely, RV, $\log R'_{\text{HK}}$, and BIS series, following the same name conventions as in Rajpaul et al. (2015). Also in this case we assumed a circular orbit for the USP planet. We assigned Gaussian priors on the orbital period and central time of transit of TOI-1807 b based on the results of Case 1¹³, and uniform priors to all the other parameters, including the rotation period P_{rot} . We ran the sampler for 100 000 steps, considering the first 25 000 as burn-in, and using a thinning factor of 200. The results of the modeling are reported in Fig. 12 and in Table 4. The true mass of the planet has been derived by taking into account the uncertainty on the stellar mass and the inclination distribution obtained from Case 1. We found that stellar activity and planet parameters values are in agreement with those found in case 1; however, the error on the RV semi-amplitude K_b is slightly smaller than the error found in case 1 ($\sim 38 \text{ cm s}^{-1}$ versus $\sim 45 \text{ cm s}^{-1}$), highlighting again the advantages of this approach on young and intermediate-age stars (e.g., Barragán et al. 2019). We noted that the residuals of the fit of the $\log R'_{\text{HK}}$ series shown in panel b of Fig. 12 present some significant variations and that the model does not fit perfectly the data. This problem has been already highlighted by Barragán et al. (2022b), and it could be ascribed to instrumental systematics or second-order astrophysical effects not included in the model.

Besides the multi-dimensional GP framework, we tested other three approaches for the modeling of stellar activity, all involving the use of Gaussian processes trained on spectral indexes only: a quasi-periodic kernel as the one of Scenario 1; a GP framework-like approach where the quasi-periodic kernel and its first derivative are employed for the RV and the BIS data-sets, but covariance matrices of each data-set are computed independently, that is, only the hyper-parameters are shared rather than assuming a single underlying GP; a quasi-periodic with cosine kernel as introduced by Perger et al. (2021). Priors on planetary parameters and MCMC settings were the same as the GP framework analysis. The use of different models for the

¹³ As these parameters are constrained by photometry, it is legitimate to use the results of the previous analysis as priors even if the RV and $\log R'_{\text{HK}}$ data-sets are in common.

Table 3. Priors and results of the model of planet b from the combined analysis of the light curve and RV series (Case 1).

Stellar activity			
Parameter	Unit	Prior	Value
Common RV+log R'_{HK} +light curve			
Rotational period (P_{rot})	days	$\mathcal{U}(8.0, 10.0)$	8.83 ± 0.08
<i>Quasi-periodic kernel</i>			
Decay Timescale of activity (P_{dec})	days	$\mathcal{U}(10.0, 100.0)$	$14.3^{+1.2}_{-1.1}$
Coherence scale (w)		...	$0.26^{+0.03}_{-0.02}$
Amplitude of the RV signal	m s^{-1}	$\mathcal{U}(0.01, 1500.00)$	$25.2^{+2.6}_{-2.2}$
Uncorrelated RV jitter ($\sigma_{\text{jitter}}^{\text{RV}}$)	m s^{-1}	...	$0.69^{+0.53}_{-0.45}$
RV offset (γ^{RV})	m s^{-1}	...	-6838.3 ± 4.2
<i>SHOTterm+RotationTerm kernel</i>			
Standard deviation of the rotation	ppt	...	$5.2^{+2.0}_{-1.0}$
Granulation period	days	$\mathcal{U}(0.05, 5.00)$	$0.18^{+0.16}_{-0.06}$
Standard deviation of granulation	ppt	...	0.067 ± 0.010
Photometric jitter ($\sigma_{\text{jitter}}^{\text{LC}}$)	ppm	...	303 ± 7
Planet b			
Parameter	Unit	Prior	Value
Orbital Period (P_b)	days	$\mathcal{U}(0.549, 0.550)$	$0.549374^{+0.000010}_{-0.000013}$
Central time of the first transit ($T_{0,b}$)	BJD	$\mathcal{U}(2458899.3, 2458899.4)$	$2458899.3449^{+0.0008}_{-0.0005}$
Duration of the transit ($T_{14,b}$)	hours	...	$0.98^{+0.03}_{-0.02}$
Limb darkening (u_1)		$\mathcal{N}(0.47, 0.05)$	0.46 ± 0.05
Limb darkening (u_2)		$\mathcal{N}(0.18, 0.05)$	0.17 ± 0.05
Impact factor (b_b)		...	$0.53^{0.09}_{-0.11}$
Orbital inclination (i_b)	deg	...	82.0 ± 2.0
Orbital eccentricity (e_b)		fixed	0
Semi-major-axis-to-stellar-radius ratio ((a_b/R_\star))		...	3.8 ± 0.2
Orbital Semi-major axis (a_b)	au	...	0.0120 ± 0.0003
Planetary-to-stellar-radius ratio ($(R_{p,b}/R_\star)$)		...	0.0182 ± 0.0006
Planetary radius ($R_{p,b}$)	R_\oplus	...	1.37 ± 0.09
RV semi-amplitude (K_b)	m s^{-1}	$\mathcal{U}(0.01, 10)$	$2.39^{+0.45}_{-0.46}$
Planetary mass ($M_{p,b}$)	M_\oplus	...	2.57 ± 0.50
Planetary density (ρ_b)	ρ_\oplus	...	1.00 ± 0.29
Stellar density (ρ_\star)	ρ_\odot	$\mathcal{N}(2.3, 0.4)$	2.4 ± 0.4

stellar activity always resulted in a RV semi-amplitude of TOI-1807 b and the rotational period of the star matching well within 1σ with respect to the previous results, with error bars similar to the case of the photometrically trained GP. The only parameter showing a significant change across different GP kernels is the timescale of the decay of the active regions, which has no impact on the modeling of the USP planet.

5.3. Case 3: Search for the second planet

Armed with the knowledge that many USP planets belong to multi-planet systems, we searched for the signature of a second planet in our RV data-set. We employed the same GP activity models (as illustrated in the previous sections) and added a second planet with orbital period between 1 and 300 days in addition to the USP planet. We did not assume any circularity for the orbit of the second planet, nevertheless we imposed a Gaussian prior on e_b centered around zero and with standard deviation equal to 0.098, following Van Eylen et al. (2019). The outcome of the MCMC was initially confusing, because in all cases we obtained a significant ($>5\sigma$) detection of a planet, but with the period and semi-amplitude drastically changing depending

on the activity model employed in the analysis. Most notably, employing the GP framework resulted in a period of the additional planet extremely close to the stellar rotational period ($P_c \simeq 8.5$ days versus $P_{\text{rot}} \simeq 8.8$ days). We repeated the analysis using the dynamic nested sampling algorithm (Higson et al. 2019; Buchner 2016) implemented in the dynesty package (Speagle 2020), with the double goal of checking the posterior distributions for the parameters of the additional planet and computing the Bayesian evidence of the two-planet models with respect to the single-planet one. The analysis confirmed the presence of a marked multi-modality in the posterior of the additional planet, with contrasting results regarding the Bayesian evidence between models with the same activity treatment but different number of planets (e.g., $\Delta \ln \mathcal{Z} \approx 2$ when using a quasi-periodic with derivative kernel, $\Delta \ln \mathcal{Z} \approx 6$ when using a quasi-periodic with cosine kernel). We tentatively explain the initial detection as the keplerian absorbing part of the strong activity signal, although a detailed analysis of the behavior of the GP/Keplerian modeling is beyond the scope of this paper. We note, however, how testing different assumptions on the stellar activity and the use of different posterior samplers averted the claim of a likely false positive detection. More importantly, in all cases the posterior

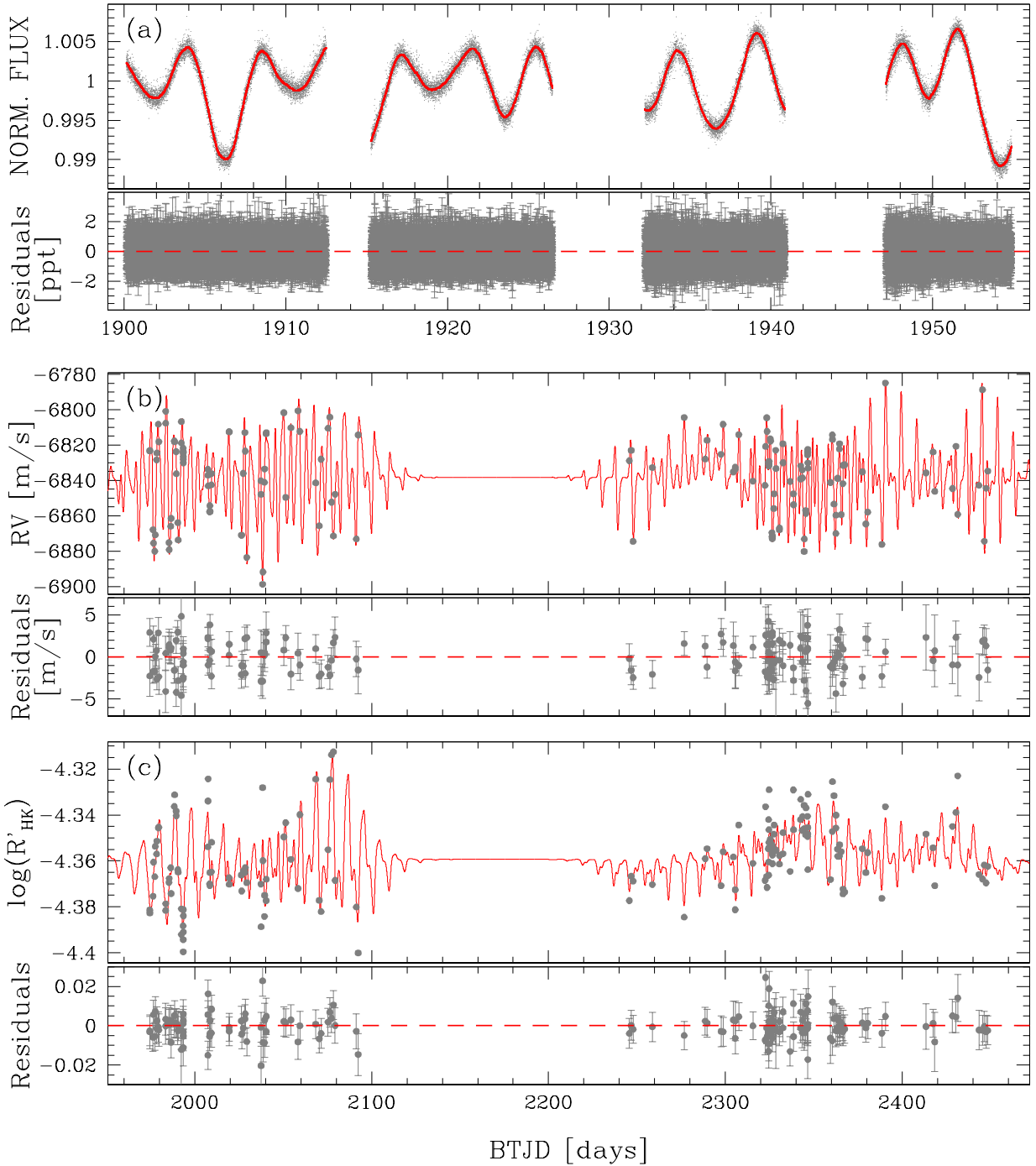


Fig. 10. Overview of the modeling of the stellar activity performed for the Case 1. *Panel a* shows the light curve (in gray) of the star obtained with TESS short cadence data; the model of the activity obtained with the GP fit is reported in red. The panel below is the plot of the residuals after the subtraction of the model to the light curve. *Panels b and c* represent the RV and $\log R'_{\text{HK}}$ series of TOI-1807 (gray points): the stellar activity models are illustrated in red, while the residuals obtained after the subtraction of the model to the observed data are reported in the plots below each panel.

distribution of the semi-amplitude of the USP planet in the two-planet model closely matched the one obtained with the corresponding single-planet model, independently of the sampler used in the analysis, thus confirming the robustness of our detection.

5.4. Expected relativistic apsidal precession of TOI-1807 b

Due to the closeness of TOI-1807 b to its hosting star, it is reasonable to ask whether some general relativistic effects are

expected¹⁴. If we compare the case of this planet to the well-studied case of Mercury (whose measured apsidal line precession led to a confirmation of the validity of General relativity), we see that TOI-1807 b actually orbits in a regime of stronger gravitational field than Mercury does. Indeed, the ratio of its pericenter to the Schwarzschild radius (r_S) of its hosting star divided by the same quantity for Mercury is ≈ 0.05 , so if for

¹⁴ Special relativity can be ruled out because, even if the planet orbits very fast, $\beta = v/c \approx 7.93 \times 10^{-4}$.

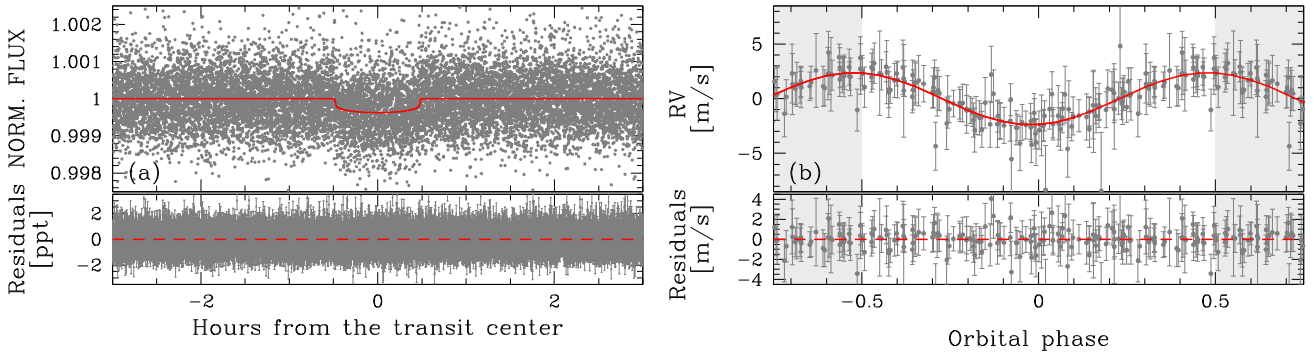


Fig. 11. Photometric and RV modeling of TOI-1807 b planetary signal obtained in Case 1. *Panel a* shows the folded transits in the light curve of TOI-1807 after the subtraction of the stellar activity signal, and the model of the transits (red line). In the panel below, the residuals of the light curve after the subtraction of the planetary transit model. *Panel b* shows the RV curve of the star after removing the stellar activity contribution, phased with the period of TOI-1807 b; the red line represents the model used to measure the RV semi-amplitude of the curve. The region between the two gray shaded areas corresponds to one orbital phase. In the panel below the RV residuals after model subtraction are shown.

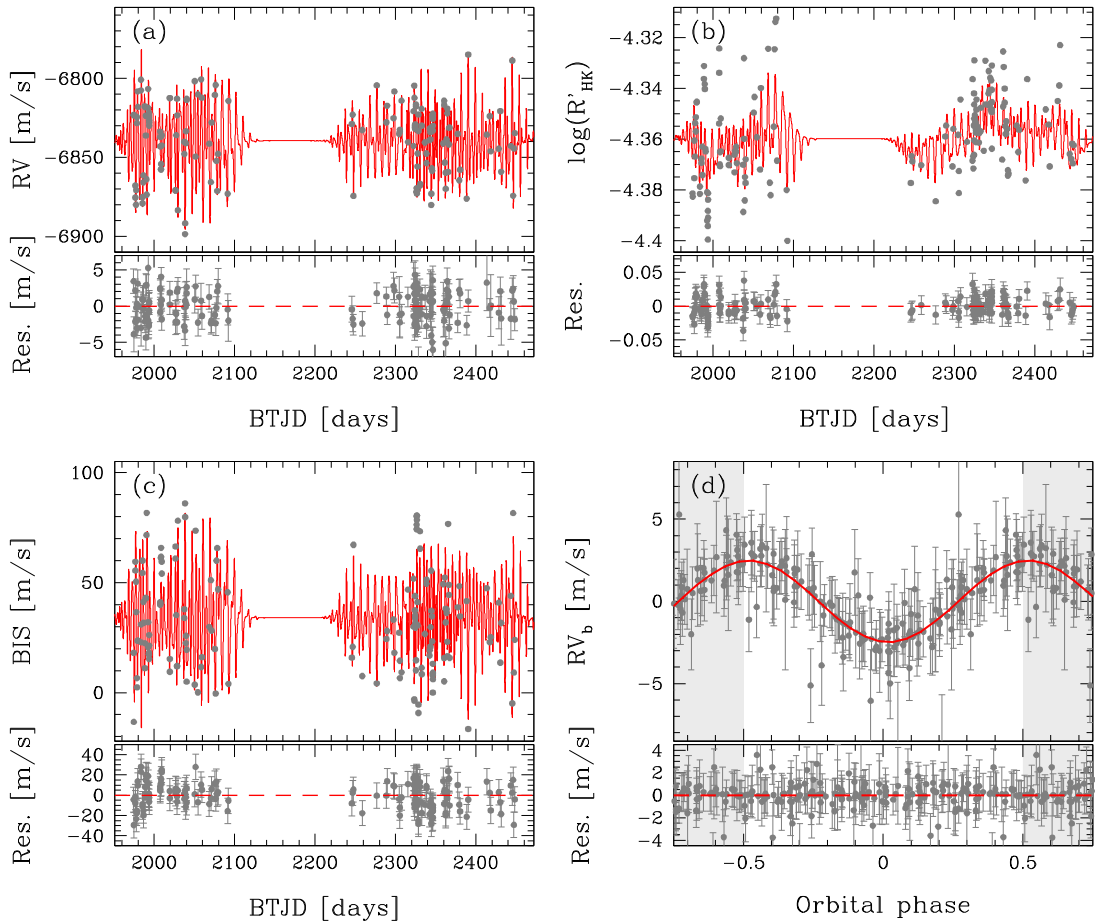


Fig. 12. Overview of the activity+planet modeling in the spectroscopic series obtained in case 2. *Panels a, b, and c* show the RV, $\log R'_{\text{HK}}$, and BIS series, respectively (gray points). Red lines represent the models of the stellar activity obtained in the GP framework we used. The panels below report the difference between the observed points and the stellar activity models. *Panel d* shows the RV curve of the star after the subtraction of the stellar activity and phased with the period of TOI-1807 b; model of the RV series is reported in red; the region between the two gray shaded areas corresponds to one orbital phase.

Mercury General Relativity matters, this is a fortiori true also for TOI-1807 b.

Adopting the data of Tables 2 and 4 for the hosting star and planet, respectively, we calculated the expected 1st order general relativistic precession of TOI-1807 b and compared it to the semi-major axis precession of planet Mercury, which is $\delta\varphi_{\text{Mer}} \sim 0.1$ arcsec per period.

We calculated the $\delta\varphi$ of TOI-1807 b by using the formula:

$$\delta\varphi = \delta\varphi_{\text{Mer}} \frac{M_{\star} + M_{\text{P,b}}}{M_{\odot} + M_{\text{Mer}}} \frac{a_{\text{Mer}} (1 - e_{\text{Mer}}^2)}{a_{\text{b}}}, \quad (1)$$

where M_{\star} , $M_{\text{P,b}}$ and a_{b} indicate the mass of the hosting star BD+39 2643 and the mass and semi-major axis of the hosted

Table 4. Priors and results of the model of planet b from the analysis of spectroscopic series with GP framework (Case 2).

GP framework parameters			
Parameter	Unit	Prior	Value
Uncorrelated RV jitter ($\sigma_{\text{jitter},0}^{\text{RV}}$)	m s ⁻¹	...	0.79 ^{+0.51} _{-0.49}
RV offset (γ_0^{RV})	m s ⁻¹	...	-6839.6 ± 1.1
Uncorrelated BIS jitter ($\sigma_{\text{jitter},0}^{\text{BIS}}$)	m s ⁻¹	...	12.30 ^{+0.83} _{-0.76}
BIS offset (γ_0^{BIS})	m s ⁻¹	...	34.0 ± 1.4
Uncorrelated log R'_{HK} jitter ($\sigma_{\text{jitter},0}^{\log R'_{\text{HK}}}$)	0.0132 ^{+0.0010} _{-0.0009}
log R'_{HK} offset ($\gamma_0^{\log R'_{\text{HK}}}$)	-4.360 ± 0.003
V_c	m s ⁻¹	...	1.2 ^{+1.9} _{-1.9}
V_r	m s ⁻¹	...	27.8 ^{+4.3} _{-3.4}
B_c	m s ⁻¹	...	-1.9 ^{+1.7} _{-1.8}
B_r	m s ⁻¹	...	-23.8 ^{+3.2} _{-3.9}
L_c	-0.0110 ^{+0.0019} _{-0.0020}
Stellar activity			
Parameter	Unit	Prior	Value
Rotational period (P_{rot})	days	$\mathcal{U}(8.0, 9.5)$	8.84 ± 0.08
Decay Timescale of activity (P_{dec})	days	$\mathcal{U}(10.0, 1000.0)$	12.85 ^{+1.15} _{-1.12}
Coherence scale (w)	...	$\mathcal{U}(0.01, 0.60)$	0.43 ^{+0.04} _{-0.04}
Planet b			
Parameter	Unit	Prior	Value
Orbital Period (P_b)	days	$\mathcal{N}(0.549374, 0.00002)$	0.549380 ^{+0.000015} _{-0.000016}
Central time of the first transit ($T_{0,b}$)	BJD	$\mathcal{N}(2458899.3449, 0.0008)$	2458899.3449 ^{+0.0008} _{-0.0008}
Orbital eccentricity (e_b)	...	fixed	0
Semi-major-axis-to-stellar-radius ratio ((a_b/R_\star))	3.7 ± 0.2
Orbital Semi-major axis (a_b)	au	...	0.0120 ± 0.0002
RV semi-amplitude (K_b)	m s ⁻¹	$\mathcal{U}(0.01, 10)$	2.48 ^{+0.38} _{-0.39}
Planetary mass ($M_{\text{P},b}, i = 82 \pm 2$ deg)	M_\oplus	...	2.67 ± 0.43
Planetary density (ρ_b)	ρ_\oplus	...	1.04 ± 0.28

TOI-1807 b planet (e_b is assumed zero, see Table 4), respectively, while M_{Mer} , a_{Mer} , and e_{Mer} refer to the mass, the semi-major axis and orbital eccentricity of Mercury, respectively. We obtained $\delta\varphi \simeq 2.35\delta\varphi_{\text{Mer}} \simeq 0.23$ arcsec per orbit, which is a significantly large value. On the other side, gravitational redshift z_b of the TOI-1807 b planet would be impossible to detect, being the ratio:

$$\frac{1 + z_b}{1 + z_{\text{Mer}}} = \frac{\sqrt{1 - (r/r_S)_{\text{Mer}}}}{\sqrt{1 - (r/r_S)_b}} \sim 1.000000065, \quad (2)$$

that is, having evaluated Mercury's r/r_S at pericenter, TOI-1807 b shows almost the same very small gravitational redshift of Mercury around the Sun.

6. Discussion and conclusions

In this work we confirmed the planetary nature and presented the characterization of the youngest USP planet discovered so far, TOI-1807 b, detected in the TESS light curve of the active K dwarf star BD+39 2643.

We derived the properties of the host star (effective temperature, mass, radius, lithium content, etc.) and we analyzed its activity by using ground-based photometric and spectroscopic

observations; in this way we also obtained a first estimate of the rotation period of the star ($P_{\text{rot}} \sim 8.8$ days). We identified all the stars comoving with TOI-1807 (and TOI-2076) and, through a gyrochronological analysis performed by using TESS light curves and literature results, we obtained an age of 300 ± 80 Myr for TOI-1807.

Combining the light curves obtained with TESS in two sectors with the exquisite spectroscopic data-set collected with HARPS-N at TNG (161 measurements over 2 yr, collected with a USP-specific observational strategy), we modeled the activity of the star by using a GP approach. We considered different approaches for the modeling of the stellar activity: the first trained on photometry (case 1) and the second trained on spectroscopy (case 2). In the two cases, we obtained measurements of the stellar rotation in agreement, that is: $P_{\text{rot}} = 8.83 \pm 0.08$ days and $P_{\text{rot}} = 8.84 \pm 0.08$ days for cases 1 and 2, respectively. The results of the stellar activity modeling are reported in Tables 3 and 4 and illustrated in Figs. 10 and 12.

Simultaneously with the activity, we modeled the USP signal well detectable both in the light curve and in the RV series after the removal of the signal due to stellar activity. The modeling of the planet signal both in the photometric and spectroscopic series is illustrated in Figs. 11 and 12. As reported in Tables 3 and 4, the USP planet TOI-1807 b orbits its host star in $P_b = 13.1849 \pm$

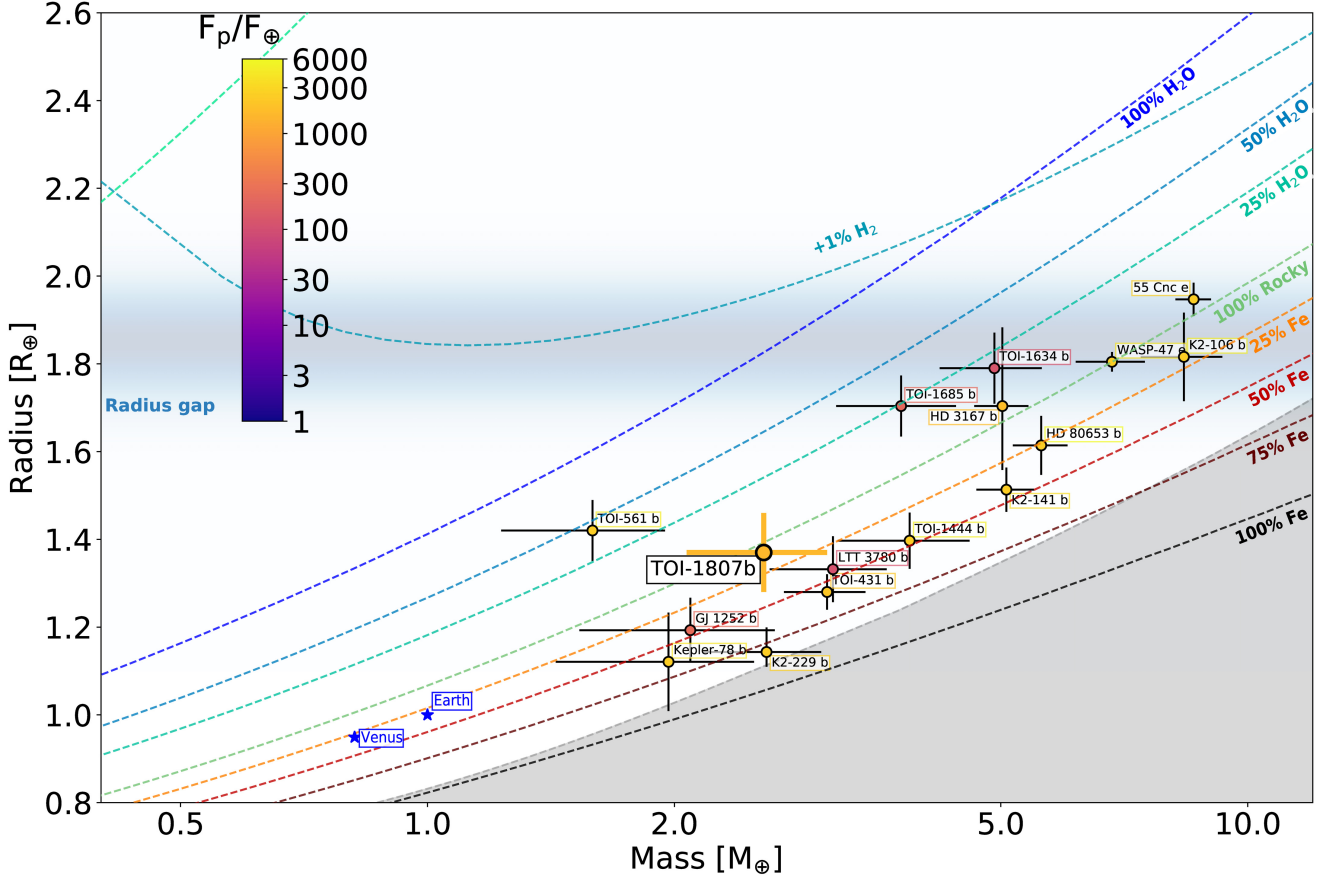


Fig. 13. Mass-radius diagram for known ultra-short period planets with mass and radius measurements more precise than 30% and having Earth/Neptune sizes and masses. Points are color-coded according to the incidental flux (in Earth units) received by the planet. TOI-1807 b is highlighted with a larger point and thick contours. For this plot, we used the TOI-1807 b’s mass obtained in case 1. The dashed colored lines are the theoretical mass-radius curves for different chemical compositions according to Zeng et al. (2019). The shaded area represents the maximum value of iron content predicted by collisional stripping (Marcus et al. 2010). Data from The Extrasolar Planets Encyclopaedia¹⁵.

0.0002 h; we measured a planetary radius $R_{p,b} = 1.37 \pm 0.09 R_{\oplus}$ and a mass $M_{p,b} = 2.57 \pm 0.50 M_{\oplus}$ in case 1 and $M_{p,b} = 2.67 \pm 0.43 M_{\oplus}$ in case 2.

Because of the closeness of TOI-1807 b to the host star, we expected a relativistic apsidal precession of its orbit. We calculated it by using the well known relativistic apsidal precession of Mercury as a proxy. We found an apsidal precession $\delta\varphi \sim 0.23$ arcsec per orbit, which is twice the apsidal precession measured for Mercury.

TOI-1807 b belongs to the small sample of USP planets with masses and radii measurements more precise than 30%. We report this sample in Fig. 13, limiting the analysis to the planets with masses and radii between Earth and Neptune values. In the mass-radius diagram we report the theoretical mass-radius curves for different chemical composition; we also report the iron content limit predicted by Marcus et al. (2010, gray area). The density of TOI-1807 b is $\rho_b = 1.00 \pm 0.29 \rho_{\oplus}$ ($=5.5 \pm 1.6 \text{ g cm}^{-3}$) considering case 1, or $\rho_b = 1.04 \pm 0.28 \rho_{\oplus}$ ($=5.7 \pm 1.5 \text{ g cm}^{-3}$) in case 2, and it is consistent with a rocky terrestrial composition (silicates and iron), probably with an iron core between 25% and 50% of the total mass, in line with the large part of USP planets that follow the Earth-like composition line. On the basis of the distance of the planet from the host star ($a \sim 0.012$ AU), the high incident flux ($F_p \approx 1600 F_{\oplus}$), and the analysis of the mass-radius diagram, we excluded the presence

of any thick envelope composed by H/He; this means that in its 300 Myr lifetime, TOI-1807 b has probably already lost most of its atmosphere via photo-evaporation processes, which is in line with the expectations for these kinds of exoplanets (Lopez 2017).

We analyzed the age versus planetary radius distribution for close-in planets ($P_{\text{orb}} < 100$ days), as done in Nardiello et al. (2021). The results are shown in Fig. 14: we considered both confirmed and candidate exoplanets orbiting stars in stellar clusters, associations, and moving groups (black circles), whose ages are well constrained by using different methods to derive the stellar age (isochrone fitting, gyrochronology, etc.). These objects (and the associated references) are listed in Table 5. We also considered USP planets ($P_{\text{orb}} < 1$ days) in literature¹⁶ having a mass $M < 10 M_J$ or no mass measurements, and age estimates better than 50%: they are shown as gray squares in Fig. 14. We highlight that TOI-1807 b is the youngest USP planet discovered so far, and that all the other USP planets are older than 0.5-1.0 Gyr. As reported in Nardiello et al. (2021), for close-in exoplanets, there is a trend of the radius as a function of the age: objects having $R_p \lesssim 3.5\text{--}4 R_{\oplus}$ are more concentrated at ages > 100 Myr¹⁷; planets having radii $4 R_{\oplus} \lesssim R_p \lesssim 12 R_{\oplus}$ are distributed at

¹⁶ Selected from the NASA Exoplanet Archive, <https://exoplanetarchive.ipac.caltech.edu/>

¹⁷ However, the lack of young planets in this radius interval could be linked to an observational bias due to the difficulty of identifying shallow transits around very active stars.

¹⁵ <http://exoplanet.eu/>, updated to April 2022.

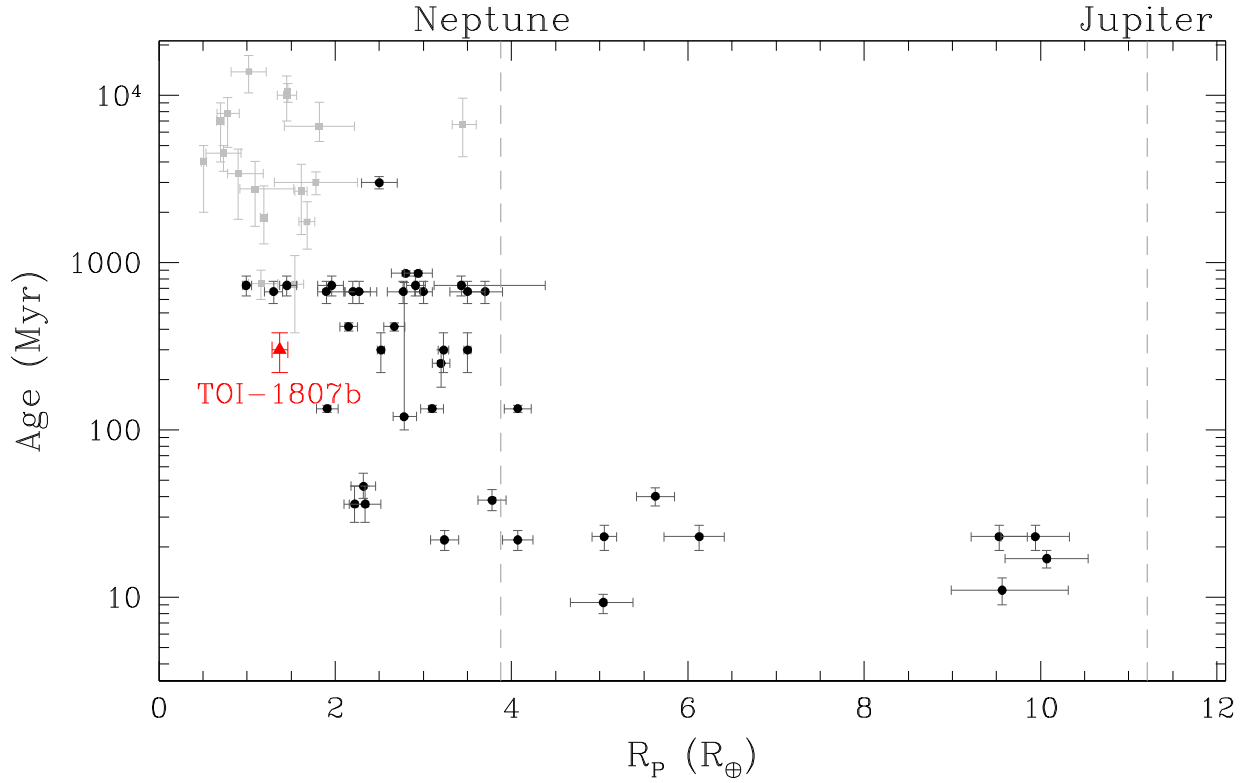


Fig. 14. Age versus planetary radius distribution for planets in stellar clusters, associations, and moving groups, whose ages are well constrained (black circles). Grey squares represent the USP planets whose age is measured with an uncertainty lower than 50 per cent. TOI-1807 b is represented as a red triangle. See text for details.

Table 5. Confirmed and candidate close-in ($P_{\text{orb}} < 100$ days) exoplanets with well measured ages.

Object	Cluster/association	Age (Myr)	R_p (R_{\oplus})	Reference	Object	Cluster/association	Age (Myr)	R_p (R_{\oplus})	Reference
K2-33 b	Upp-Sco	$9.3^{+1.1}_{-1.1}$	$5.04^{+0.34}_{-0.37}$	Mann et al. (2016b)	TOI-2076 c	TOI-1807 MG	300^{+80}_{-80}	$3.50^{+0.04}_{-0.04}$	Osborn et al. (2022)
TOI-1227 b	Low Cen Crux OB	11^{+2}_{-2}	$9.6^{+0.8}_{-0.6}$	Mann et al. (2022)	TOI-2076 d	TOI-1807 MG	300^{+80}_{-80}	$3.23^{+0.06}_{-0.06}$	Osborn et al. (2022)
HIP 67522 b	Sco-Cen	17^{+2}_{-2}	$10.07^{+0.47}_{-0.47}$	Rizzuto et al. (2020)	HD 63433 b	UMa	414^{+23}_{-23}	$2.15^{+0.10}_{-0.10}$	Mann et al. (2020)
AU Mic b	AU Mic	22^{+3}_{-3}	$4.07^{+0.17}_{-0.17}$	Martoli et al. (2021)	HD 63433 c	UMa	414^{+23}_{-23}	$2.67^{+0.12}_{-0.12}$	Mann et al. (2020)
AU Mic c	AU Mic	22^{+3}_{-3}	$3.24^{+0.16}_{-0.16}$	Martoli et al. (2021)	K2-95 b	Praesepe	670^{+100}_{-100}	$3.7^{+0.2}_{-0.2}$	Mann et al. (2017)
V 1298 Tau b	Tau	23^{+4}_{-4}	$9.53^{+0.32}_{-0.32}$	Feinstein et al. (2022)	K2-100 b	Praesepe	670^{+100}_{-100}	$3.8^{+0.2}_{-0.2}$	Barragán et al. (2019)
V 1298 Tau c	Tau	23^{+4}_{-4}	$5.05^{+0.14}_{-0.14}$	Feinstein et al. (2022)	K2-101 b	Praesepe	670^{+100}_{-100}	$3.0^{+0.1}_{-0.1}$	Mann et al. (2017)
V 1298 Tau d	Tau	23^{+4}_{-4}	$6.13^{+0.28}_{-0.28}$	Feinstein et al. (2022)	K2-102 b	Praesepe	670^{+100}_{-100}	$1.3^{+0.1}_{-0.1}$	Mann et al. (2017)
V 1298 Tau e	Tau	23^{+4}_{-4}	$9.94^{+0.39}_{-0.39}$	Feinstein et al. (2022)	K2-103 b	Praesepe	670^{+100}_{-100}	$2.2^{+0.1}_{-0.1}$	Mann et al. (2017)
KOI-7368 b	Cep-Her	36^{+10}_{-8}	$2.22^{+0.12}_{-0.12}$	Bouma et al. (2022b)	K2-104 b	Praesepe	670^{+100}_{-100}	$1.9^{+0.2}_{-0.1}$	Mann et al. (2017)
KOI-7913 b	Cep-Her	36^{+10}_{-8}	$2.34^{+0.12}_{-0.18}$	Bouma et al. (2022b)	K2-264 b	Praesepe	670^{+100}_{-100}	$2.27^{+0.20}_{-0.16}$	Rizzuto et al. (2018)
Kepler-1627 b	δ Lyr	38^{+6}_{-5}	$3.78^{+0.16}_{-0.16}$	Bouma et al. (2022a)	K2-264 c	Praesepe	670^{+100}_{-100}	$2.77^{+0.20}_{-0.18}$	Rizzuto et al. (2018)
DS TucA b	Tuc-Hor	40^{+5}_{-5}	$5.63^{+0.22}_{-0.21}$	Benatti et al. (2019)	HD 283869 b	Hyades	730^{+100}_{-100}	$1.96^{+0.13}_{-0.16}$	Vanderburg et al. (2018)
Kepler-1643 b	Cep-Her	46^{+9}_{-7}	$2.32^{+0.14}_{-0.14}$	Bouma et al. (2022b)	K2-25 b	Hyades	730^{+100}_{-100}	$3.43^{+0.95}_{-0.31}$	Mann et al. (2016a)
K2-284 b	Cas-Tau	120^{+640}_{-20}	$2.78^{+0.14}_{-0.12}$	David et al. (2018)	K2-136A b	Hyades	730^{+100}_{-100}	$0.99^{+0.06}_{-0.04}$	Mann et al. (2018)
TOI-451 b	Psc-Eri	$134^{+6.5}_{-6.5}$	$1.91^{+0.12}_{-0.12}$	Newton et al. (2021)	K2-136A c	Hyades	730^{+100}_{-100}	$2.91^{+0.11}_{-0.10}$	Mann et al. (2018)
TOI-451 c	Psc-Eri	$134^{+6.5}_{-6.5}$	$3.10^{+0.13}_{-0.13}$	Newton et al. (2021)	K2-136A d	Hyades	730^{+100}_{-100}	$1.45^{+0.11}_{-0.08}$	Mann et al. (2018)
TOI-451 d	Psc-Eri	$134^{+6.5}_{-6.5}$	$4.07^{+0.15}_{-0.15}$	Newton et al. (2021)	K-66 b	NGC 6811	863^{+30}_{-30}	$2.80^{+0.16}_{-0.16}$	Meibom et al. (2013)
TOI-1098 b	Melange-1	250^{+50}_{-70}	$3.2^{+0.1}_{-0.1}$	Tofflemire et al. (2021)	K-67 b	NGC 6811	863^{+30}_{-30}	$2.94^{+0.16}_{-0.16}$	Meibom et al. (2013)
TOI-2076 b	TOI-1807 MG	300^{+80}_{-80}	$2.52^{+0.04}_{-0.04}$	Osborn et al. (2022)	K2-231 b	Ruprecht 147	3000^{+250}_{-250}	$2.5^{+0.2}_{-0.2}$	Curtis et al. (2018)

ages < 100 Myr and the lack of planets at older ages cannot be attributed to any observational bias: on the contrary, they should be more easily detectable. This trend can be interpreted in the context of atmosphere loss of low mass close-in planets linked to photoevaporation mechanisms that happen on timescales of < 100 – 200 Myr (Owen 2019; Owen et al. 2020). As we already

reported in the analysis of the mass-radius diagram, TOI-1807 b has no extended atmosphere. This is in agreement with its location in the age-planetary radius diagram: indeed, it is located in the region of small-radii ($R_p \lesssim 4 R_{\oplus}$), “middle-age” (100–1000 Myr), close-in, low-mass planets that have probably already lost their atmospheres during their early life. The host star is

characterized by an X-ray emission, L_X , close to the median value for stars of the same spectral type and age (e.g., Micela 2002; Preibisch & Feigelson 2005); therefore, we expect that the planet may have suffered a significant mass loss due to its small distance from the host star and to its small mass. Indeed, low-gravity planets are subject to more intense evaporation than the most massive planets (Penz & Micela 2008). After a few hundred million years, the planet may have lost all of its atmosphere and simultaneously contracted to its present size. Its radius puts the planet at the low size peak of the bimodal distribution of planetary radii observed in planets with orbital periods smaller than 100 days (Fulton et al. 2017). Modirrousta-Galian et al. (2020) demonstrated that evaporation due to energy radiation can produce the observed bimodal distribution. They also predict that the 90% of the planets at the $\sim 1.3 R_{\oplus}$ peak completely lost their envelope, consistently with the hypothesis that TOI-1807 b is today without atmosphere.

Because many USP planets are hosted by multi-planet systems, we also checked for the presence of a second non-transiting planet orbiting TOI-1807 (Case 3). Even if we obtained some significant detection (in some cases, with a significance $>5\sigma$) in the RV series, we found that period and semi-amplitude of a hypothetical planet c changed drastically on the basis of the activity model used for the analysis (while almost nothing changes for planet b). Comparing the Bayesian evidence of cases 1 and 2 with case 3 and analyzing the previously reported facts, we concluded that any detection obtained in this analysis is due to a false positive (probably linked to the stellar activity modeling) and that new data are mandatory for the detection of an hypothetical second planet orbiting TOI-1807.

Acknowledgements. The authors thank the anonymous referee for carefully reading the paper and for the useful comments and suggestions that have contributed to improving the quality of the manuscript. DN acknowledges the support from the French Centre National d'Etudes Spatiales (CNES). This work has been supported by the PRIN-INAF 2019 "Planetary systems at young ages (PLATEA)". We acknowledge financial support from the ASI-INAF agreement n.2018-16-HH.0. This paper includes data collected by the TESS mission. Funding for the TESS mission is provided by the NASA Explorer Program. This work has made use of data from the European Space Agency (ESA) mission *Gaia* (<https://www.cosmos.esa.int/gaia>), processed by the *Gaia* Data Processing and Analysis Consortium (DPAC, <https://www.cosmos.esa.int/web/gaia/dpac/consortium>). Funding for the DPAC has been provided by national institutions, in particular the institutions participating in the *Gaia* Multilateral Agreement. This work makes use of observations collected at the Asiago Schmidt 67/92 cm telescope (Asiago, Italy) of the INAF – Osservatorio Astronomico di Padova. This research has made use of the Keck Observatory Archive (KOA), which is operated by the W.M. Keck Observatory and the NASA Exoplanet Science Institute (NExSci), under contract with the National Aeronautics and Space Administration (Prog. ID H6aH, PI Boesgaard; Prog. ID N038Hr, PI Fischer; Prog. ID H198Hr, H212Hr, H170Hr, PI Shkolnik; Prog. ID A297Hr, PI Fischer; Prog. ID C103Hr, PI Bowler) Based on data obtained from the ESO Science Archive Facility (Prog. ID 091.C-0216(A), PI Rodriguez; Prog. ID 090.D-0133(A), PI Datson; Prog. ID 072.C-0488(E), PI Mayor, and 183.C-0972(A), PI Udry). Based on data retrieved from the SOPHIE archive at Observatoire de Haute-Provence (OHP), available at atlas.obs-hp.fr/sophie (Prog. ID 09B.PNP.CON.S, 11A.PNP.CON.S, 17A.PNCG.SOUB). Data at IRTF/iSHELL were obtained by A. Sohani, F. Zohrabi, D. Vermilion, S. Arnez, C. Geneser, A. Tanner, K. Collins, J. Berberian, I. Helm, and P. Newman.

References

Aguilera-Gómez, C., Ramírez, I., & Chanamé, J. 2018, *A&A*, 614, A55
 Ambikasaran, S., Foreman-Mackey, D., Greengard, L., Hogg, D. W., & O'Neil, M. 2015, *IEEE Trans. Pattern Anal. Mach. Intell.*, 38, 252
 Ammler-von Eiff, M., & Guenther, E. W. 2009, *A&A*, 508, 677
 Anglada-Escudé, G., & Butler, R. P. 2012, *ApJS*, 200, 15
 Apai, D., Nardiello, D., & Bedin, L. R. 2021, *ApJ*, 906, 64
 Asaiain, R., Figueras, F., Torra, J., & Chen, B. 1999, *A&A*, 341, 427
 Astudillo-Defru, N., Delfosse, X., Bonfils, X., et al. 2017, *A&A*, 600, A13

Bailer-Jones, C. A. L., Rybizki, J., Fouesneau, M., Mantelet, G., & Andrae, R. 2018, *AJ*, 156, 58
 Baliunas, S. L., Donahue, R. A., Soon, W. H., et al. 1995, *ApJ*, 438, 269
 Baratella, M., D'Orazi, V., Biazzo, K., et al. 2020a, *A&A*, 640, A123
 Baratella, M., D'Orazi, V., Carraro, G., et al. 2020b, *A&A*, 634, A34
 Barbato, D., Pinamonti, M., Sozzetti, A., et al. 2020, *A&A*, 641, A68
 Barragán, O., Aigrain, S., Kubyskhina, D., et al. 2019, *MNRAS*, 490, 698
 Barragán, O., Aigrain, S., Rajpaul, V. M., & Zicher, N. 2022a, *MNRAS*, 509, 866
 Barragán, O., Armstrong, D. J., Gandolfi, D., et al. 2022b, *MNRAS*, 514, 1606
 Barros, S. C. C., Demangeon, O., Díaz, R. F., et al. 2020, *A&A*, 634, A75
 Bell, C. P. M., Mamajek, E. E., & Naylor, T. 2015, *MNRAS*, 454, 593
 Benatti, S., Nardiello, D., Malavolta, L., et al. 2019, *A&A*, 630, A81
 Benatti, S., Damasso, M., Borsari, F., et al. 2021, *A&A*, 650, A66
 Bergfors, C., Brandner, W., Janson, M., et al. 2010, *A&A*, 520, A54
 Boisse, I., Bouchy, F., Hébrard, G., et al. 2011, *A&A*, 528, A4
 Bonomo, A. S., Zeng, L., Damasso, M., et al. 2019, *Nat. Astron.*, 3, 416
 Boro Saikia, S., Marvin, C. J., Jeffers, S. V., et al. 2018, *A&A*, 616, A108
 Borucki, W. J., Koch, D., Basri, G., et al. 2010, *Science*, 327, 977
 Bouma, L. G., Curtis, J. L., Masuda, K., et al. 2022a, *AJ*, 163, 121
 Bouma, L. G., Kerr, R., Curtis, J. L., et al. 2022b, AAS, submitted [arXiv:2205.01112]
 Bowler, B. P., Shkolnik, E. L., Liu, M. C., et al. 2015, *ApJ*, 806, 62
 Bowler, B. P., Hinkley, S., Ziegler, C., et al. 2019, *ApJ*, 877, 60
 Brandt, T. D., McElwain, M. W., Turner, E. L., et al. 2014, *ApJ*, 794, 159
 Brewer, J. M., Fischer, D. A., Valenti, J. A., & Piskunov, N. 2016, *ApJS*, 225, 41
 Buchner, J. 2016, *Stat. Comput.*, 26, 383
 Burggraaf, O., Talens, G. J. J., Spronck, J., et al. 2018, *A&A*, 617, A32
 Butters, O. W., West, R. G., Anderson, D. R., et al. 2010, *A&A*, 520, L10
 Butler, R. P., Vogt, S. S., Laughlin, G., et al. 2017, *AJ*, 153, 208
 Caballero, J. A. 2010, *A&A*, 514, A98
 Cale, B., Plavchan, P., LeBrun, D., et al. 2019, *AJ*, 158, 170
 Carleo, I., Malavolta, L., Lanza, A. F., et al. 2020, *A&A*, 638, A5
 Carleo, I., Desidera, S., Nardiello, D., et al. 2021, *A&A*, 645, A71
 Casali, G., Spina, L., Magrini, L., et al. 2020, *A&A*, 639, A127
 Castelli, F., & Kurucz, R. L. 2003, in *IAU Symposium*, 210, *Modelling of Stellar Atmospheres*, eds. N. Piskunov, W. W. Weiss, & D. F. Gray, A20
 Chiang, E., & Laughlin, G. 2013, *MNRAS*, 431, 3444
 Cifuentes, C., Caballero, J. A., Cortés-Contreras, M., et al. 2020, *A&A*, 642, A115
 Claret, A. 2018, *A&A*, 618, A20
 Cosentino, R., Lovis, C., Pepe, F., et al. 2012, *SPIE Conf. Ser.*, 8446, 84461V
 Curtis, J. L., Vanderburg, A., Torres, G., et al. 2018, *AJ*, 155, 173
 da Silva, L., Girardi, L., Pasquini, L., et al. 2006, *A&A*, 458, 609
 Dalal, S., Kiefer, F., Hébrard, G., et al. 2021, *A&A*, 651, A11
 David, T. J., Mamajek, E. E., Vanderburg, A., et al. 2018, *AJ*, 156, 302
 David, T. J., Petigura, E. A., Luger, R., et al. 2019, *ApJ*, 885, L12
 Desidera, S., Covino, E., Messina, S., et al. 2015, *A&A*, 573, A126
 Dias, W. S., Monteiro, H., Moitinho, A., et al. 2021, *MNRAS*, 504, 356
 Dutra-Ferreira, L., Pasquini, L., Smiljanic, R., Porto de Mello, G. F., & Steffen, M. 2016, *A&A*, 585, A75
 Eisenbeis, T., Ammler-von Eiff, M., Roell, T., et al. 2013, *A&A*, 556, A53
 Feinstein, A. D., David, T. J., Montet, B. T., et al. 2022, *ApJ*, 925, L2
 Foreman-Mackey, D. 2018, *RNAAS*, 2, 31
 Foreman-Mackey, D., Hogg, D. W., Lang, D., & Goodman, J. 2013, *PASP*, 125, 306
 Foreman-Mackey, D., Agol, E., Ambikasaran, S., & Angus, R. 2017, *AJ*, 154, 220
 Fuhrmann, K. 2008, *MNRAS*, 384, 173
 Fulton, B. J., Petigura, E. A., Howard, A. W., et al. 2017, *AJ*, 154, 109
 Gagné, J., Lafrenière, D., Doyon, R., Malo, L., & Artigau, É. 2015, *ApJ*, 798, 73
 Gagné, J., Mamajek, E. E., Malo, L., et al. 2018, *ApJ*, 856, 23
 Gaia Collaboration (Brown, A. G. A., et al.) 2018, *A&A*, 616, A1
 Gaia Collaboration (Brown, A. G. A., et al.) 2021a, *A&A*, 649, A1
 Gaia Collaboration (Smart, R. L., et al.) 2021b, *A&A*, 649, A6
 Galicher, R., Marois, C., Macintosh, B., et al. 2016, *A&A*, 594, A63
 Gálvez, M. C., Montes, D., Fernández-Figueroa, M. J., & López-Santiago, J. 2006, *Ap&SS*, 304, 59
 Gelman, A., & Rubin, D. B. 1992, *Stat. Sci.*, 7, 457
 Gillen, E., Briegal, J. T., Hodgkin, S. T., et al. 2020, *MNRAS*, 492, 1008
 Gomes da Silva, J., Figueira, P., Santos, N., & Faria, J. 2018, *J. Open Source Softw.*, 3, 667
 Gomes da Silva, J., Santos, N. C., Adibekyan, V., et al. 2021, *A&A*, 646, A77
 Goodman, J., & Weare, J. 2010, *Commun. Appl. Math. Comput. Sci.*, 5, 65
 Gray, R. O., Corbally, C. J., Garrison, R. F., McFadden, M. T., & Robinson, P. E. 2003, *AJ*, 126, 2048
 Griffin, R. F., & Filiz Ak, N. 2010, *Ap&SS*, 330, 47

- Grünblatt, S. K., Howard, A. W., & Haywood, R. D. 2015, *ApJ*, **808**, 127
- Günther, M. N., Zhan, Z., Seager, S., et al. 2020, *AJ*, **159**, 60
- Halbwachs, J. L., Mayor, M., & Udry, S. 2012, *MNRAS*, **422**, 14
- Hansen, B. M. S., & Murray, N. 2012, *ApJ*, **751**, 158
- Hartman, J. D., Bakos, G. Á., Noyes, R. W., et al. 2011, *AJ*, **141**, 166
- Hatzes, A. P. 2014, *A&A*, **568**, A84
- Haywood, R. D., Collier Cameron, A., Queloz, D., et al. 2014, *MNRAS*, **443**, 2517
- Hedges, C., Hughes, A., Zhou, G., et al. 2021, *AJ*, **162**, 54
- Higson, E., Handley, W., Hobson, M., & Lasenby, A. 2019, *Stat. Comput.*, **29**, 891
- Hippke, M., & Heller, R. 2019, *A&A*, **623**, A39
- Howell, S. B., Sobeck, C., Haas, M., et al. 2014, *PASP*, **126**, 398
- Hunter, A., Macgregor, A. B., Szabo, T., Wellington, C., & Bellgard, M. I. 2012, *Source Code Biol. Med.*, **7**, 1
- Ida, S., & Lin, D. N. C. 2010, *ApJ*, **719**, 810
- Jayasinghe, T., Kochanek, C. S., Stanek, K. Z., et al. 2018, *MNRAS*, **477**, 3145
- Jeffers, S. V., Schöfer, P., Lamert, A., et al. 2018, *A&A*, **614**, A76
- Jenkins, J. S., Jones, H. R. A., Pavlenko, Y., et al. 2008, *A&A*, **485**, 571
- Jenkins, J. M., Twicken, J. D., McCauliff, S., et al. 2016, *SPIE Conf. Ser.*, **9913**, 99133E
- Johnson, D. R. H., & Soderblom, D. R. 1987, *AJ*, **93**, 864
- Kim, B., An, D., Stauffer, J. R., et al. 2016, *ApJS*, **222**, 19
- Kipping, D. M. 2010, *MNRAS*, **408**, 1758
- Kipping, D. M. 2013, *MNRAS*, **435**, 2152
- Kiraga, M. 2012, *Acta Astron.*, **62**, 67
- Koen, C., & Eyer, L. 2002, *MNRAS*, **331**, 45
- Kraus, A. L., Shkolnik, E. L., Allers, K. N., & Liu, M. C. 2014, *AJ*, **147**, 146
- Kreidberg, L. 2015, *PASP*, **127**, 1161
- Lacedelli, G., Malavolta, L., Borsato, L., et al. 2021, *MNRAS*, **501**, 4148
- Lallement, R., Capitanio, L., Ruiz-Dern, L., et al. 2018, *A&A*, **616**, A132
- Lamm, M. H., Bailer-Jones, C. A. L., Mundt, R., Herbst, W., & Scholz, A. 2004, *A&A*, **417**, 557
- Lamman, C., Baranec, C., Berta-Thompson, Z. K., et al. 2020, *AJ*, **159**, 139
- Lanza, A. F., Bonomo, A. S., Moutou, C., et al. 2010, *A&A*, **520**, A53
- Lee, E. J., & Chiang, E. 2017, *ApJ*, **842**, 40
- Libralato, M., Bedin, L. R., Nardiello, D., & Piotto, G. 2016a, *MNRAS*, **456**, 1137
- Libralato, M., Nardiello, D., Bedin, L. R., et al. 2016b, *MNRAS*, **463**, 1780
- Lind, K., Asplund, M., & Barklem, P. M. 2009, *A&A*, **503**, L541
- Lopez, E. D. 2017, *MNRAS*, **472**, 245
- Lopez, E. D., & Fortney, J. J. 2013, *ApJ*, **776**, 2
- López-Santiago, J., Micela, G., & Montes, D. 2009, *A&A*, **499**, 129
- Lovis, C., Dumusque, X., Santos, N. C., et al. 2011, *ArXiv e-prints* [arXiv:1107.5325]
- Lu, H.-p., Zhang, L.-y., Shi, J., et al. 2019, *ApJS*, **243**, 28
- Makarov, V. V., & Kaplan, G. H. 2005, *AJ*, **129**, 2420
- Malavolta, L. 2016, *PyORBIT: Exoplanet orbital parameters and stellar activity*, *Astrophysics Source Code Library*, [record ascl:1612.008]
- Malavolta, L., Nascimbeni, V., Piotto, G., et al. 2016, *A&A*, **588**, A118
- Malavolta, L., Mayo, A. W., Loudon, T., et al. 2018, *AJ*, **155**, 107
- Maldonado, J., Eiroa, C., Villaver, E., Montesinos, B., & Mora, A. 2015, *A&A*, **579**, A20
- Mallonn, M., von Essen, C., Weingrill, J., et al. 2015, *A&A*, **580**, A60
- Mallonn, M., Herrero, E., Juvan, I. G., et al. 2018, *A&A*, **614**, A35
- Malo, L., Doyon, R., Lafrenière, D., et al. 2013, *ApJ*, **762**, 88
- Malo, L., Artigau, É., Doyon, R., et al. 2014, *ApJ*, **788**, 81
- Mann, A. W., Gaidos, E., Mace, G. N., et al. 2016a, *ApJ*, **818**, 46
- Mann, A. W., Newton, E. R., Rizzuto, A. C., et al. 2016b, *AJ*, **152**, 61
- Mann, A. W., Gaidos, E., Vanderburg, A., et al. 2017, *AJ*, **153**, 64
- Mann, A. W., Vanderburg, A., Rizzuto, A. C., et al. 2018, *AJ*, **155**, 4
- Mann, A. W., Johnson, M. C., Vanderburg, A., et al. 2020, *AJ*, **160**, 179
- Mann, A. W., Wood, M. L., Schmidt, S. P., et al. 2022, *AJ*, **163**, 156
- Marcus, R. A., Sasselov, D., Stewart, S. T., & Hernquist, L. 2010, *ApJ*, **719**, L45
- Martioti, E., Hébrard, G., Correia, A. C. M., Laskar, J., & Lecavelier des Etangs, A. 2021, *A&A*, **649**, A177
- McQuillan, A., Aigrain, S., & Mazeh, T. 2013, *MNRAS*, **432**, 1203
- Meibom, S., Torres, G., Fressin, F., et al. 2013, *Nature*, **499**, 55
- Meshkat, T., Mawet, D., Bryan, M. L., et al. 2017, *AJ*, **154**, 245
- Messina, S., Lanzafame, A. C., Feiden, G. A., et al. 2016, *A&A*, **596**, A29
- Messina, S., Lanzafame, A. C., Malo, L., et al. 2017, *A&A*, **607**, A3
- Messina, S., Nardiello, D., Desidera, S., et al. 2022, *A&A*, **657**, L3
- Micela, G. 2002, in *The Evolving Sun and its Influence on Planetary Environments*, eds. B. Montesinos, A. Gimenez, & E. F. Guinan, *Astronomical Society of the Pacific Conference Series*, **269**, 107
- Modirrousta-Galian, D., Locci, D., & Micela, G. 2020, *ApJ*, **891**, 158
- Nardiello, D. 2020, *MNRAS*, **498**, 5972
- Nardiello, D., Bedin, L. R., Nascimbeni, V., et al. 2015, *MNRAS*, **447**, 3536
- Nardiello, D., Libralato, M., Bedin, L. R., et al. 2016a, *MNRAS*, **463**, 1831
- Nardiello, D., Libralato, M., Bedin, L. R., et al. 2016b, *MNRAS*, **455**, 2337
- Nardiello, D., Borsato, L., Piotto, G., et al. 2019, *MNRAS*, **490**, 3806
- Nardiello, D., Piotto, G., Deleuil, M., et al. 2020, *MNRAS*, **495**, 4924
- Nardiello, D., Deleuil, M., Mantovan, G., et al. 2021, *MNRAS*, **505**, 3767
- Newton, E. R., Irwin, J., Charbonneau, D., et al. 2016, *ApJ*, **821**, 93
- Newton, E. R., Mann, A. W., Kraus, A. L., et al. 2021, *AJ*, **161**, 65
- Nordstrom, B., & Andersen, J. 1985, *A&AS*, **61**, 53
- Nordström, B., Mayor, M., Andersen, J., et al. 2004, *A&A*, **418**, 989
- Norton, A. J., Wheatley, P. J., West, R. G., et al. 2007, *A&A*, **467**, 785
- Oelkers, R. J., Rodriguez, J. E., Stassun, K. G., et al. 2018, *AJ*, **155**, 39
- Osborn, H. P., Bonfanti, A., Gandolfi, D., et al. 2022, <https://doi.org/10.1051/0004-6361/202243065>
- Owen, J. E. 2019, *Annu. Rev. Earth Planet. Sci.*, **47**, 67
- Owen, J. E., & Lai, D. 2018, *MNRAS*, **479**, 5012
- Owen, J. E., & Wu, Y. 2013, *ApJ*, **775**, 105
- Owen, J. E., Shaikhislamov, I. F., Lammer, H., Fossati, L., & Khodachenko, M. L. 2020, *Space Sci. Rev.*, **216**, 129
- Pecaut, M. J., & Mamajek, E. E. 2013, *ApJS*, **208**, 9
- Penz, T., & Micela, G. 2008, *A&A*, **479**, 579
- Pepe, F., Mayor, M., Galland, F., et al. 2002, *A&A*, **388**, 632
- Pepper, J., Pogge, R. W., DePoy, D. L., et al. 2007, *PASP*, **119**, 923
- Perger, M., Anglada-Escudé, G., Ribas, I., et al. 2021, *A&A*, **645**, A58
- Petrovich, C., Deibert, E., & Wu, Y. 2019, *AJ*, **157**, 180
- Plavchan, P., Barclay, T., Gagné, J., et al. 2020, *Nature*, **582**, 497
- Pollacco, D. L., Skillen, I., Collier Cameron, A., et al. 2006, *PASP*, **118**, 1407
- Preibisch, T., & Feigelson, E. D. 2005, *ApJS*, **160**, 390
- Quinn, S. N., White, R. J., Latham, D. W., et al. 2012, *ApJ*, **756**, L33
- Quinn, S. N., White, R. J., Latham, D. W., et al. 2014, *ApJ*, **787**, 27
- Rajpaul, V., Aigrain, S., Osborne, M. A., Reece, S., & Roberts, S. 2015, *MNRAS*, **452**, 2269
- Rasmussen, C. E., & Williams, C. K. I. 2006, *Gaussian processes for machine learning, Adaptive computation and machine learning* (MIT Press), I–XVIII, 1
- Rayner, J., Tokunaga, A., Jaffe, D., et al. 2016, *SPIE Conf. Ser.*, **9908**, 990884
- Reiners, A. 2006, *A&A*, **446**, 267
- Rhee, J. H., Song, I., Zuckerman, B., & McElwain, M. 2007, *ApJ*, **660**, 1556
- Riaz, B., Gizis, J. E., & Harvin, J. 2006, *AJ*, **132**, 866
- Ricker, G. R., Winn, J. N., Vanderspek, R., et al. 2015, *J. Astron. Telescopes Instrum. Syst.*, **1**, 014003
- Riedel, A. R., Alam, M. K., Rice, E. L., Cruz, K. L., & Henry, T. J. 2017, *ApJ*, **840**, 87
- Rizzuto, A. C., Vanderburg, A., Mann, A. W., et al. 2018, *AJ*, **156**, 195
- Rizzuto, A. C., Newton, E. R., Mann, A. W., et al. 2020, *AJ*, **160**, 33
- Roberts, D. H., Lehar, J., & Dreher, J. W. 1987, *AJ*, **93**, 968
- Sahu, K. C., Casertano, S., Bond, H. E., et al. 2006, *Nature*, **443**, 534
- Sanchis-Ojeda, R., Rappaport, S., Winn, J. N., et al. 2014, *ApJ*, **787**, 47
- Schlichting, H. E. 2018, in *Handbook of Exoplanets*, eds. H. J. Deeg, & J. A. Belmonte, 141
- Schlichting, H. E., Sari, R., & Yalinewich, A. 2015, *Icarus*, **247**, 81
- Schlieder, J. E., Lépine, S., & Simon, M. 2012, *AJ*, **143**, 80
- Schröder, C., Reiners, A., & Schmitt, J. H. M. M. 2009, *A&A*, **493**, 1099
- Sestito, P., & Randich, S. 2005, *A&A*, **442**, 615
- Shkolnik, E. L., Anglada-Escudé, G., Liu, M. C., et al. 2012, *ApJ*, **758**, 56
- Shkolnik, E. L., Allers, K. N., Kraus, A. L., Liu, M. C., & Flagg, L. 2017, *AJ*, **154**, 69
- Skrutskie, M. F., Cutri, R. M., Stiening, R., et al. 2006, *AJ*, **131**, 1163
- Smith, J. C., Stumpe, M. C., Van Cleve, J. E., et al. 2012, *PASP*, **124**, 1000
- Snedden, C. A. 1973, PhD thesis, The University of Texas at Austin.
- Sobeck, J. S., Kraft, R. P., Sneden, C., et al. 2011, *AJ*, **141**, 175
- Soderblom, D. R., Jones, B. F., Balachandran, S., et al. 1993a, *A&A*, **106**, 1059
- Soderblom, D. R., Pilachowski, C. A., Fedele, S. B., & Jones, B. F. 1993b, *A&A*, **105**, 2299
- Sousa, S. G., Santos, N. C., Adibekyan, V., Delgado-Mena, E., & Israelian, G. 2015, *A&A*, **577**, A67
- Speagle, J. S. 2020, *MNRAS*, **493**, 3132
- Stassun, K. G., Oelkers, R. J., Pepper, J., et al. 2018, *AJ*, **156**, 102
- Storn, R., & Price, K. 1997, *J. Global Optim.*, **11**, 341
- Strassmeier, K., Washuettl, A., Granzer, T., Scheck, M., & Weber, M. 2000, *A&AS*, **142**, 275
- Strassmeier, K. G., Granzer, T., Weber, M., et al. 2004, *Astron. Nachr.*, **325**, 527
- Strassmeier, K. G., Weber, M., Granzer, T., & Järvinen, S. 2012, *Astron. Nachr.*, **333**, 663
- Stumpe, M. C., Smith, J. C., Van Cleve, J. E., et al. 2012, *PASP*, **124**, 985
- Stumpe, M. C., Smith, J. C., Catanzarite, J. H., et al. 2014, *PASP*, **126**, 100

- Suárez Mascareño, A., Rebolo, R., & González Hernández, J. I. 2016, *A&A*, **595**, A12
- Takeda, Y., & Kawanamoto, S. 2005, *PASJ*, **57**, 45
- Terquem, C., & Papaloizou, J. C. B. 2007, *ApJ*, **654**, 1110
- Tofflemire, B. M., Rizzuto, A. C., Newton, E. R., et al. 2021, *AJ*, **161**, 171
- Torres, C. A. O., Quast, G. R., da Silva, L., et al. 2006, *A&A*, **460**, 695
- Trilling, D. E., Bryden, G., Beichman, C. A., et al. 2008, *ApJ*, **674**, 1086
- Valsecchi, F., Rasio, F. A., & Steffen, J. H. 2014, *ApJ*, **793**, L3
- Van Eylen, V., Albrecht, S., Huang, X., et al. 2019, *AJ*, **157**, 61
- Vanderburg, A., Mann, A. W., Rizzuto, A., et al. 2018, *AJ*, **156**, 46
- Vigan, A., Bonavita, M., Biller, B., et al. 2017, *A&A*, **603**, A3
- Voges, W., Aschenbach, B., Boller, T., et al. 2000, *IAU Circ.*, **7432**, 3
- Waite, I. A., Marsden, S. C., Carter, B. D., et al. 2011, *PASA*, **28**, 323
- West, A. A., Weisenburger, K. L., Irwin, J., et al. 2015, *ApJ*, **812**, 3
- Wichmann, R., Schmitt, J. H. M. M., & Hubrig, S. 2003, *A&A*, **399**, 983
- Winn, J. N., Sanchis-Ojeda, R., & Rappaport, S. 2018, *New A Rev.*, **83**, 37
- Wright, J. T., Marcy, G. W., Butler, R. P., & Vogt, S. S. 2004, *ApJS*, **152**, 261
- Wright, E. L., Eisenhardt, P. R. M., Mainzer, A. K., et al. 2010, *AJ*, **140**, 1868
- Wright, N. J., Drake, J. J., Mamajek, E. E., & Henry, G. W. 2011, *ApJ*, **743**, 48
- Zechmeister, M., & Kürster, M. 2009, *A&A*, **496**, 577
- Zeng, L., Jacobsen, S. B., Sasselov, D. D., et al. 2019, *Proc. Natl. Acad. Sci. U.S.A.*, **116**, 9723
- Žerjal, M., Zwitter, T., Matijević, G., et al. 2017, *ApJ*, **835**, 61
- Zhu, W., & Dong, S. 2021, *ARA&A*, **59**, 291
- Zuckerman, B., Rhee, J. H., Song, I., & Bessell, M. S. 2011, *ApJ*, **732**, 61
- Zuckerman, B., Vican, L., Song, I., & Schneider, A. 2013, *ApJ*, **778**, 5
- ⁵ INAF – Osservatorio Astrofisico di Catania, via S. Sofia 78, 95123 Catania, Italy
- ⁶ INAF – Osservatorio Astronomico di Roma, Via Frascati 33, 00078 Monte Porzio Catone (Roma), Italy
- ⁷ INAF – Osservatorio Astronomico di Palermo, Piazza del Parlamento, 1, 90134 Palermo, Italy
- ⁸ INAF – Osservatorio Astrofisico di Torino, via Osservatorio 20, 10025 Pino Torinese, Italy
- ⁹ Astrophysics Group, Cavendish Laboratory, JJ Thomson Avenue, Cambridge CB3 0HE, UK
- ¹⁰ Dipartimento di Fisica – Università di Roma La Sapienza, P.le A. Moro 5, 00185 Roma, Italy
- ¹¹ Department of Physics and Astronomy, George Mason University, 4400 University Drive, Fairfax, VA 22030, USA
- ¹² INAF – Osservatorio Astronomico di Trieste, via Tiepolo 11, 34143 Trieste, Italy
- ¹³ INAF – Osservatorio Astronomico di Brera, Via E. Bianchi 46, 23807 Merate (LC), Italy
- ¹⁴ Astronomy Department, Indiana University, Bloomington, IN 47405-7105, USA
- ¹⁵ INAF – Osservatorio Astronomico di Capodimonte, Salita Moiariello 16, 80131 Naples, Italy
- ¹⁶ Department of Physics, University of Rome “Tor Vergata”, Via della Ricerca Scientifica 1, 00133 Rome, Italy
- ¹⁷ Max Planck Institute for Astronomy, Königstuhl 17, 69117 Heidelberg, Germany
- ¹⁸ INAF – Osservatorio Astronomico di Cagliari, via della Scienza 5, 09047 Selargius (CA), Italy
- ¹⁹ Fundación Galileo Galilei – INAF, Rambla José Ana Fernandez Pérez 7, 38712 Breña Baja, TF, Spain
- ²⁰ Instituto de Astrofísica de Canarias, C/Vía Lactea s/n, E-38205 La Laguna (Tenerife), Spain
- ²¹ Departamento de Astrofísica, Univ. de La Laguna, Av. del Astrofísico F. Sánchez, s/n, 38205 La Laguna (Tenerife), Spain
-
- ¹ INAF – Osservatorio Astronomico di Padova, Vicolo dell’Osservatorio 5, 35122 Padova, Italy
e-mail: domenico.nardiello@inaf.it
- ² Aix Marseille Univ, CNRS, CNES, LAM, 13000 Marseille, France
- ³ Dipartimento di Fisica e Astronomia “Galileo Galilei” – Università di Padova, Vicolo dell’Osservatorio 3, 35122 Padova, Italy
- ⁴ Leibniz-Institut für Astrophysik Potsdam (AIP), An der Sternwarte 16, 14482 Potsdam, Germany

Appendix A: Light curve correction

In Fig. A.1, we reported a comparison between the raw SAP light curve (red points), the light curve corrected by the TESS team (PDCSAP, blue points) and the light curve corrected using the PATHOS pipeline and adopted in this work (green points).

Appendix B: Comoving objects

Appendix B.1: Search for comoving objects

In order to improve the age constraints for our targets and better understand their dynamical environment, we searched for wide physical companions and comoving objects. We first noticed, as also done by Hedges et al. (2021), that the planet hosts TOI-1807 and TOI-2076 have very similar space velocity, having a difference of about 0.5 km s^{-1} considering all the three coordinates, and consistent age diagnostics. Therefore, they are likely to be comoving and coeval. In order to look for additional comoving objects, we made use of the catalog from Gaia Collaboration (2021b), which includes the U, V, and W space velocities for *Gaia* stars within 100 pc with available radial velocity. We searched over the whole sky for targets within 60 pc which have a space velocity δUVW (considering the three components) which differ by less than 4 km s^{-1} with respect to the mean of TOI-1807 and TOI-2076; 76 objects fulfilling these criteria were identified, some of which previously known as being young and/or active. Few additional objects can be considered to be physical companions of one of the selected targets. We noticed that the space velocities of TOI-1807 and TOI-2076 somewhat resemble those of B3 subgroup of the Local Association identified by Asiain et al. (1999). An age of $300 \pm 120 \text{ Myr}$ was estimated in their study from isochrone fitting of early type stars.

As is widely known from the literature (see, e.g., López-Santiago et al. 2009), interlopers with similar kinematics but different ages are likely to exist. For intermediate age groups (a few hundreds of Myr old), the existence itself of some groups is questioned (see, e.g., Zuckerman et al. 2013, for the Castor moving group). To shed further light on the possibility of a group of coeval objects, we considered the selected targets individually, deriving age indicators from the literature and public data, when available.

Appendix B.2: TESS data reduction

Out of 79 stars among wide companions and comoving objects, 55 were observed by TESS in one or more Sectors. We obtained the light curves of these stars from the Full Frame Images (FFIs) by using the PATHOS pipeline described in detail by Nardiello et al. (2019) and also reported in Section 2.1. We selected the best aperture for each target comparing their mean rms distributions, as described in detail by Nardiello et al. (2020) and Messina et al. (2022).

Appendix B.3: Rotation period

We analyzed the TESS light curves of all 55 stars to measure the rotation period. Details on the procedure can be found in Messina et al. (2022). Briefly, we used three different methods: Generalized Lomb-Scargle (GLS; Zechmeister & Kürster 2009), CLEAN (Roberts et al. 1987) and AutoCorrelation Function (ACF; McQuillan et al. 2013) in order to provide a "grade" of confidence on the correctness of the measured rotation periods ("A" if the three methods provided a similar value; "B"

when only two methods found a similar value; "C" when period estimates differed across all three methods). We selected only rotation periods with grade "A" and "B" and with False Alarm Probability (FAP) $< 0.1\%$. We followed the method used by Lamm et al. (2004) to compute the error associated with the period determination. On a total sample of 55 stars, we measured 34 periods with grade A and 7 periods with grade B (see Table B.1). Data from the literature have been considered as well. Five targets have the rotation measured by HATNET (Hartman et al. 2011), two by Mearth (West et al. 2015) one by ASAS (Kiraga 2012), two by ASAS-SN (Jayasinghe et al. 2018), five by KELT (Oelkers et al. 2018), and one by Mascara (Burggraaff et al. 2018). Overall, the rotation period is measured for 47 targets.

Appendix B.4: Other age indicators

Additional age diagnostics were derived from the literature or from available high-resolution spectra. For TOI-2076, we exploited the spectra gathered by the GAPS program, analyzed the same way as those of TOI-1807, being published in a forthcoming paper in preparation. We also analyzed reduced spectra available in public archives: SOPHIE¹⁸ (3 objects), FEROS¹⁹ (1 object), and HIRES/Keck²⁰ (6 objects)

The resulting measurements of Li 6708Å doublet are listed in Table B.1.

Appendix B.5: A plausible group of coeval and comoving objects

From the comparison of the age indicators, the results is that TOI-1807, TOI-2076, and additional 24 comoving stars exhibit similar ages, intermediate between Pleiades and Hyades. Using Group X (age $300 \pm 60 \text{ Myr}$, Messina et al. 2022) and the open cluster NGC 3532 (age $415 \pm 30 \text{ Myr}$ Dias et al. 2021) as comparisons, the estimated age for these stars is of $300 \pm 80 \text{ Myr}$. Other 32 stars among the comoving objects appear to have different ages (in most cases, older) and are then classified as kinematic interlopers. Finally, 18 stars have an ambiguous status (mostly because of lack of information beside kinematics or because of the uncertainty in the age determination).

The 23 kinematically selected stars which result to have an age similar to TOI-1807 and TOI-2076 are moderately clustered on the sky (Fig. B.1) and are at a similar distance (median 42.1 pc, rms 7.4 pc). The other three stars (ASAS J041255-1418.6, HD 34652, and UCAC2 9643914) are located in a different region of the sky. The stars classified with ambiguous or discrepant age are instead scattered over the whole sky.

Appendix B.6: Individual objects

Description of individual systems is provided below

HD 123 = V640 Cas A = TIC 604446831 Triple system, formed by a G2 + G8 star separated by $1.44''$, with the secondary being itself a spectroscopic binary. After a deblending of 2MASS magnitude, the star lies above similar-color members of Group X in the period-color diagram, implying an age slightly older than 300 Myr and similar to Hyades. Li EW (Takeda & Kawanomoto 2005) and $\log R'_{HK}$ (Boro

¹⁸ <http://atlas.obs-hp.fr/sophie/>

¹⁹ <http://archive.eso.org/cms.html>

²⁰ <https://koa.ipac.caltech.edu/cgi-bin/K0A/>

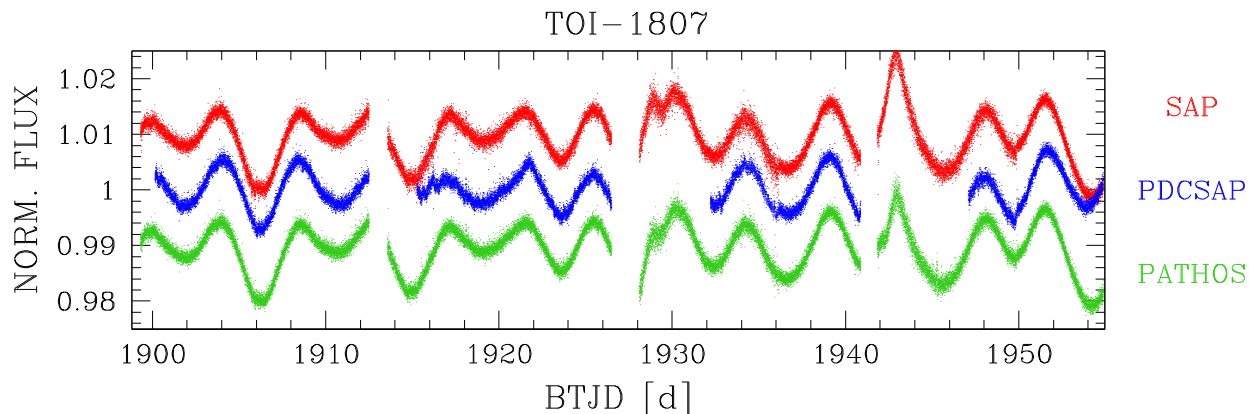


Fig. A.1. Comparison between the raw SAP light curve of TOI-1807 (in red) and the same light curve corrected by using the PDC (in blue) and the PATHOS (in green) pipelines.

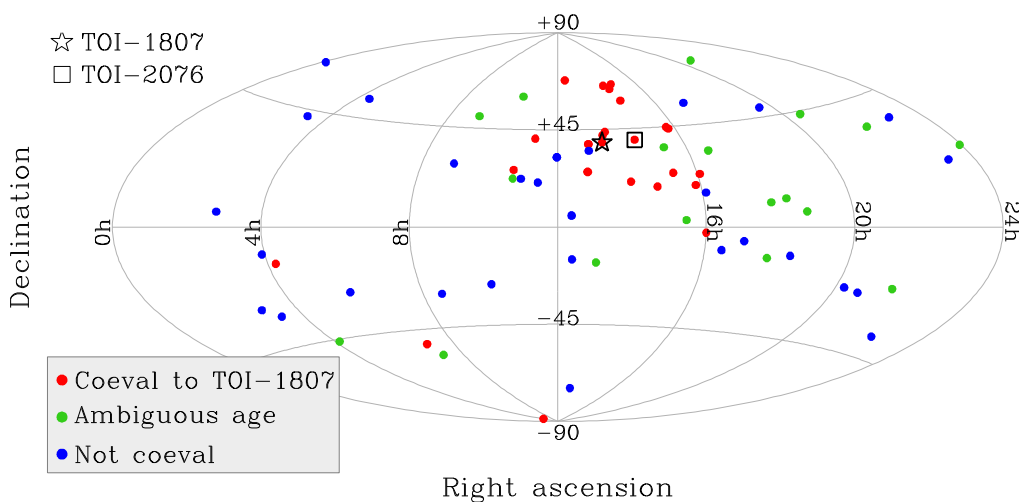


Fig. B.1. Right ascension and declination for the kinematically selected stars with U,V,W close to that of TOI-1807 and TOI-2076. Stars coeval to TOI-1807 and TOI-2076, not coeval, or with undetermined age are plotted with different colors. TOI-1807 and TOI-2076 are indicated with a star symbol and a square, respectively.

Saikia et al. 2018) are also compatible with this age assignment. Fuhrmann (2008) noted instead a lower activity level for the secondary, suggesting that the primary is somewhat rejuvenated by accretion of angular momentum. Independently of this speculation, the system results older than TOI-1807.

UCAC4 180-001659 = TIC 231019115 M1 dwarf, proposed as a member of Tuc-Hor association by Riedel et al. (2017). However, in the period-color diagram, this target lies significantly above similar-color members of Group X, implying an age older than 300 Myr. Also, Li non detection and gravity from 7699 Å line (Riedel et al. 2017) are compatible with a main sequence object, not particularly young. RV by Riedel et al. (2017) and *Gaia* EDR3 are discrepant at 2.5σ level, suggesting the possibility that the star is an SB. BANYAN group assignment using *Gaia* data also supports a field object (87% probability). We conclude that the star is a field M dwarf somewhat older than TOI-1807.

HD 17250C = TIC 318841149 Isolated component (separation 494'') of a triple system. The other two components (HD17250 A and B) form a tight pair (separation 1.9'') and do not satisfy our kinematic selection criteria for objects co-

moving with TOI-1807 and TOI-2076. The system has been considered in the literature as a possible member of Tuc-Hor association (e.g., Zuckerman et al. 2011). Our own kinematic analysis with BANYAN Σ and *Gaia* data yields membership probabilities for Tuc-Hor of 98.7% and 89% for HD 17250 A and C, respectively. HD 17250 C is expected to be a M2.5 star from its colors. Its position on color-magnitude diagram (CMD) is well above the main sequence and compatible with the age of Tuc-Hor, unless it is itself an unresolved binary. Instead, in the period-color diagram, HD 17250 C, with period graded B, is well above the sequence of Group X members, suggesting an age much older than 300 Myr. Considering the uncertainty in the period determination and the other evidence supporting the membership to Tuc-Hor association, we conclude that this system is likely to be much younger than TOI-1807.

HD 18414 = TIC 91556441 TESS data show a significant but irregular non-periodic variability. There are no indication of youth in the literature beside kinematics.

Wolf 140 = TIC 416098108 M3.5 star. The long rotation period reported by Newton et al. (2016) and the low levels of

H α activity (Lu et al. 2019; Cifuentes et al. 2020) indicate that this object is an old interloper.

HD 20776 = TIC 44628969 The TESS light curve of this target appeared non variable during the time span of observations. The low $v \sin i$ of the star (1.0 km s^{-1} , Nordström et al. 2004) and lack of X-ray detection also support an old age.

2MASS J03550477-1032415 = TIC 55441420 Ultra-cool object (spectral type M8.5) with signatures of low gravity (Gagné et al. 2015). A very young age is also supported by the strong Li line and activity (Shkolnik et al. 2017). The TESS light curve of this target appeared non variable during the time span of observations. The star is flagged as possible member of β Pic MG in the above studies while our own BANYAN analysis with *Gaia* EDR3 parameters supports membership to Columba association (92%). Independently on the membership assignment, the object is much younger than TOI-1807.

HD 26413 = TIC 152473055 Triple system, formed by a F3 primary with one companion (B) at 0.8-1.5'' and another one (C) at 18''. From absolute mag, B and C are expected to be a K2/K3 and a M3 star, respectively. The RV of the primary from *Gaia* DR2 and Nordstrom & Andersen (1985) differ by 13.2 km s^{-1} , suggesting the presence of a fourth component. The very short photometric periodicity ($P = 0.395 \text{ d}$) likely refers to the brightest F3 component and arises from flux rotational modulation (it is compatible with the observed $v \sin i$ and stellar radius) rather than from pulsations, considering the significant evolution of the light curve amplitude during the TESS observations; the last likely due to active region growth and decay. The position on the CMD is slightly above main sequence implying an age older than TOI-1807, unless the photometry is significantly contaminated by the unknown spectroscopic component. The position on the period-color diagram is roughly consistent with that of Group X, although the period distribution is poorly defined at these blue colors.

ASAS J041255-1418.6 = TIC 332660818 It is a M1 star. We measured from TESS photometry a rotation period $P = 7.3 \pm 1.0 \text{ d}$ in agreement with the literature value $P = 7.30 \text{ d}$ from ASAS (Kiraga 2012). The rotation period is fully compatible with that of similar-color members of Group X, implying an age of about 300 Myr. There is no lithium to be seen in the archive FEROS spectrum we analyzed, as also found by Bowler et al. (2019), indicating age older than about 100 Myr. High levels of chromospheric and coronal activity have been measured (Bowler et al. 2019; Žerjal et al. 2017).

HD 34652 = TIC 317383399 We measured from TESS photometry a rotation period $P = 1.753 \pm 0.026 \text{ d}$ and a secondary period (of comparable power in both GLS and CLEAN periodograms) $P = 1.527 \text{ d}$ likely arising from surface differential rotation. In the period-color diagram, this lies among similar-color members of Group X, then compatible with an age of about 300 Myr. The isochrone fitting (using PARAM, da Silva et al. 2006) yields an inconclusive value of $970 \pm 800 \text{ Myr}$. The X-ray emission ($R_X = -4.89$) is close to the median value of Hyades members of similar color, but compatible with fairly broad range of ages. We conclude that this star may have a similar age to TOI-1807 but the limited sensitivity of age diagnostics for mid-F stars does not allow us firm conclusions.

HD 27857 = TIC 470480305 Moderately young G5 star. Both the rotation period from TESS photometric time series and Li EW by Kim et al. (2016) indicate an age much older than TOI-1807 and slightly older than the Hyades.

UCAC2 20545888 = TIC 33062967 Emission-line M dwarf. In the period-color diagram, TIC 33062967 lies significantly above similar-color members of Group X, implying a likely older age than 300 Myr.

UCAC2 9643914 = TIC 238088359 M dwarf with large RUWE in *Gaia* EDR3 (11.0) indicating a spatially unresolved binary. We measured from TESS photometry a rotation period $P = 2.82 \pm 0.10 \text{ d}$ superimposed to a secondary period of about 20 d. The position in the period-color diagram is consistent with similar-color members of Group X. The star has also prominent X-ray emission ($R_X = -3.2$).

GSC 08558-01964 = TIC 294154590 Close binary star (M1.5+M4, projected separation 1.1'', Bergfors et al. 2010) The star results quite active in H α , is X-ray bright (Riaz et al. 2006) and with fast rotation from $v \sin i$ measurement (Malo et al. 2014). Instead, there are no determinations of the rotation period. Therefore, the star may have similar age to TOI-1807 and Group X but considering the spectral type and the additional uncertainties due to its binarity, we are not able to put tight constraints on system age.

HD 72687 = TIC 283397452 We measured from TESS photometry a rotation period $P = 3.87 \pm 0.31 \text{ d}$ in agreement with the literature value $P = 3.84 \text{ d}$ from KELT (Oelkers et al. 2018). Considering additional age diagnostics such as lithium (Torres et al. 2006), this star appears younger than similar-color members of Group X.

HD 76332 = TIC 126312524 Moderately active star and binary system, as revealed by the large RUWE in *Gaia* EDR3 and, more recently, by the RV + astrometry analysis ($a = 78 \text{ mas}$, mass of companion $0.47 M_\odot$ Dalal et al. 2021). We measured from the TESS photometry a rotation period $P = 10.7 \pm 1.1 \text{ d}$ in agreement with the literature value $P = 13.25 \text{ d}$ from KELT (Oelkers et al. 2018). The position in the color-period diagram suggests an age significantly older than 300 Myr. This is also supported by the Li EW measured by us on SOPHIE spectra ($49.9 \pm 1.0 \text{ m}\text{\AA}$), which is below that of Hyades stars of similar color.

TYC 3430-1344-1 = TIC 456344030 Its position in the period-color diagram is slightly above similar-color members of NGC 3532, implying an age slightly older than 300 Myr. There are no additional data on age indicators to further constrain the system age.

TYC 6621-759-1 = TYC 309024402 Star with large RUWE in *Gaia* EDR3 (7.30) and then probable tight binary system. Its position in the period-color diagram is significantly above similar-color members of NGC 3532, implying an age much older than 300 Myr. There are no other indication of youth in the literature beside kinematics.

TYC 4144-944-1 = TIC 355868825 We measured, based on TESS photometry, a rotation period $P = 11.4 \pm 2.9 \text{ d}$ in agreement with the literature value $P = 12.75 \text{ d}$ from KELT (Oelkers et al. 2018). The rotation period is slightly slower than similar-color members of Group X, indicating a slightly older age than 300 Myr.

40 LMi = TIC 241197867 It is a A4Vn star identified as close binary by Galicher et al. (2016). It also has significant $\Delta\mu$ signature. From the H band magnitude, the companion is expected to be a M2.5/M3 star from Mamajek tables. The system has also an X-ray counterpart from *Chandra* observations. Assuming this is entirely originating from the late type companion, we estimated $R_X = -2.8$, compatible with both Pleiades and Hyades early M dwarfs. Isochrone age is $300 \pm 200 \text{ Myr}$. We conclude that the star has an age of a few hundreds of Myr, then compatible with the age of TOI-1807, but with significant uncertainty.

- UCAC4 562-049479 = TIC 95776155** Its position in the period-color diagram is consistent with similar-color members of NGC 3532, implying an age of about 300 Myr.
- LP 373-35 = TIC 84925818** We measured from TESS photometry a rotation period $P = 18 \pm 6$ d in rough agreement with the literature values $P = 23.8$ d from MEarth (West et al. 2015; Newton et al. 2016). Its position in the period-color diagram suggests an age much older than that of Group X.
- 2MASS J11155546+4049569 = TIC 450332591** We measured from TESS photometry a rotation period $P = 4.72 \pm 0.41$ d in agreement with the literature values $P = 4.764$ d from HATNET (Hartman et al. 2011). Its position in the period-color diagram suggests an age similar to that of Group X. The X-ray luminosity ($R_X = -2.8$) and the moderate $H\alpha$ emission are consistent with this age estimate.
- HD 99419 = TIC 3901189** Rotation period is not available. Indicators from archive SOPHIE spectra (EW Li well below the Hyades locus, slow $v \sin i_*$, low RV scatter, modest chromospheric emission) indicate an age significantly older than TOI-1807.
- HD 103928 = TIC 99302268** and **HD 103928B = TIC 99302269** Binary system with components separated by $7''$. The primary is a late A/early F star, while the estimated spectral type of the secondary from absolute magnitude and colors is around M1-M2.5. A photometric period of 0.70 d is reported by Koen & Eyer (2002), possibly due to the pulsations of the primary. Assuming that all the X-ray flux is originating from the secondary, the X-ray luminosity is below the loci of Hyades and Pleiades M dwarfs, suggesting an older age, although possibly compatible with the lower edge of their distributions. Isochrone fitting of the primary is also inconclusive (550 ± 450 Myr). There is then some indication that the system is older than TOI-1807, although the same age cannot be ruled out considering the large uncertainties.
- 17 Vir = TIC 377227654** and **17 VirB** Visual binary, formed by a F8 and a K5 star. The low levels of chromospheric and coronal activity (e.g., Wright et al. 2004) and the 3.1 ± 0.7 Gyr isochrone age (Aguilera-Gómez et al. 2018) show that this pair is an old kinematic interloper.
- TYC 4394-114-1 = TIC 148910632** K star flagged as a candidate member of the AB Dor association by Schlieder et al. (2012); however our own BANYAN analysis with *Gaia* parameters rules out membership in any known association. The position on the color-period diagram is consistent with similar-color members of Group X, implying an age of about 300 Myr.
- UCAC4 376-064366 = TIC 40560697** The periodogram analysis of TESS data did not provide any reliable rotation period. There is no indication of youth in the literature beside kinematic. This M dwarf is then probably older than TOI-1807.
- LX Com = HIP 62758 = HD 111813 = TIC 450335652** and **BD+26 2401 = HIP 62794 = TIC 156514310** They form a very wide common proper motion pair (separation $373'' = 14150$ au). BD+26 2401 is an SB2 with orbital solution (period 19.436 ± 0.001 d Halbwegs et al. 2012). This is likely responsible for the significant RUWE. Both stars are X-ray sources, with R_X of -4.59 and -4.55 for LX Com and BD+26 2401, respectively. For LX Com we measured on TESS data a rotation period of $P = 3.9 \pm 0.25$. Since the light curve is clearly double dip, it implies that the rotation period is $P \times 2 = 7.8$ d in good agreement with Strassmeier et al. (2000) who derived a period of 7.74 d. For BD+26 2401, we measured a period of $P = 20.3 \pm 3$ d using GLS and CLEAN methods, which may be related to the orbital period of the binary. We thus did not consider it for dating purposes. We instead rely on indicators of LX Com, which are all compatible with an age intermediate between Hyades and Pleiades.
- L68-145 = TIC 361397288** This star is moderately active (Žerjal et al. 2017) but it lies well above the period distribution of Group X members, being likely significantly older (most likely with age similar to Hyades and Praesepe).
- GJ 490A = TIC 950125199** Quadruple system formed by two pairs of M dwarfs separated by $16''$. GJ 490A and GJ 490B have projected separations of $0.10''$ and $0.17''$, respectively (Bowler et al. 2015). We measured from TESS photometry a primary rotation period $P = 3.37 \pm 0.21$ d in agreement with the literature values $P = 3.17$ d from Wright et al. (2011) and $P = 3.36$ d from Norton et al. (2007), as well as a secondary period $P = 0.4681$ d, which likely belongs to one of the unresolved secondary components. This star lies well inside the period distribution of Group X members. However, a quite broad range of ages are possible considering the rotation distribution of M dwarfs with measured ages. The system was also proposed to be a member of younger groups, such as Tuc-Hor (Shkolnik et al. 2012) and AB Dor (Malo et al. 2013). BANYAN analysis using *Gaia* EDR3 parameters indicates a field object. Kinematic parameters and group assignment should be taken with caution considering the multiplicity of the system. The marginal detection of lithium on HIRES/Keck spectra, although uncertain because of the difficulty in continuum placement for such cool object, supports an age significantly younger than that of TOI-1807.
- HD 112733 = TIC 17740825** and **HD 112733B = TIC 17740827** They form a wide pair ($36.0'' \sim 1500$ au), with the secondary being itself a SB in short-period orbit (Gálvez et al. 2006; Strassmeier et al. 2012). The system was flagged as possible member of Hercules-Lyra association by Eisenbeiss et al. (2013). They note a small (about 2 km s^{-1}) discrepancy in W velocity with respect to the bulk of the association. The age indicators discussed by Eisenbeiss et al. (2013) are in agreement with the adopted age for Her-Lyr. The system was considered in several works on young stars and planet searches with ages ranging from 100 Myr (Meshkat et al. 2017), 250 Myr (Vigan et al. 2017), 260 Myr (Brandt et al. 2014). From the TESS time series, where the two components are unresolved, we measured a photometric period of 5.15 ± 0.48 d days, while Strassmeier et al. (2012) reported a tentative $H\alpha$ period of 2.3 days. The TESS light curve is less noisy for an aperture centered on the secondary, suggesting that the periodicity belongs to this component. Assuming the photometric period belongs to the secondary, the position on period-color diagram would imply an age younger than that of the Pleiades. An age similar to Group X and TOI-1807 would be possible if the rotational curve is double-dip and the rotation period is actually two times the observed one. Even more likely, the presence of the close companion should have altered the rotation of the star through tidal effects and indeed our photometric period is marginally consistent with the orbital period by Griffin & Filiz Ak (2010) and Strassmeier et al. (2012). Focusing on lithium EW, we estimate a most probable age of 250 Myr but compatible with the 300 Myr of Group X within errors.
- HD 113414 = TIC 1727745** Li EW by Waite et al. (2011) and X-ray emission ($R_X = -4.23$) are close to the locus of Pleiades, suggesting a similar age. In the period-color diagram, the star is close to the sequence of members of Group X, but the age sensitivity of rotation period is quite limited

for F7/F8 stars and the measurement is also compatible with Pleiades. We conclude that the star is likely younger than Group X.

HIP 65775 = HD 117378 = TIC 288405352 F9.5 star, with astrometric acceleration and significant proper motion differences (Makarov & Kaplan 2005). The RV from Nordström et al. (2004) (2 epochs) and *Gaia* DR2 agree within errors. The star is active, as resulting from X-ray and chromospheric emission (Gray et al. 2003). Our rotation period from TESS light curve (4.38 d) is fully compatible with the expectation from the activity level and projected rotational velocity. The position on the color-period diagram is consistent with similar-color members of Group X, implying an age of about 300 Myr. The Li EW measured by us on HIRES/Keck spectra is intermediate between Hyades and Pleiades median values for stars of similar color, fully supporting the 300 Myr age.

TYC 3032-368-1 = TIC 288487378 Triple system, with an isolated primary at 20'' from a close pair of very low mass stars (*Gaia* **1501788886175060608** and *Gaia* **1501788881878538496**). Only the primary is included in the *Gaia* Collaboration (2021b) catalog. We derived a rotation period of 12.2 days, which most likely belongs to the primary considering the faintness of the low mass companions ($\Delta G > 7$). The position on the color-period diagram is consistent with similar-color members of Group X, implying an age of about 300 Myr. The X-ray luminosity is intermediate between Hyades and Pleiades of similar color and compatible with the proposed age.

HIP 68732 = TIC 135154868 Triple system, as the comoving object **StKM 1-1119** at 62'' is itself a close pair (sep 1''). The position of the primary on the color-period diagram is consistent with similar-color members of Group X, implying an age of about 300 Myr. The X-ray source 1RXS J140409.4+204449 lies at 18'' from the secondary and 45'' from the primary. The X-ray luminosity is a bit lower than expected from the rotation age.

RX J1419.0+6451 = TIC 166087190 M3 star proposed as a member of AB Dor MG by Malo et al. (2013). Membership analysis with BANYAN including *Gaia* astrometry instead leads to field object classification. The position on the color-period diagram is consistent with similar-color members of Group X. The star has also prominent X-ray emission ($R_X = -3.03$).

TOI-2076 = TIC 27491137 Host of a multi-planet system (Hedges et al. 2021; Osborn et al. 2022). It will be discussed in a forthcoming paper. For the purpose of this work, we note that in the period-color diagram, TIC 27491137 lies in the same position of similar-color members of Group X, implying a likely age of 300 Myr. The other age indicators are also compatible with an age close to that of TOI-1807.

HD 127821 = TIC 166178883 Mid F-type star with IR excess due to debris disk as a separation of about 210 au (Rhee et al. 2007). The position on CMD is compatible with TOI-1807 and Group X age. The short photometric period (0.57 days) could also be compatible with those of Group X members, although the origin (pulsation vs rotation) cannot be conclusively determined from available data. If due to rotation, coupled with the $v \sin i_* = 55.6 \text{ km s}^{-1}$ (Reiners 2006), a stellar inclination of 29 deg is derived. The X-ray emission from ROSAT and $\log R_{HK}$ (Schröder et al. 2009) are also compatible with the Group X age although these have limited age sensitivity for mid-F type stars.

HD 129425 = TIC 158496710 The position on the color-period diagram is consistent with similar-color members of Group

X, implying an age of about 300 Myr. The Li EW we measured on SOPHIE spectra (79.8 mÅ) is also consistent with this age assignment.

HD 130460 = TIC 282855338 The highly significant photometric period is most likely due to rotational modulations, although pulsations cannot be ruled out, considering the spectral type of the star. If due to rotation, it would imply an inclination of about 45 deg when coupled with the observed $v \sin i$ (28 km s^{-1} , Nordström et al. 2004). The position on the color-period diagram is consistent with similar-color members of Group X, implying an age of about 300 Myr. The star was observed with *Spitzer*, with no IR excess found (Trilling et al. 2008). The isochrone age is inconclusive. The X-ray emission ($R_X = -4.69$) is slightly above the median values of Hyades members of similar colors.

BD+18 2930 = TIC 345299634 There is no rotation period available. The X-ray emission ($R_X = -4.44$) is intermediate between Hyades and Pleiades and $v \sin i_*$ (Nordström et al. 2004) is compatible with the Group X rotation sequence for an orientation close to edge-on. Therefore, we consider the star as a possible but unconfirmed object coeval to TOI-1807.

TYC 2569-1485-1 = TIC 272610678 The three rotation period search methods provide different values (grade C); however, a visual inspection of the light curve shows the $P = 9.89$ d the most convincing and in fair agreement with the literature value $P = 11.82$ d from HATNET (Hartman et al. 2011), which position this target consistently with the similar-color members of Group X.

TYC 2025-810-1 = TIC 357500019 The rotation period is slightly slower than similar-color members of Group X whereas fits well into the distribution of the NGC 3532 members.

HD 137897 = TIC 371267644 Visual binary (separation 5'', ΔG 5.63 mag). There are no specific indications of youth beside kinematics.

UCAC4 675-059372 = TIC 156000373 We measured from TESS photometry a rotation period $P = 2.20 \pm 0.04$ d in very good agreement with the literature values $P = 2.20$ d from HATNET (Hartman et al. 2011) and $P = 2.2047$ d from ASAS-SN (Jayasinghe et al. 2018). This star appears slightly faster than similar-color members of Group X, whereas it may belong to those stars transiting from the fast to the slow rotation sequence.

TYC 3059-299-1 = TIC 282941472 We measured from TESS photometry a rotation period $P = 6.58 \pm 0.40$ d in good agreement with the literature values $P = 6.61$ d from ASAS-SN (Jayasinghe et al. 2018) and $P = 6.46$ d from HATNET (Hartman et al. 2011). This star appears marginally faster than similar-color members of Group X, whereas it may belong to those stars transiting from the fast to the slow rotation sequence. The star is also very bright in X ray ($R_X = -3.26$).

UCAC4 544-056450 = TIC 307915958 The position on the color-period diagram is consistent with similar-color members of Group X, implying an age of about 300 Myr.

2MASS J16001203-0230594 = TIC 168457615 The activity and gravity indicators (Bowler et al. 2019; Žerjal et al. 2017), the lithium non-detection and the position in the CMD close to MS are consistent with an age of a few hundreds of Myr but we do not have a determination of rotation period to fully confirm and refine it.

LSPM J1604+2331 = TIC 445889890 It is a M5 star. We measured from TESS photometry a rotation period $P = 0.756 \pm 0.005$ d in good agreement with the literature value $P = 0.7564$ d from MEarth (West et al. 2015). With respect to

similar-color members of Group X, this star appears slower and therefore likely older. However, it is possible that the observed colors are altered by binarity, as the star has a very large RUWE (9.8) in *Gaia* EDR3. ROBO-AO observations by Lamman et al. (2020) did not resolve the binary. The position on CMD is slightly above the main sequence, possibly due to the contribution by the unresolved companion. The star has also high levels of magnetic and coronal activity. Overall, we consider it as a possible but unconfirmed coeval object to TOI-1807 and Group X.

HD 144489 = TIC 172712253 Rotation period is not available. X-ray emission and $v \sin i_*$ (from SOPHIE archive spectra) suggest an age older than the Hyades, while Li EW is similar to Hyades member of similar color. Therefore, the star is likely older than TOI-1807.

HD 148319 = TIC 163915173 The Li EW measured by us is similar to that of Hyades members and below the expectations for a 300 Myr object. Activity measurements span fairly broad range, from $\log R_{HK} = -4.49$ to -4.62 (Jenkins et al. 2008; Butler et al. 2017; Gomes da Silva et al. 2021), which is consistent with an age close to Hyades. Finally the application of chemical abundances clock provides an age of 800 Myr (Casali et al. 2020). Therefore, the star is likely older than TOI-1807.

2MASS J16371518+3331426 = TIC 57031688 We measured from TESS photometry a rotation period $P = 11.5 \pm 1.2$ d in agreement with the literature value $P = 10.99$ d from HATNET survey (Hartman et al. 2011). Its position on the period-color diagram is significantly above similar-color members of Group X, implying an older age than 300 Myr. The star has a large RUWE (3.34) suggesting unresolved multiplicity.

BD-05 4394 = TIC 41038121 The low levels of chromospheric activity (Astudillo-Defru et al. 2017) and RV jitter (rms 2.5 m s^{-1} from archive HARPS spectra) make it likely that it is significantly older than TOI-1807.

μ **Dra = TIC 198355687** Quadruple system, formed by a pair of F6 stars (one of which is itself a SB) separated by $2''$ and an additional component (M3) at $12''$. The periodogram analysis of TESS data shows significant but irregular variability, likely because of superposition of variability of the components, which are blended in TESS observations. The system is considered part of the Castor MG by Caballero (2010). Only the primary matches our kinematic selection criteria, and there are significant proper motion difference with respect to the other components. Considering the parameters of the more isolated component C, less affected by orbital motion, we infer that this object is not comoving with TOI-1807 and the other targets identified here, although it may have similar age (likely slightly older).

TYC 5668-239-1 = TIC 418673682 There are no specific indications of youth in the literature apart for kinematics.

HD 162199 = TIC 446245637 There are no indication of youth in the literature apart for the photometric period of 0.93d reported by Oelkers et al. (2018).

2MASS J18153959+1152077 = TIC 391453943 Star with high RUWE, indicating binarity. There are no available TESS data and additional indications of youth in the literature. The age remains then unconstrained.

HD 168746 = TIC 18097734 RV planet host (Pepe et al. 2002). Confirmed old star from low levels of chromospheric and coronal activity and isochrone age.

TYC 460-624-1 = TIC 449263348 The rotation period reported by Kiraga (2012), 16.18d, is longer than Group X

members of similar color but within the distribution of NGC 3532 members. Chromospheric emission (Jeffers et al. 2018) and X-ray emission are compatible with an age intermediate between Group X and the Hyades.

KIC 11087368 = TIC 26960092 The periodogram analysis of TESS data did not provided any reliable rotation period, and a grade C was assigned. The low activity level in $H\alpha$ (Lu et al. 2019) supports the interpretation of an old interloper.

2MASS J20144598-2306214 = TIC 71480177 Active M3-M4 dwarf, considered for membership in the Tuc-Hor association by Kraus et al. (2014) but rejected on the basis of the discrepant radial velocity. Our own BANYAN analysis adopting *Gaia* ERD3 parameters also indicates a field object. The activity level and UV excess are compatible with a very young age, with the Li non detection being non conclusive considering the spectral type of the star. The position in CMD is above main-sequence, indicating a young age, similar to Tuc-Hor or slightly older. While a tidally-locked binary with similar components might also explain the observed characteristics, the object is likely much younger than TOI-1807.

1RXS J203300.7+435147 = TIC 188452312 The high RUWE indicates that the star is likely an unresolved binary. The periodogram analysis of TESS data did not reveal any reliable rotation period. The X-ray luminosity is at lower bound of Pleiades members of similar colors. This is consistent with a 300 Myr age but with large uncertainties.

EM* StHA 182 = 2MASS J20434114-2433534 = TIC 269940990 This star is identified as a member of β Pic MG in several literature sources (e.g., Bell et al. 2015). Application of BANYAN Σ on-line tool including *Gaia* EDR3 data supports membership. The star is known to be a close binary (projected separation $1.45''$, ΔG 0.07 mag); individual spectral types M3.7 and M4.1). We derived from TESS data a rotation period of 0.98 days (Grade A), similar to that derived by Günther et al. (2020) on Sectors 1-2 only. A longer period (1.610d) was instead provided by Messina et al. (2017). Its position on the period-color diagram is consistent with similar-color members of a variety of objects such as IC2391, Pleiades, and Group X. The rotation period is faster than the typical ones for β Pic MG members, but possibly compatible with few other very fast rotators members (mostly binaries). A marginally significant Li EW is measured by us on HIRES/Keck spectra ($5.3 \pm 2.5 \text{ m}\text{\AA}$). If confirmed, this would strongly support the very young age of β Pic MG members and rule out older ages (Messina et al. 2016). The position on CMD (after correction for binarity when applicable) is well above main sequence and consistent with other β Pic MG members. We then conclude that this object is significantly younger than TOI-1807 and TOI-2046.

HD 198767 = TIC 387511797 It is a G0 star with very high RUWE in *Gaia* EDR3, suggesting unresolved binarity. We measured from TESS photometry a rotation period $P = 6.19 \pm 0.07$ d in agreement with the literature values $P = 6.55$ from KELT (Oelkers et al. 2018) and $P = 6.21$ d from Mascara (Burggraaff et al. 2018). This star appears slightly slower and therefore a bit older than similar-color members of Group X. The Li EW measurement (Wichmann et al. 2003) is intermediate between Hyades and Pleiades loci, closer to the latter one. The X-ray luminosity is intermediate between Pleiades and Hyades.

2MASS J21364848-2200541 = TIC 441026957 The rotation period is slower than similar-color members of Group X whereas still compatible with members of NGC 3532.

BD+34 4580 = TIC 236671835 We measured from TESS photometry a rotation period $P = 10.1 \pm 1.0$ d. We note that the rotation period $P = 1.238$ d reported by Oelkers et al. (2018) is likely a beat of the rotation period measured by us. In the period-color diagram this star appears marginally older than 300 Myr, possibly compatible within errorbars.

UCAC4 260-199238 = TIC 152889010 The periodogram analysis of TESS data did not provide any reliable rotation period. There is no other indication of youth in the literature beside the kinematics.

BD+36 4976 = TIC 418960381 This star is slower than similar-color members of Group X and therefore, likely older than 300 Myr.

UCAC4 558-143573 = TIC 436525094 Low activity in $H\alpha$ is reported by Lu et al. (2019), suggesting a moderately old age.

BD+24 4863 = TIC 269786865 There are no TESS data available and no other indication of youth in the literature beside kinematics. The age of this star is then unknown.

Appendix C: Combined analysis of HARPS-N and iSHELL data sets

Appendix C.1: Observations and data reduction of iSHELL data

We observed TOI-1807 with the iSHELL spectrograph (Rayner et al. 2016) on the NASA Infrared Telescope Facility. 232 exposures were recorded in KGAS mode ($2.18 - 2.47 \mu\text{m}$) with an integration time of 300 seconds on 23 nights between June 14th, 2020 – January 26th, 2022. The median S/N per spectral pixel is ≈ 30 and ranges from 20–40 due to variable weather conditions at Maunakea. Spectra are reduced and RVs are computed using updated methods to those described in Cale et al. (2019). The RVs from individual exposures and echelle orders were co-added within a night to generate one RV per night TOI-1807 was observed. In doing so, we discarded two exposures from UT date February 9th, 2021, all exposures from June 10th, 2021, and two exposures from June 15th, 2021 due to low S/N (< 15) from poor weather conditions at Maunakea. The median error bar of the co-added iSHELL RVs is 8.8 m s^{-1} .

Appendix C.2: Analysis of HARPS-N and iSHELL RVs

We run PyORBIT both on the HARPS-N and iSHELL data, by using the same configuration and priors described in Sect. 5.1 (case 1), but excluding the modeling of the light curve. In this analysis we excluded the iSHELL RV measurements obtained between May 28th, 2021 and June 6th, 2021, because characterized by anomalous high values ($\sim 100 \text{ m s}^{-1}$ above the mean iSHELL RVs); we also compared these measurements with HARPS-N RVs collected in the same days and we have had confirmation that they are affected by some kind of systematic. The results of the modeling are reported in Table C.1. The adopted iSHELL RVs follow the trend due to the stellar activity, as shown in Fig. C.1; because of the large errors, the iSHELL RVs did not contribute to the measurement of the planet parameters and for this reason, we decided not to use them for the analysis of our work.

Appendix D: GP framework results with different tools

We compared the results obtained with the GP framework modeling implemented in PyORBIT (Sect. 5.2), with those obtained (by using the same initial conditions) with the original software by Rajpaul et al. (2015) and with the modeling obtained with `pyaneti` (Barragán et al. 2022a). The comparison is reported in Table D.1. All the results are in agreement within the errors.

Appendix E: Spectroscopic time series

The spectroscopic time series (RV, BIS, $\log R'_{\text{HK}}$, see tables E.1, E.2, and E.3) will be available in electronic format as supplementary material of the paper.

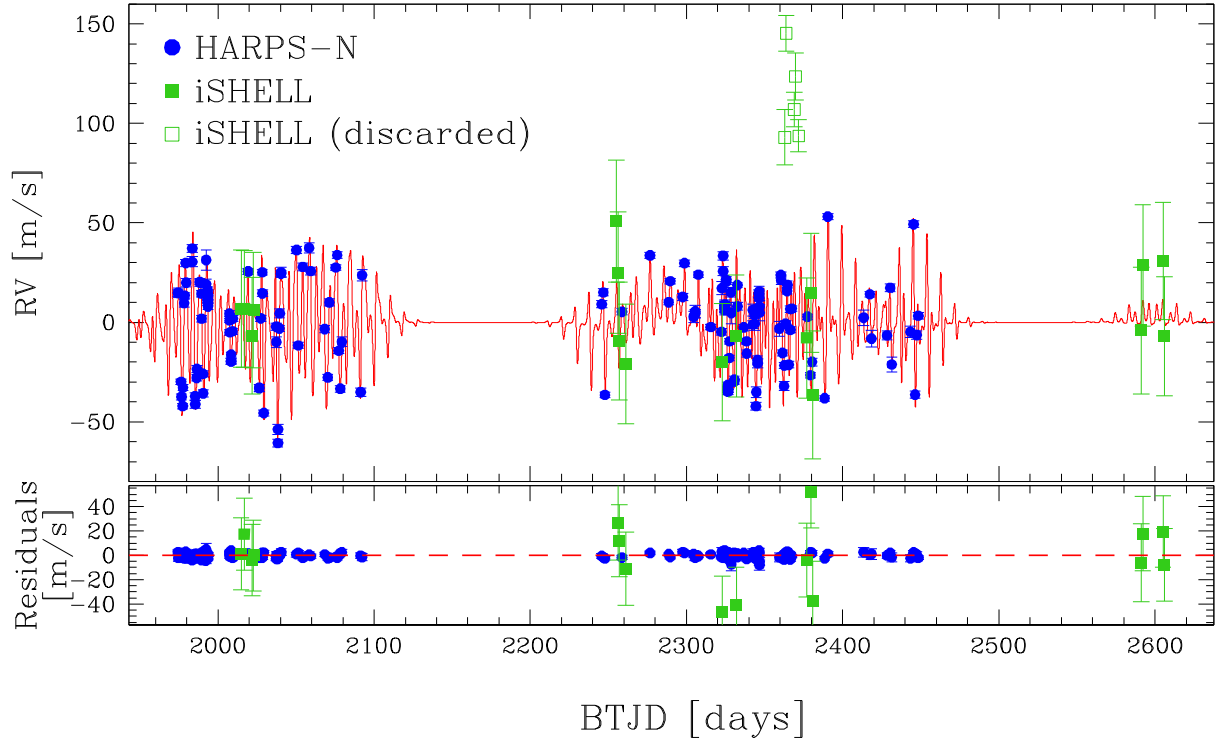


Fig. C.1. Joint analysis of HARPS-N and iSHELL RVs. Top panel shows the activity modeling of HARPS-N (blue points) and iSHELL (green squares) data by using the same configuration used for case 1, as described in Sect. 5.1. Empty squares represent the iSHELL measurements we discarded (see text for details). Bottom panel illustrates the residual after subtracting the model (shown in red in top panel).

Table C.1. Priors and results of the model of planet b from the analysis of combined HARPS-N and iSHELL spectroscopic series.

Stellar activity			
Parameter	Unit	Prior	Value
Rotational period (P_{rot})	days	$\mathcal{U}(8.0, 10.0)$	8.89 ± 0.09
Decay Timescale of activity (P_{dec})	days	$\mathcal{U}(10.0, 100.0)$	$14.3^{+1.2}_{-1.2}$
Coherence scale (w)	$0.26^{+0.03}_{-0.02}$
Amplitude of the RV signal (HARPS-N)	m/s	$\mathcal{U}(0.01, 1500.00)$	$25.2^{+2.6}_{-2.2}$
Amplitude of the RV signal (iSHELL)	m/s	$\mathcal{U}(0.01, 1500.00)$	$50.1^{+19.2}_{-23.6}$
Uncorrelated HARP-N RV jitter ($\sigma_{\text{jitter}}^{\text{RV,HARPS-N}}$)	m s^{-1}	...	$0.69^{+0.53}_{-0.45}$
HARPS-N RV offset ($\gamma^{\text{RV,HARPS-N}}$)	m s^{-1}	...	-6838.3 ± 4.2
Uncorrelated iSHELL RV jitter ($\sigma_{\text{jitter}}^{\text{RV,iSHELL}}$)	m s^{-1}	...	$42.9^{+20.00}_{-17.8}$
iSHELL RV offset ($\gamma^{\text{RV,iSHELL}}$)	m s^{-1}	...	-1.0 ± 17.6
Planet b			
Parameter	Unit	Prior	Value
Orbital Period (P_b)	days	$\mathcal{U}(0.549, 0.550)$	$0.549418^{+0.000043}_{-0.000046}$
Central time of the first transit ($T_{0,b}$)	BJD	$\mathcal{U}(2458899.3, 2458899.4)$	$2458899.330875^{+0.03}_{-0.02}$
Orbital eccentricity (e_b)		fixed	0
Semi-major-axis-to-stellar-radius ratio ((a_b/R_*))	3.7 ± 0.2
Orbital Semi-major axis (a_b)	au	...	0.0120 ± 0.0003
RV semi-amplitude (K_b)	m s^{-1}	$\mathcal{U}(0.01, 10)$	$2.31^{+0.46}_{-0.49}$
Planetary mass ($M_{p,b}$, $i = 82 \pm 2$ deg)	M_{\oplus}	...	2.45 ± 0.52

Table D.1. Comparison between the results obtained with GP framework modeling implemented in different software.

Parameter	Unit	Rajpaul et al. (2015)	pyaneti	PyORBIT
Uncorrelated RV jitter ($\sigma_{\text{jitter},0}^{\text{RV}}$)	m s ⁻¹	0.23 ^{+0.01} _{-0.26}	0.70 ^{+0.60} _{-0.50}	0.79 ^{+0.51} _{-0.49}
RV offset (γ_0^{RV})	m s ⁻¹	-6839.4 ± 0.8	-6839.5 ± 1.2	-6839.6 ± 1.1
Uncorrelated BIS jitter ($\sigma_{\text{jitter},0}^{\text{BIS}}$)	m s ⁻¹	12.31 ^{+0.71} _{-0.84}	12.30 ^{+0.8} _{-0.8}	12.30 ^{+0.83} _{-0.76}
BIS offset (γ_0^{BIS})	m s ⁻¹	33.8 ± 1.1	34.0 ± 1.5	34.0 ± 1.4
Uncorrelated log R' _{HK} jitter ($\sigma_{\text{jitter},0}^{\log R'_{\text{HK}}}$)		0.0133 ^{+0.0009} _{-0.0010}	0.0130 ^{+0.0010} _{-0.0010}	0.0132 ^{+0.0010} _{-0.0009}
log R' _{HK} offset ($\gamma_0^{\log R'_{\text{HK}}}$)		-4.359 ± 0.001	-4.360 ± 0.003	-4.360 ± 0.003
V_c	m s ⁻¹	0.9 ^{+1.7} _{-1.7}	-1.4 ^{+2.3} _{-2.2}	1.2 ^{+1.9} _{-1.9}
V_r	m s ⁻¹	25.0 ^{+2.4} _{-3.1}	28.5 ^{+4.5} _{-3.7}	27.8 ^{+4.3} _{-3.4}
B_c	m s ⁻¹	-1.7 ^{+1.5} _{-1.5}	1.9 ^{+1.9} _{-1.8}	-1.9 ^{+1.7} _{-1.8}
B_r	m s ⁻¹	-21.2 ^{+2.8} _{-2.3}	-24.4 ^{+3.4} _{-4.1}	-23.8 ^{+3.2} _{-3.9}
L_c		-0.0010 ^{+0.0018} _{-0.0015}	0.0110 ^{+0.0020} _{-0.0020}	-0.0110 ^{+0.0019} _{-0.0020}
Rotational period (P_{rot})	days	8.85 ± 0.07	8.84 ± 0.08	8.84 ± 0.08
Decay Timescale of activity (P_{dec})	days	12.41 ^{+1.10} _{-0.99}	12.90 ^{+1.20} _{-1.20}	12.85 ^{+1.15} _{-1.12}
Coherence scale (w)		0.40 ^{+0.03} _{-0.03}	0.44 ^{+0.04} _{-0.04}	0.43 ^{+0.04} _{-0.04}
Orbital Period (P_b)	days	0.549381 ^{+0.000015} _{-0.000015}	0.549388 ^{+0.000024} _{-0.000024}	0.549380 ^{+0.000015} _{-0.000016}
Central time of the first transit ($T_{0,b}$)	BJD	2458899.3449 ^{+0.0008} _{-0.0008}	2458899.3449 ^{+0.0008} _{-0.0008}	2458899.3449 ^{+0.0008} _{-0.0008}
RV semi-amplitude (K_b)	m s ⁻¹	2.53 ^{+0.36} _{-0.36}	2.49 ^{+0.38} _{-0.39}	2.48 ^{+0.38} _{-0.39}

Table E.1. First season of HARPS-N RV, BIS, and log R'_{HK} measurements of TOI-1807.

JD-2450000	RV (km s ⁻¹)	σ_{RV} (km s ⁻¹)	log R' _{HK}	$\sigma_{\log R'_{\text{HK}}}$	BIS (km s ⁻¹)	JD-2450000	RV (km s ⁻¹)	σ_{RV} (km s ⁻¹)	log R' _{HK}	$\sigma_{\log R'_{\text{HK}}}$	BIS (km s ⁻¹)
8974.46441595	-6.8233	0.0015	-4.3814	0.0029	0.0181	9008.51021374	-6.8543	0.0010	-4.3707	0.0018	0.0658
8974.61600577	-6.8231	0.0023	-4.3827	0.0054	-0.0133	9008.58962957	-6.8576	0.0010	-4.3651	0.0019	0.0617
8975.51827612*	-6.7910	0.0011	-4.3606	0.0020	-0.0020	9009.40084674	-6.8425	0.0013	-4.3648	0.0025	0.0595
8975.63956639*	-6.8383	0.0035	-4.3627	0.0088	-0.0520	9009.50183513	-6.8361	0.0013	-4.3519	0.0026	0.0541
8976.44347286	-6.8679	0.0012	-4.3754	0.0022	0.0555	9019.38956783	-6.8125	0.0011	-4.3674	0.0021	0.0153
8976.65122857	-6.8755	0.0014	-4.3606	0.0029	0.0595	9019.45377624	-6.8125	0.0013	-4.3702	0.0025	0.0095
8977.41639792	-6.8801	0.0011	-4.3669	0.0020	0.0504	9026.38768335	-6.8710	0.0015	-4.3662	0.0032	0.0609
8977.62983603	-6.8708	0.0013	-4.3537	0.0026	0.0366	9026.50468897	-6.8710	0.0015	-4.3731	0.0031	0.0664
8978.44811542	-6.8284	0.0017	-4.3570	0.0035	0.0066	9027.38664056	-6.8360	0.0012	-4.3645	0.0022	0.0352
8978.59219355	-6.8245	0.0011	-4.3514	0.0019	0.0024	9028.40158054	-6.8129	0.0012	-4.3650	0.0022	0.0120
8979.39425788	-6.8082	0.0017	-4.3456	0.0036	0.0235	9028.49611091	-6.8234	0.0014	-4.3630	0.0028	0.0121
8979.62786819	-6.8181	0.0020	-4.3453	0.0046	0.0236	9029.39434628	-6.8836	0.0013	-4.3695	0.0025	0.0781
8983.51984327	-6.8076	0.0024	-4.3816	0.0062	0.0310	9037.38815359	-6.8402	0.0016	-4.3701	0.0033	0.0339
8983.56943540	-6.8009	0.0019	-4.3787	0.0045	0.0229	9037.50453450	-6.8479	0.0026	-4.3887	0.0071	0.0379
8985.41144889	-6.8752	0.0017	-4.3694	0.0037	0.0544	9038.38668478	-6.8987	0.0019	-4.3281	0.0039	0.0860
8985.55519063	-6.8792	0.0017	-4.3677	0.0037	0.0600	9038.52708029	-6.8918	0.0025	-4.3599	0.0072	0.0798
8986.40951622	-6.8659	0.0015	-4.3630	0.0031	0.0412	9039.38863040	-6.8411	0.0013	-4.3842	0.0025	0.0225
8986.57451820	-6.8615	0.0017	-4.3742	0.0038	0.0317	9039.51469822	-6.8335	0.0021	-4.3750	0.0052	0.0258
8988.42992979	-6.8176	0.0013	-4.3363	0.0025	0.0111	9040.37477881	-6.8136	0.0014	-4.3773	0.0028	0.0050
8988.58227026	-6.8182	0.0014	-4.3312	0.0028	0.0224	9040.47274672	-6.8129	0.0024	-4.3680	0.0062	0.0195
8989.43032134	-6.8237	0.0014	-4.3383	0.0027	0.0430	9050.37744444	-6.8017	0.0017	-4.3496	0.0033	0.0036
8989.58069423	-6.8362	0.0015	-4.3403	0.0031	0.0429	9051.39733395	-6.8496	0.0013	-4.3434	0.0023	0.0736
8990.45362751	-6.8639	0.0012	-4.3639	0.0024	0.0716	9054.37401342	-6.8102	0.0017	-4.3593	0.0037	0.0001
8990.60241476	-6.8737	0.0015	-4.3649	0.0031	0.0817	9058.40701370	-6.8006	0.0023	-4.3720	0.0056	0.0117
8992.38380996	-6.8188	0.0025	-4.3809	0.0066	0.0320	9059.37938790	-6.8123	0.0017	-4.3399	0.0029	0.0161
8992.46549471	-6.8067	0.0050	-4.3921	0.0175	0.0205	9068.36923554	-6.8414	0.0015	-4.3244	0.0024	0.0299
8993.40261228	-6.8217	0.0014	-4.3883	0.0030	0.0173	9070.37216797	-6.8657	0.0013	-4.3772	0.0025	0.0511
8993.44472770	-6.8237	0.0013	-4.3943	0.0027	0.0181	9071.38883149	-6.8280	0.0015	-4.3821	0.0034	0.0282
8993.48428541	-6.8244	0.0025	-4.3996	0.0061	0.0174	9075.37245446	-6.8105	0.0012	-4.3551	0.0021	0.0198
8993.52620408	-6.8265	0.0015	-4.3910	0.0031	0.0153	9076.36724852	-6.8042	0.0015	-4.3246	0.0030	-0.0004
8993.56836579	-6.8280	0.0013	-4.3813	0.0027	0.0214	9077.36882563	-6.8523	0.0013	-4.3138	0.0022	0.0600
8993.60875678	-6.8300	0.0013	-4.3839	0.0028	0.0262	9078.36645711	-6.8714	0.0014	-4.3125	0.0028	0.0657
9007.40029000	-6.8337	0.0012	-4.3539	0.0021	0.0399	9079.36222621	-6.8478	0.0023	-4.3685	0.0059	0.0469
9007.50066506	-6.8371	0.0009	-4.3339	0.0015	0.0405	9091.35641808	-6.8731	0.0020	-4.3801	0.0055	0.0456
9007.58233770	-6.8431	0.0010	-4.3243	0.0018	0.0411	9092.35503638	-6.8143	0.0027	-4.4001	0.0082	0.0040
9008.39959635	-6.8577	0.0013	-4.3700	0.0025	0.0612						

* Not used during planet and stellar activity modelling.

Table E.2. Second season of HARPS-N RV, BIS and $\log R'_{\text{HK}}$ measurements of TOI-1807.

JD-2450000	RV (km s ⁻¹)	σ_{RV} (km s ⁻¹)	$\log R'_{\text{HK}}$	$\sigma_{\log R'_{\text{HK}}}$	BIS (km s ⁻¹)	JD-2450000	RV (km s ⁻¹)	σ_{RV} (km s ⁻¹)	$\log R'_{\text{HK}}$	$\sigma_{\log R'_{\text{HK}}}$	BIS (km s ⁻¹)
9245.71820728	-6.8289	0.0016	-4.3773	0.0034	0.0159	9338.52325852	-6.8537	0.0015	-4.3464	0.0030	0.0514
9246.75235034	-6.8230	0.0016	-4.3667	0.0033	0.0208	9342.47056341	-6.8392	0.0017	-4.3420	0.0029	0.0168
9247.80531298	-6.8745	0.0012	-4.3688	0.0023	0.0672	9342.60351957	-6.8318	0.0028	-4.3332	0.0059	0.0193
9258.72515565	-6.8327	0.0015	-4.3703	0.0031	0.0075	9343.48228209	-6.8341	0.0019	-4.3467	0.0036	0.0209
9276.70613765	-6.8044	0.0012	-4.3845	0.0024	0.0042	9343.61577051	-6.8386	0.0033	-4.3407	0.0073	0.0298
9288.63117172	-6.8279	0.0010	-4.3590	0.0018	0.0244	9344.52135958	-6.8802	0.0018	-4.3358	0.0030	0.0554
9289.62913153	-6.8173	0.0011	-4.3547	0.0019	0.0280	9344.65394516	-6.8731	0.0026	-4.3459	0.0057	0.0372
9297.53293888	-6.8252	0.0017	-4.3708	0.0037	0.0332	9345.42856827	-6.8570	0.0021	-4.3486	0.0040	0.0347
9298.67051675	-6.8083	0.0015	-4.3560	0.0029	0.0181	9345.58234475	-6.8586	0.0020	-4.3369	0.0037	0.0233
9304.55013936	-6.8352	0.0027	-4.3583	0.0067	0.0272	9346.40817978	-6.8236	0.0018	-4.3406	0.0033	0.0080
9305.55635483	-6.8336	0.0020	-4.3813	0.0043	0.0145	9346.45210101	-6.8256	0.0015	-4.3494	0.0027	0.0131
9305.56656304	-6.8325	0.0030	-4.3726	0.0073	0.0066	9346.52170370	-6.8243	0.0017	-4.3483	0.0031	0.0000
9307.57306441	-6.8141	0.0010	-4.3444	0.0017	0.0092	9346.61142104	-6.8224	0.0025	-4.3638	0.0068	0.0091
9315.56461272	-6.8404	0.0011	-4.3611	0.0020	0.0468	9346.64270406	-6.8301	0.0030	-4.3455	0.0087	0.0086
9322.42066058	-6.8428	0.0014	-4.3685	0.0030	0.0518	9346.69584931	-6.8331	0.0040	-4.3310	0.0117	0.0061
9322.71609101	-6.8208	0.0033	-4.3364	0.0098	0.0300	9359.40602561	-6.8412	0.0037	-4.3681	0.0108	0.0493
9323.41920484	-6.8046	0.0019	-4.3668	0.0042	-0.0030	9360.45664208	-6.8142	0.0013	-4.3472	0.0026	0.0157
9323.54739509	-6.8123	0.0020	-4.3716	0.0046	-0.0037	9360.57386843	-6.8168	0.0020	-4.3255	0.0038	0.0051
9324.38355936	-6.8294	0.0018	-4.3548	0.0039	0.0439	9361.39599194	-6.8534	0.0013	-4.3316	0.0022	0.0523
9324.43312945	-6.8304	0.0022	-4.3662	0.0050	0.0374	9362.45681500	-6.8700	0.0021	-4.3457	0.0045	0.0381
9324.47732934	-6.8319	0.0022	-4.3420	0.0050	0.0309	9362.57358987	-6.8597	0.0013	-4.3401	0.0025	0.0319
9324.52385554	-6.8300	0.0022	-4.3605	0.0053	0.0336	9363.42179882	-6.8388	0.0011	-4.3549	0.0019	0.0379
9324.56852995	-6.8310	0.0023	-4.3544	0.0053	0.0344	9363.56161612	-6.8389	0.0014	-4.3580	0.0028	0.0362
9324.61286873	-6.8312	0.0016	-4.3519	0.0034	0.0351	9364.42230071	-6.8222	0.0014	-4.3580	0.0026	0.0231
9324.65635104	-6.8310	0.0015	-4.3464	0.0029	0.0295	9364.55892371	-6.8192	0.0017	-4.3530	0.0038	0.0166
9324.70296982	-6.8292	0.0023	-4.3290	0.0054	0.0318	9365.54275951	-6.8593	0.0015	-4.3560	0.0030	0.0767
9325.40108234	-6.8165	0.0013	-4.3506	0.0024	0.0101	9366.45758326	-6.8418	0.0012	-4.3744	0.0024	0.0490
9325.53454990	-6.8177	0.0012	-4.3523	0.0022	0.0147	9366.56998321	-6.8314	0.0016	-4.3723	0.0035	0.0444
9326.36722874	-6.8696	0.0012	-4.3543	0.0022	0.0763	9367.45813011	-6.8311	0.0011	-4.3736	0.0021	0.0158
9326.40955361	-6.8722	0.0011	-4.3535	0.0021	0.0743	9377.43036413	-6.8352	0.0011	-4.3547	0.0020	0.0388
9326.45132294	-6.8718	0.0010	-4.3532	0.0018	0.0801	9379.40317741	-6.8646	0.0012	-4.3651	0.0023	0.0484
9326.49485147	-6.8730	0.0012	-4.3552	0.0023	0.0804	9380.44381032	-6.8579	0.0018	-4.3564	0.0040	0.0347
9326.53833370	-6.8716	0.0012	-4.3565	0.0021	0.0785	9388.45962108	-6.8762	0.0011	-4.3763	0.0020	0.0416
9326.60411837	-6.8717	0.0012	-4.3575	0.0022	0.0805	9390.47008063	-6.7849	0.0013	-4.3364	0.0023	-0.0165
9326.64815613	-6.8717	0.0011	-4.3612	0.0019	0.0742	9413.46189904	-6.8357	0.0038	-4.3483	0.0094	0.0475
9327.42357917	-6.8559	0.0010	-4.3484	0.0018	0.0411	9417.42186840	-6.8239	0.0010	-4.3543	0.0019	0.0229
9327.55162999	-6.8476	0.0010	-4.3444	0.0018	0.0306	9418.44355285	-6.8462	0.0042	-4.3708	0.0134	0.0252
9328.47268336	-6.8229	0.0022	-4.3551	0.0053	-0.0092	9428.43009929	-6.8446	0.0021	-4.3450	0.0050	0.0409
9328.65304685	-6.8333	0.0053	-4.3556	0.0181	-0.0054	9430.41405431	-6.8207	0.0018	-4.3389	0.0040	0.0136
9330.49354193	-6.8679	0.0012	-4.3614	0.0022	0.0733	9431.40611978	-6.8592	0.0036	-4.3230	0.0099	0.0317
9330.63536494	-6.8669	0.0016	-4.3577	0.0033	0.0654	9443.37940582	-6.8428	0.0027	-4.3659	0.0074	0.0440
9332.54051802	-6.8193	0.0010	-4.3569	0.0017	0.0113	9445.36272734	-6.7887	0.0015	-4.3678	0.0032	-0.0049
9332.66888067	-6.8300	0.0018	-4.3477	0.0033	0.0084	9446.37889092	-6.8744	0.0016	-4.3618	0.0037	0.0816
9336.61763016	-6.8406	0.0015	-4.3646	0.0031	0.0267	9447.39404862	-6.8444	0.0019	-4.3696	0.0048	0.0091
9338.43760288	-6.8476	0.0011	-4.3291	0.0020	0.0495	9448.38183570	-6.8347	0.0013	-4.3624	0.0027	0.0240

Table E.3. iSHELL RV measurements of TOI-1807.

JD-2450000	RV (m s ⁻¹)	σ_{RV} (m s ⁻¹)
9014.835956239	-24.7	7.2
9016.809708646	-24.7	6.8
9021.801696615	-38.2	6.5
9022.801223677	-25.3	5.3
9255.144664628	50.9	11.3
9256.160684256	-6.5	10.5
9257.103522918	-40.9	7.3
9261.168549077	-52.4	9.6
9322.949459804	-51.6	7.1
9331.867578560	-38.4	11.0
9362.909338106*	93.0	13.9
9363.866398826*	145.3	9.0
9368.917426278*	107.0	8.6
9369.863219064*	123.6	11.8
9371.816766591*	93.7	8.1
9376.921081772	-39.3	9.8
9379.854432749	-16.6	8.5
9380.852652085	-68.0	14.7
9591.139044181	-35.5	14.0
9592.159119182	-2.9	10.8
9605.085212320	-0.7	7.1
9606.087809338	-38.4	8.6

* Not used during planet and stellar activity modeling.

Table B.1. Our measurements of rotation periods, Li EW, and age classification of the kinematically selected targets comoving with TOI-1807.

ID	TIC	α (J2000.0) (deg.)	δ (J2000.0) (deg.)	G (mag)	$(G - K_{\text{mass}})_0$ (mag)	P (d)	σ (d)	grade	EW Li mÅ	Coeval
HD 123	604446831	1.565889	58.4367	6.196	1.860	9.67	0.21	A		N?
UCAC4 180-001659	231019115	27.274584	-54.1992	12.209	3.353					N?
HD 17250C	318841149	41.469222	5.4901	12.588	3.400	20	4	B		N?
HD 18414	91556441	44.175443	-30.8602	8.756	1.583			C		N?
Wolf 140	416098108	49.529217	42.6692	12.178	3.739					N
HD 20776	44628969	49.912190	-34.0237	9.077	1.692			C		N?
2MASS J03550477-1032415	55441420	58.769894	-10.5449	17.529	5.550			C		N
HD 26413	152473055	62.141159	-45.8648	6.540	0.945	0.395	0.003	A		?
ASAS J041255-1418.6	332660818	63.232301	-14.3164	11.914	3.276	7.34	1.05	A	0	Y?
HD 34652	317383399	65.319224	-87.8129	7.384	0.952	1.753	0.026	A		Y?
HD 27857	470480305	66.609138	52.5048	7.893	0.659	12.9	3.3	A		N
UCAC2 20545888	33062967	88.514907	-27.3237	12.496	3.493	21	9	B		N
UCAC2 9643914	238088359	105.01363	-51.3543	12.568	3.467	2.82	0.10	A		Y?
GSC 08558-01964	294154590	107.74969	-56.5499	8.108	1.397					?
HD 72687	283397452	128.31408	-29.9566	8.107	1.395	3.87	0.31	A		N?
HD 76332	126312524	134.09563	28.6679	8.416	1.569	10.8	2.1	A	49.9±1.0	N?
TYC 3430-1344-1	456344030	136.24858	50.4177	9.854	1.941	10.6	2.9	A		?
TYC 6621-759-1	309024402	151.10760	-26.2086	10.889	2.557	23	8	B		N?
TYC 4144-944-1	355868825	157.00903	60.0963	10.304	2.177	11.4	2.9	A		?
40 LMi	241197867	160.75784	26.3256	5.483	0.432					Y?
UCAC4 562-049479	95776155	160.78268	22.3020	12.197	3.178	13.0	3.0	A		?
LP 373-35	84925818	164.26578	22.2889	14.797	4.449	18	6	B		N
2MASS J11155546+4049569	450332591	168.98113	40.8325	13.686	3.655	4.72	0.41	A	54.8±1.6	Y
HD 99419	3901189	171.61328	20.5181	7.788	1.302					N
HD 103928	99302268	179.52989	32.2739	6.344	0.744					N?
HD 103928B	99302269	179.52800	32.2728	12.154	3.466					N?
17 Vir	377227654	185.63349	05.3054	6.326	1.169					N
17 Vir B	377227655	185.63126	05.3108	9.016	2.274					N
TYC 4394-114-1	148910632	185.83058	67.9022	10.827	2.437	10.5	0.2	A		Y?
TIC 40560697	40560697	185.91647	-14.9889	12.261	3.481			C		N?
LX Com	450335652	192.91004	25.5088	8.840	1.846	7.80	0.56	A	78.8±4.7	Y?
BD+26 2401	156514310	193.00904	25.4566	9.436	2.489	20	3	B	5.6±0.7	Y?
L68-145	361397288	193.62125	-74.5023	11.021	3.293	20	3	A		N?
GJ 490A	950125199	194.41755	35.2250	9.765	3.210	3.37	0.21	A	25.8±105	N?
HD 112733	17740825	194.63321	38.2788	8.472	1.620	5.15	0.48	A		Y?
HD 112733B	17740827	194.64583	38.2801	9.002	2.125	5.15	0.48	A	111.9±1.1	Y?
HD 113414	1727745	195.91254	-16.3366	7.598	1.147	3.18	0.20	A		?
TOI-1807	180695581	201.28332	38.9225	9.675	2.105	8.68	0.17	A	104.0±1.0	Y
HD 117378	288405352	202.26368	42.2383	7.491	1.244	4.40	0.17	A	102.2±1.5	Y
TYC 3032-368-1	288487378	203.85894	43.7658	10.489	2.591	12.2	0.3	A		Y?
HIP 68732	135154868	211.04165	20.7591	9.787	2.271	10.0	1.0	B		Y?
RX J1419.0+6451	166087190	214.76373	64.8629	13.173	3.614	0.425	0.001	A	0	Y?
TOI-2076	27491137	217.39268	39.7904	8.910	1.820	7.29	0.12	A	89.4±3.0	Y

Table B.1. Continued.

ID	TIC	α (J2000.0) (deg.)	δ (J2000.0) (deg.)	G (mag)	$(G - K_{2\text{Mass}})_0$ (mag)	P (d)	σ (d)	grade	EW Li mÅ	Coeval
HD 127821	166178883	217.69196	63.1858	5.991	0.976	0.570	0.001	A		Y?
HD 129425	158496710	220.04402	57.7132	7.739	1.159	3.78	0.05	A	79.8±3.0	Y?
HD 130460	282855338	221.31925	65.3300	7.092	1.037	1.595	0.005	A		Y?
BD+18 2930	345299634	221.73805	18.3003	9.251	1.715	—	—	C		Y?
TYC 2569-1485-1	272610678	229.68640	35.9487	11.070	2.749	—	—	A		?
TYC 2025-810-1	357500019	229.81312	24.3271	10.576	2.574	11.6	2.6	A		Y?
HD 137897	371267644	232.13727	03.1104	9.014	1.505	—	—	A		?
UCAC4 675-059372	156000373	235.92797	44.8477	12.386	3.372	2.20	0.04	A		Y?
TYC 3059-299-1	282941472	236.59651	44.0541	11.226	2.806	6.58	0.40	A		Y?
UCAC4 544-056450	307915958	237.91306	18.6732	12.138	3.237	4.05	0.31	A		Y?
2MASS J16001203-0230594	168457615	240.05012	-02.5165	11.675	3.254	—	—	A		Y?
LSPM J1604+2331	445889890	241.05512	23.5274	13.317	4.218	0.756	0.005	A		Y?
HD 144489	172712253	241.39598	15.2575	8.524	1.422	—	—	A	83.3±5.2	N?
HD 148319	163915173	246.87854	-10.1429	8.411	1.348	—	—	A	74.0±7.8	N?
2MASS J16371518+3331426	57031688	249.31323	33.5285	13.405	3.499	11.5	1.2	A		?
BD-05 4394	41038121	255.70661	-06.0684	10.052	3.107	—	—	A		N?
μ Dra	198355687	256.33385	54.4700	5.513	1.756	—	—	A		N?
TYC 5668-239-1	418673682	266.11879	-13.0744	10.095	3.107	—	—	A		?
HD 162199	446245637	267.34646	10.3388	8.174	1.697	—	—	A		?
2MASS J18153959+1152077	391453943	273.91499	11.8688	12.597	3.517	—	—	A		?
HD 168746	18097734	275.45743	-11.9227	7.772	1.519	—	—	A		N
TYC 460-624-1	449263348	281.29279	06.3378	10.004	3.198	—	—	A		?
KIC 11087368	26960092	293.46911	48.6578	13.447	3.683	—	—	C		N?
2MASS J20144598-2306214	71480177	303.69160	-23.1060	12.792	3.847	—	—	A		N?
1RXS J203300.7+435147	188452312	308.25105	43.8633	—	—	—	—	A		?
EM* SHHA 182	269940990	310.92140	-24.5648	—	—	—	—	A	5.3±2.5	N?
HD 198767	387511797	312.07519	69.1418	7.817	1.265	6.19	0.07	A		?
2MASS J21364848-2200541	441026957	324.20204	-22.0151	12.363	3.382	14.5	3.9	A		?
BD+34 4580	236671835	329.90301	35.6840	9.256	1.955	10.0	1.0	A		?
UCAC4 260-199238	152889010	337.59242	-38.1578	12.392	3.119	—	—	C		N?
BD+36 4976	418960381	345.03034	36.9331	9.423	1.954	17	6	B		N?
UCAC4 558-143573	436525094	349.12987	21.5425	12.087	3.426	—	—	A		N?
BD+24 4863	269786865	359.36201	25.1090	9.250	1.658	—	—	A		?

Notes. Sources of data for Li EW measurements: ASAS J041255-1418.6: FEROS, Prog. ID 091.C-0216(A), PI Rodriguez; HD 76332: FEROS, Prog. ID 090.D-0133(A), PI Datson; HD 99419: SOPHIE, Prog. ID 09B.PNP.CONNS; LX Com: HIRES/Keck, Prog. ID H6aH, PI Boesgaard; BD+26 2401: HIRES/Keck, Prog. ID N038Hr, PI Fischer; GJ 490A: HIRES/Keck, Prog. ID H198Hr, H170Hr, PI Shkolnik; HD 112733B: HIRES/Keck, Prog. ID H6aH, PI Boesgaard; TOI-1807: HARPS-N (this paper, Sect. 3.3) HD 117378 : HIRES/Keck, Prog. ID A297Hr, PI Fischer; RX J1419.0+6451: HIRES/Keck, Prog. ID C103Hr, PI Bowler; TOI-2076: HARPS-N (GAPS team, priv. comm.); HD 129425: SOPHIE, Prog. ID 17A.PNCG.SOUB, PI Soubiran; HD 144489: SOPHIE, Prog. ID 11A.PNP.CONNS; HD 148319: HARPS, Prog. ID 072.C-0488(E), PI Mayor and I83.C-0972(A), PI Udry; EM* SHHA 182: HIRES/Keck, Prog. ID H198Hr, H212Hr, H170Hr, PI Shkolnik